EFFECT OF VENETIAN BLINDS ON OVERALL HEAT TRANSFER THROUGH WINDOW SYSTEMS: A FINITE ELEMENT NUMERICAL SOLUTION

by

Ping Ye

A thesis submitted to the Department of Mechanical Engineering
in conformity with the requirements for the degree
of Master of Science (Engineering)

Queen's University
Kingston, Ontario, Canada
May, 1997

ABSTRACT

A numerical study of two-dimensional heat transfer through glazing units with venetian blinds has been undertaken. The following situations have been modeled: (A) natural convection over an isothermal flat plate with a venetian blind; and (B) combined heat transfer through an insulated glazing unit (IGU) with an internal venetian blind.

The natural convective heat transfer characteristics of an isothermal, vertical flat plate adjacent to a set of blind louvers has been numerically evaluated. Results are presented for five different blade-to-plate spacings (d=15, 20, 25, 30, 40 *mm*) and four different blade angles (θ=0°, 45°, -45°, and 80°). For simplification, the louvers were treated as zero-thickness baffles. Some of the results from this work were compared with those from the experimental work of Machin (1997).

For the IGU systems with internal venetian blinds, the combined convective and radiative heat transfer in IGU cavities, along with conduction in the solid portions, have been simulated for several different louver angles (i.e., 0°, 45°, -45°, 75°, and -75°). In addition, the combined heat transfer on an indoor glass surface was investigated to obtain the indoor combined heat transfer coefficient, h_i. This was used subsequently as the indoor boundary condition for the evaluation of the 2-D combined heat transfer through an IGU system. In order to be able to compare the results of this numerical modeling work with those from the published and well-accepted work, the simulation of laminar natural convection in an IGU cavity was also performed.

The results of this work compare well with previous experimental and numerical work and demonstrate the use of these techniques in the modelling of complex fenestration systems.

ACKNOWLEDGEMENTS

I wish to acknowledge my gratitude to my research supervisor, Dr. S.J. Harrison of the Department of Mechanical Engineering for his guidance and encouragement during the research.

I would, also, like to express my appreciation to Dr. P.H. Oosthuizen of Mechanical Engineering, Queen's University and Dr. D. Naylor of Ryerson Polytechnic University (Toronto) for their invaluable support.

Finally, I wish to acknowledge my appreciation to the National Science and Engineering Research Council, (NSERC), Queen's University, the Department of Mechanical Engineering and the Solar Calorimetry Laboratory for the funding they provided through the fellowship, award, teaching assistantship and research assistantship.

TABLE OF CONTENTS

LIST OF TABLES

LIST OF FIGURES

NOMENCLATURE

Symbols

A	aspect ratio
A	area
A_e	area of an element
a	pitch between blades
a,b,c	constants
C	a function of Prandtl number (a constant for air)
c_p	specific heat
d	plate-to-blade spacing
d,e	constants
F	force
F_{ik}	view factor from surface i to surface k
g	gravitational acceleration
h	heat transfer coefficient
J	Jacobian matrix
k	thermal conductivity
L	height
m	mass
$\vec{n}$	normal vector
p	pressure
q	heat flux
$\dot{q}$	heat generation
q_{ref}	reference heat flux ($q_{ref} = k_f \Delta T / W$)
R	residual
r,s	natural coordinates
S	Stefan-Boltzman constant
T	dimensional temperature
T_c	cold wall temperature
T_h	hot wall temperature
t	time

t_b	thickness of blind louver
t_g	thickness of glass pane
u,v,w	x, y, z components of velocity
U,V	dimensionless X, Y components of velocity
U,V,P	column vectors of element nodal point unknowns
U_{ref}	characteristic velocity ($U_{ref} = (\alpha PrGr^{1/2})/W$)
V	volume
$\bar{V}$	fluid velocity
W	width
W	characteristic length
x,y,z	global coordinate directions
X,Y	dimensionless global coordinate directions

Greek letters

α	coefficient of thermal diffusion
β	coefficient of thermal expansion
δ	boundary layer thickness
δ_{ik}	Kronecker delta
ΔT	reference temperature difference
ε	surface emissivity
Φ	dissipation function
φ,ϑ,ψ	column vectors of the shape functions
μ	dynamic viscosity
ν	kinematic viscosity
θ	dimensionless temperature
θ	blade angle
Θ	column vector of element nodal point values of dimensionless temperature
ρ	density
σ	normal stress
τ	viscous shear stress

Subscript

c	convective
f	fluid
g	glass
i	indoor
L	average value over length L
o	outdoor
r	room
r	radiative
s	solid
T	thermal
w	wall
x,y,z	local value
∞	infinite

Superscript

m	constant
n	constant
'	dimensionless

CHAPTER 1

INTRODUCTION

1.1 BACKGROUND

The window has been a source of particular concern to energy researchers because of its potential large heat gains during the summer and losses in the winter.

For decades, the thermal performance of glazing systems, or fenestration, with different features (low-e coatings, multi-glazed units, different glazing cavity gas fills and irregular frame shapes etc.) has been extensively studied. There has been, however, very little information presented on the performance of glazing systems with blinds. This study attempts to provide an insight into the performance of this latter group of fenestration.

To address this problem, natural convection from an isothermal vertical surface adjacent to a venetian blind was studied (see fig. 1.1). To the authors' knowledge, only the experimental results from Machin (1997) exist and were reported in terms of the local and overall convective heat transfer coefficients. In addition, to analyze in detail the effects of louvers (blade-to-plate spacing d and blade angle θ) on the flow pattern, numerical simulation was required. Unfortunately, there are no numerical results reported on this subject. For the present study, a two-dimensional finite element numerical model was developed to investigate the effects of a venetian blind on the free convection heat transfer

on an isothermal vertical surface.

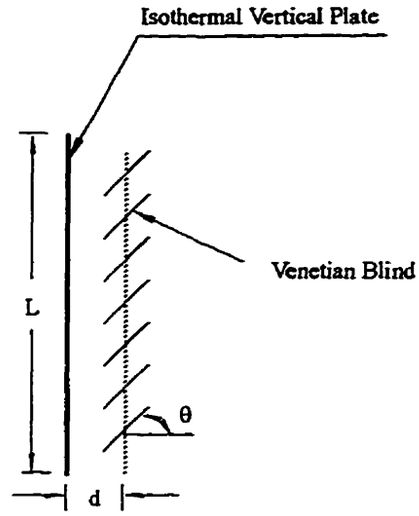

Figure 1.1 The sketch of an isothermal vertical surface adjacent to a venetian blind

The second type of the problem that was dealt with in the present thesis is the effects of internal (between-the-panes) venetian blinds on the combined heat transfer through IGU systems (fig. 1.2). There have been experimental and theoretical attempts to calculate the overall heat transfer through a window with an internal blind. For example, the results reported by Garnet (1995) indicate that the effect of blade angle on U-value is significant. As the blind is closed, the performance of the window improves, but in the open position, the effect of the blind is to reduce the thermal resistance of the window. Rheault and Bilgen (1989) give a theoretical radiation model to calculate the heat transfer through a window with a between-the-panes venetian blind. These results predicted that auxiliary heating and cooling load could be reduced by up to 36% and 47% for winter and summer, respectively. Both studies mentioned above, however, did not establish

temperature profile or flow pattern. The presence of blinds makes it difficult to model combined heat transfer through an IGU, specially with respect to the effect of blade angle. This study makes a contribution towards the solution of this difficult problem by presenting a finite element numerical model for combined heat transfer through IGU systems with internal blinds.

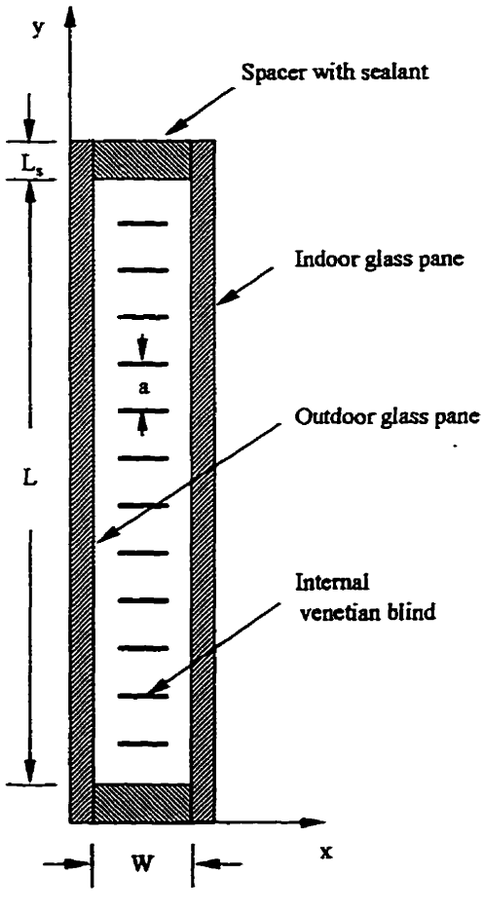

Figure 1.2 A sketch of the IGU system with a internal venetian blind

1.2 LITERATURE REVIEW

Most double-glazed windows manufactured today contain a glazing system that is packaged in the form of a sealed, insulated glazing unit (IGU). The IGU consists of two panes of glass that are separated from each other by edge spacer and seal. Heat transfer through an IGU system is a combination of all modes of heat transfer (see fig. 1.3):

(1) conduction in the solid portions;

(2) convection through air layers on the exterior (forced convection) and interior window surfaces and between glazing layers (natural convection);

(3) radiation heat transfer between glazing layers or between glazing layers and the outdoor or indoor room environment, respectively.

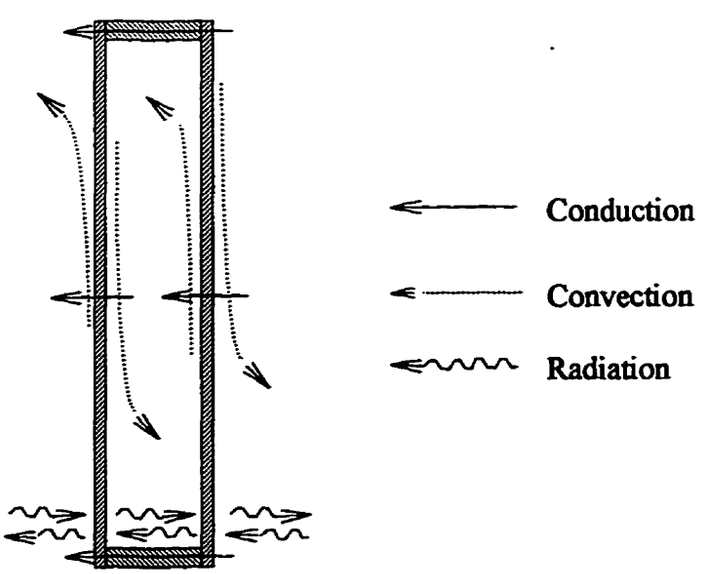

Figure 1.3 Schematic of heat transfer through an IGU

Exterior forced convective heat transfer has been investigated analytically, experimentally and numerically, for example, by Falkner and Skan (1931), Yazdanian and Klems (1994), and Curcija (1992). Conduction in the solid components of window was well characterized, e.g., by Carpenter and McGowan (1989), Reilly (1994) and Wright et al. (1994).

The previous work related to natural convection over an isothermal surface or in an IGU cavity, and the effect of venetian blinds on window thermal performance, are reviewed in the following three sections.

1.3.1 Laminar Natural Convection From an Isothermal Surface

Laminar natural convection currents formed adjacent to a heated or cooled object in a fluid of essentially infinite extent are familiar phenomena. The density of the fluid near the hot or cold surface is changed, resulting in a buoyancy effect that causes circulation of the fluid. Here the velocity and temperature distributions are interrelated; the temperature distribution, in effect, produces the velocity distribution.

Natural convection on a vertical flat plate has been extensively studied. Some comprehensive reviews of early work are available, for example, by Ede (1967). He provided a detailed review of over 110 publications concerning free convection on a vertical surface. The early development of the subject was characterized by the appearance of many papers dealing with experimental work; theoretical papers were rare. Recently this trend has reversed, and most publications have been largely concerned with analytical work.

Figure 1.4 shows the system of coordinates and the significant quantities. Figs. 1.5 and 1.6 are interferometer pictures of nature convection over a heated vertical plate in air, showing the thermal boundary layer on the plates.

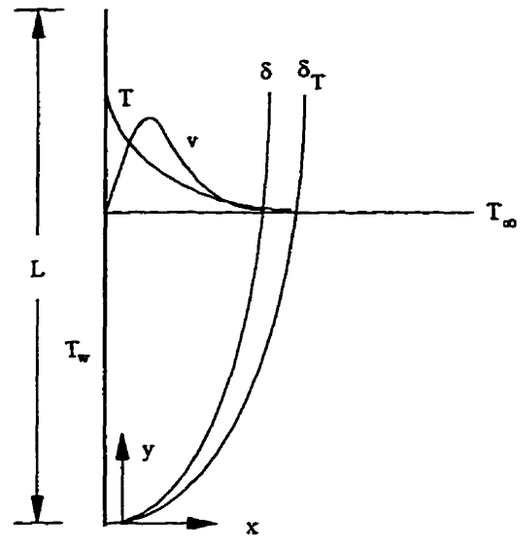

Figure 1.4 Hydrodynamic and thermal boundary layers for natural convection on a vertical plate

It can be seen from fig. 1.5 that near the leading edge the flow is laminar; farther up the plate it changes to turbulent within the boundary layer. Transition to a turbulent boundary layer occurs at a critical value of the Rayleigh number $Ra_y=g\Delta T(y^3/\nu\alpha \approx 10^9$.

Lienhard (1981) showed, by the application of dimensional analysis to natural convection on a flat vertical surface, that the Nusselt number $Nu_y=hy/k$ is a function of the Grashof number, Gr_y, and Prandtl number, Pr:

$$Nu = f(Gr, Pr) \tag{1.1}$$

Another attribute of the dimensionless functional equation is that the primary independent variable is usually the product of Gr and Pr, the Rayleigh number, Ra.

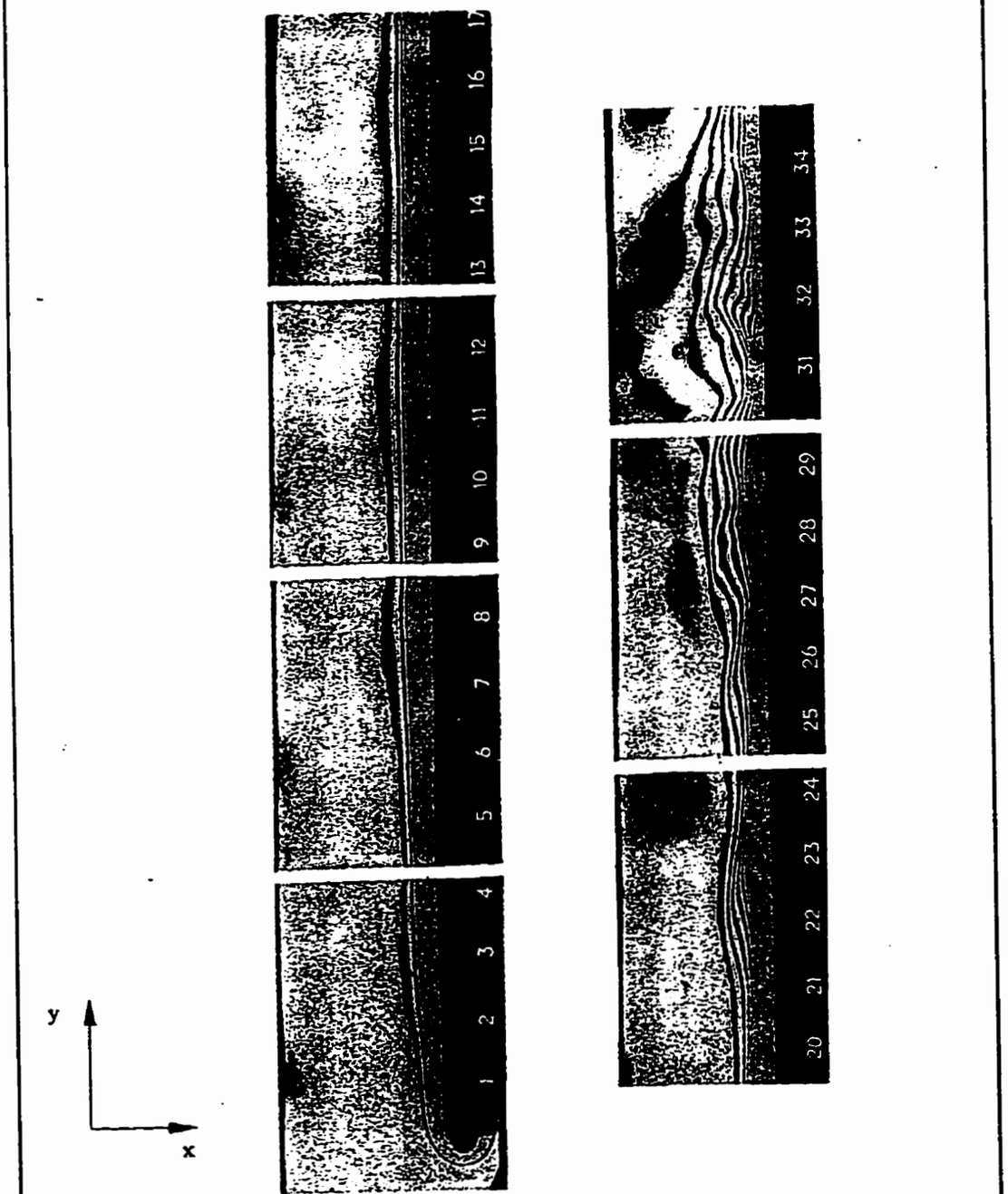

Figure 1.5 Interferometer photographs showing laminar and turbulent free-convection flow on a vertical plate. Numbers give distance in inches from the lower edge of the plate (Eckert and Soehngen 1948)

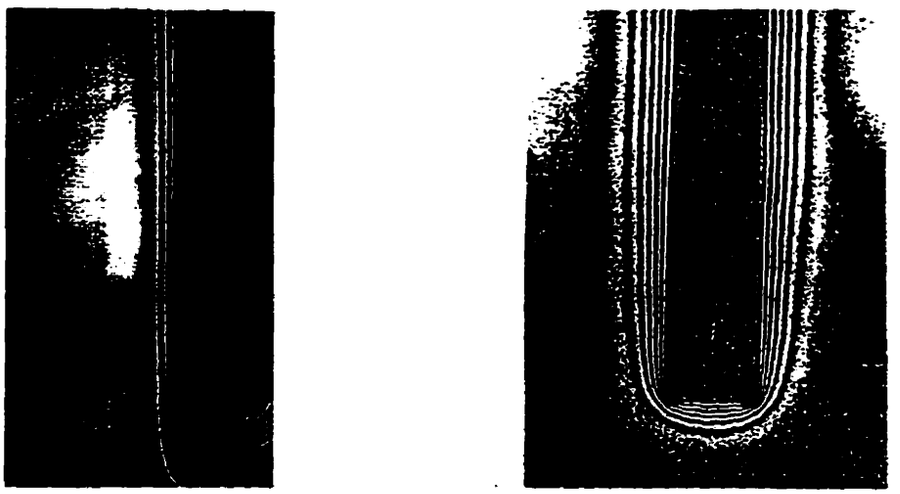

(a) Machin (1997) (b) Gryazoridis (from Mills 1992)

Figure 1.6 Thermal boundary layers on heated vertical plates.

Thus most analyses and correlations of natural convection yield

$$Nu = f(\underbrace{Ra}_{\text{primary (or most important) independent variable}}, \underbrace{Pr}_{\text{secondary parameter}}) \qquad (1.2)$$

All analytical work is based on the set of governing equations (discussed in the following chapter), representing the conservation of mass, momentum, and energy in a fluid moving under the influence of a body force. Lorenz (1881) greatly simplified these equations and reduced them to two equations. His solution leads to the following expression for the average Nusselt number over a plate of height L:

$$Nu_L = 0.548\,(Gr_L \cdot Pr)^{1/4} \tag{1.3}$$

a result which is astonishingly close to experimental data and more accurate solutions.

Pohlhausen, in collaboration with Schmidt and Beckmann (1930), applied Prandtl's boundary-layer approximation, assuming that the effects of the free convection were confined to a thin layer adjacent to the heated surface, to simplify the governing equations and reduced them to two differential equations. The solution for a single value of the Prandtl number (0.733), was obtained numerically as:

$$Nu_y = 0.39\,(Gr_y \cdot Pr)^{1/4} \tag{1.4}$$

or

$$Nu_L = 0.52\,(Gr_L \cdot Pr)^{1/4} \tag{1.5}$$

The advent of the computer permitted Ostrach (1952) and Sparrow (1956) to extend the solution over a wide range of Pr, i.e., $0.00835 \le Pr \le 1000$. Ostrach's solution for Nu may be put in the form:

$$Nu_y = (3C/4)\,(Gr_y \cdot Pr)^{1/4} \tag{1.6}$$

or

$$Nu_L = C\,(Gr_L \cdot Pr)^{1/4} \tag{1.7}$$

where C is a function of Pr, for air C=0.5153.

Le Fevre (1956) consider the extreme cases where Pr tends to zero or infinite and gave C=0.670327 for $Pr \to \infty$ and C=0.800544 $Pr^{1/4}$ for $Pr \to 0$. He also proposed an empirical expression that fits the computer solutions very closely and facilitates interpolation to other values of the Prandtl number:

$$C^4 = Pr/(2.43478 + 4.884Pr^{1/2} + 4.95283Pr) \tag{1.8}$$

For air (Pr=0.711), C=0.5154.

Ede (1967) presented a table which listed the best values available for C in eq. (1.7). For air with Pr=0.72, a value of C=0.516492 was recommended.

The analysis of natural convection using an integral method was first done by Squire (1938), assuming $\delta = \delta_T$ and

$$\frac{T - T_\infty}{T_W - T_\infty} = a + b\left(\frac{x}{\delta}\right) + c\left(\frac{x}{\delta}\right)^2 \tag{1.9}$$

and

$$u = U_c\left(\left(\frac{x}{\delta}\right) + d\left(\frac{x}{\delta}\right)^2 + e\left(\frac{x}{\delta}\right)^3\right) \tag{1.10}$$

where U_c is a function of y and has the dimensions of velocity. He obtained results for the local heat transfer from a vertical isothermal wall during natural convection:

$$Nu_y = 0.508Ra_y^{1/4}\left(\frac{Pr}{0.952 + Pr}\right)^{1/4} \tag{1.11}$$

or for a plate of length L, the overall average Nusselt number

$$Nu_L = 0.678 Ra_L^{1/4} \left(\frac{Pr}{0.952 + Pr} \right)^{1/4} \tag{1.12}$$

The detailed derivation of eq. (1.11) can be found in books of Rohsenow and Choi (1961) and Lienhard (1981).

A large number of experimental observations are available for testing the theoretical solutions. Data available for air were plotted in fig. 1.7, and can be seen to form a smooth curve, concave upwards. The straight line tangential to the curve represents Ostrach's solution, eq. (1.7); it represents the data reasonably well for Rayleigh numbers between 10^6 and 10^8, but deviates from the curve at either end. The divergence at high Rayleigh number may be due to the development of turbulence, and that at low Ra to a thickening of the boundary layer to such an extent that the boundary-layer approximation becomes invalid. Therefore the theoretical results are most suitable for the intermediate range of Rayleigh number for which the postulates of laminar boundary layer theory are applicable. A completely satisfactory theory has not been developed for either the diffusive regime (low Ra) or the turbulent regime (high Ra).

The empirical expression of Churchill and Usagi (1972) can be rewritten as follows, in terms of average Nusselt number Nu_L:

$$Nu_L = 0.670 Ra_L^{1/4} / \left(1 + 0.492/Pr^{9/16}\right)^{4/9} \tag{1.13}$$

Churchill and Chu (1975) developed a simple expression for the space-mean Nu_L in terms of the model of Churchill and Usagi (1972). The development utilized experimental values for Ra approaching zero and infinity and the theoretical solutions

obtained from laminar boundary layer theory. The correlating equation used was in the form

$$Nu_L = 0.68 + \frac{0.670 Ra_L^{1/4}}{(1 + (0.492/Pr)^{9/16})^{4/9}} \qquad (1.14)$$

Equation (1.14) is shown in fig. 1.8 to provide a good representation for all $Ra < 10^9$ while the correlation of Churchill and Usagi (1972) (eq, (1.13)) is seen to be increasingly in error for $Ra < 10^5$.

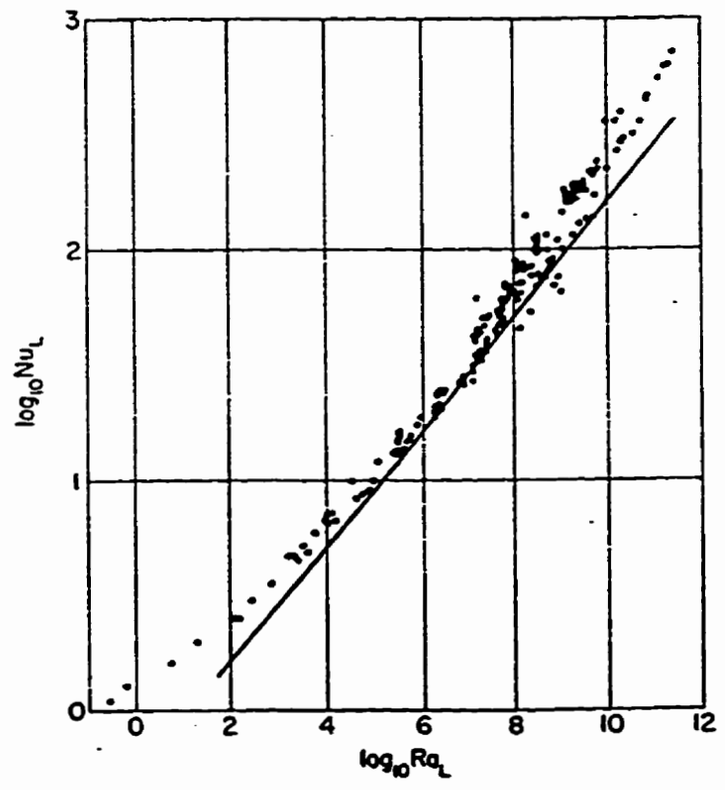

Figure 1.7 Flat plate: experimental data for air (from Ede 1967)

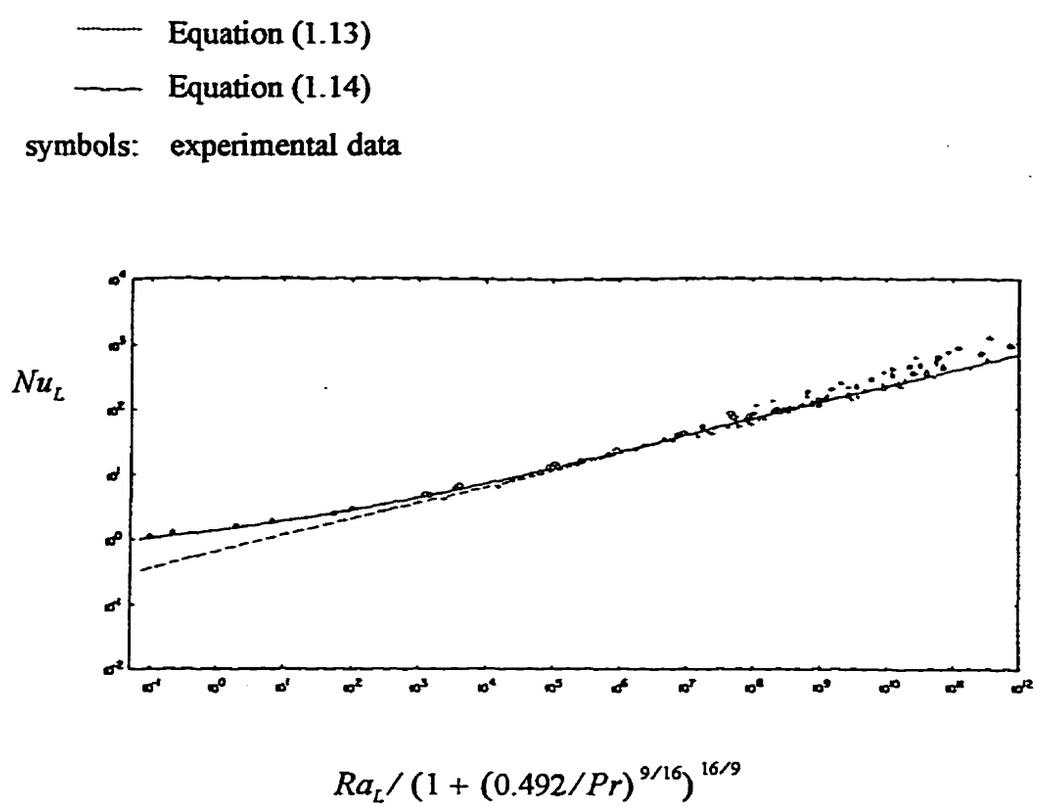

Figure 1.8 Correlating equations for the laminar regime of isothermal, vertical plates (from Churchill and Chu 1975)

Recently Curcija and Goss (1993) have performed a two-dimensional finite element solution of natural convection over an isothermal flat plate (T_w = 7.2°C, T_∞ = 21°C, L=0.5 m, and Ra_L = 1.79×10^8). They compared their results in terms of local heat transfer coefficient and Nusselt number, velocity distributions at different locations, and the overall average Nusselt number. Their predictions compared closely with the results of previous studies.

1.3.2 Laminar Natural Convection in a Cavity

Natural convection involving fluids in enclosures whose vertical sides have different temperatures has been under study for the past eighty years. The reason for this is that it is a simple free convection problem and yet has important practical applications. Among these applications are double glazing and cavity walls, where a layer of air acts as insulation between the warm interior of a building and a cold exterior. Work on such problems, prior to 1972, is discussed in an extensive review article by Ostrach (1972). He pointed out that the complexity of confined natural convection problems resulted from the fact that a boundary layer type flow would exist near the walls but there would also be a region enclosed by the boundary layer, forming a core region. The core region flow is closely coupled to the boundary layer flow. Much subsequent work continues to appear in the literature. Recently Wright and Sullivan (1989) have reviewed the literature concerned with natural convection in enclosures with particular attention paid to window heat transfer applications. Their survey covers over 90 publications concerning analytical, experimental, and numerical studies in the field of free convection in sealed glazing units.

The conventional model (see fig. 1.9) which has been widely investigated is based on the assumption that the flow and heat transfer are two-dimensional, the vertical boundary temperatures are uniform and the conditions at the horizontal surfaces are specified as having either a linear temperature profile (LTP) or zero heat flux (ZHF). Because of its simplicity, much analytical, experimental and numerical work has been performed on this problem.

Batchelor (1954) analyzed the laminar natural convection and was the first to define conduction and boundary layer flow regimes. Eckert and Carlson (1961) and Yin et al. (1978) confirmed Batchelor's work and refined it by proposing conduction, transition, and boundary layer regimes. The regimes are briefly reviewed as follows.

Conduction regime At low Rayleigh numbers ($Ra_w \leq 10^3$) it was shown that a

weak unicellular flow exists and the flow is parallel in the centre region. Heat is transferred across the cavity mainly by conduction (except in small regions at the ends of the cavity where heat is convected). No vertical temperature gradient exists in this regime. The temperature distribution across the mid-height of the cavity in this flow is linear with the result that Nu=1.

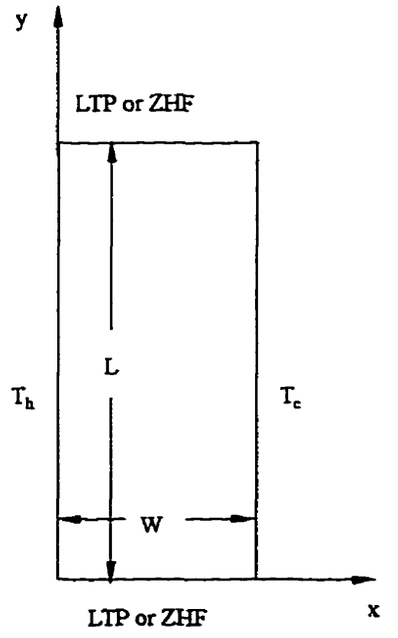

Figure 1.9 2-D Laminar Natural Convection in a Rectangular Cavity

Laminar boundary layer regime At higher temperature differences (larger $Ra_W \approx 3 \times 10^4$), the emergence of boundary layers on the vertical side-walls and a core in the centre are observed. In this, the so-called boundary layer regime, heat is transferred primarily by horizontal convection across the cavity. Gill (1966) pointed out that the boundary layer thickness is proportional to $Ra_W^{-1/4}$. In this situation higher horizontal

temperature gradients exist at the walls and a smaller horizontal temperature gradient exists in the fluid core. Heat transfer across the cavity is greater than that in the conduction regime ($Nu > 1$).

Transition regime For intermediate values of Rayleigh number (Ra_w from 10^3 to 3×10^4) the flow is said to be in the transition regime. In this situation the boundary layers are relatively thick and merge together in the center of the cavity. The major portion of the heat transfer from one plate to another occurs by convection in the boundary layers while in the center a small fraction is transferred by conduction across the flow.

Observation techniques such as interferometry have yielded valuable information regarding the flow fields; the work of Eckert and Carlson (1961), Elder (1965), Seki et al. (1978) and Vest and Aparci (1969) are important examples. By using a Mach-Zehnder interferometer, Eckert and Carlson (1961) have obtained detailed observations of the primary temperature distribution in air and established that, except in the conduction regime, the core in the centre becomes stably stratified, meaning that temperature increases with height. Near the mid-height the rise is linear. Using this fact and assuming that the horizontal velocity is zero, Elder (1965) reported an experimental study of natural convection in a rectangular enclosure using particle suspension techniques and calculated the vertical velocity and the temperature profiles near the mid-height. The profiles have the proper shape and magnitude if the vertical temperature gradient, which is a parameter in his equation, is adjusted to fit the experimental data. It was these two studies which allowed Gill (1966) to work out a boundary layer theory for the flow. Some improvements into Gill's theory have been made by Bejan (1979) and Graebel (1981).

Numerical studies have the greatest capacity to obtain fine details about the flow patterns and heat transfer. Papers by Elder (1966), Wilkes and Churchill (1966), Newell and Schmidt (1970), Spradley and Churchill (1975), Jones (1979), Raithby and Wong (1981), Korpela et al. (1982), Lee and Korpela (1983), Ramanan and Korpela (1989),

Yeoh et al. (1989), and Novak and Nowak (1993) are typical of the many applications of finite difference methods to the solution of the natural convection problem.

Making the Boussinesq approximation, that density variations are significant only in their generation of buoyancy forces, and that other fluid parameters are independent of temperature, the problem is defined by: the kinematic viscosity, ν; the thermal diffusivity, α; the acceleration due to buoyancy, $\beta g \Delta T$, where β is the coefficient of volumetric expansion; L and W. Hence, since these involve only the dimensions of length and time, three dimensionless parameters are needed to specify the system. A convenient set is:

$Pr = \nu/\alpha$, Prandtl number which is a property of fluid;

$Ra = \beta g \Delta T L^3/\alpha\nu$, Raleigh number which involves the imposed temperature difference ΔT;

$A=L/W$, aspect ratio which depends only on the geometry of the system

If the working fluid is air (most of studies are for air; $Pr \approx 0.71$), the Nusselt number will depend only on Ra and A.

Some studies, for example, experiments by El Sherbiny et al. (1982), Yin et al. (1978), Hollands et al. (1976), and Randall et al. (1979) and numerical studies by Raithby et al. (1977), Jones (1979) and Newell and Schmidt (1970) have produced heat transfer correlations. The usual form of the correlation is

$$Nu = cRa^m/A^n \tag{1.15}$$

Values of c, m and n obtained in some studies are shown in Table 1.1. It can be seen from the table that the variation is considerable.

There is a general lack of agreement on the effect of aspect ratio on the average

heat transfer coefficient. Some researchers either neglected or did not discern the dependence of Nu on A (Randall et al. 1979, Landis and Yanowitz 1966, Dropkin and Somerscales 1965). It is found in the work of Randall et al. (1979) that there is a significant aspect ratio effect on the local heat transfer profile, but the integrated average Nusselt number does not vary significantly with aspect ratio for the range studied.

A definite effect of aspect ratio has been reported, for example, by Eckert and Carlson (1961) and Newell and Schmidt (1970), but there is no agreement on the magnitude of the effect ($n = 0.1 \sim 0.265$).

Table 1.1 Some Values of c, m, and n in Equation (1.14)

Investigator	c	m	n	Range of A	Range of Ra	Comment
Eckert and Carlson (1961)	0.132	0.3	0.1	10	$5.7\times10^4 \sim 1.4\times10^5$	Exp.
Newell and Schmidt (1970)	0.173	0.315	0.265	2.5 ~ 20	$2.8\times10^3 \sim 1.0\times10^5$	Num.
Raithby et al. (1977)	0.288	0.25	0.25	$A \geq 5$	all range of Ra	Theor.
Yin et al. (1978)	0.230	0.269	0.131	4.9 ~ 78.7	$1.1\times10^3 \sim 5.0\times10^6$	Exp.
Randall et al. (1979)	0.097	0.290	0.000	9 ~ 36	$2.8\times10^3 \sim 2.2\times10^5$	Exp.
Jones (1979)	0.225	0.262	0.166	1 ~ 20	$1.9\times10^3 \sim 2.3\times10^5$	Num.
Jakob (1946)	0.196	0.250	0.111	3.12 ~ 42.2	$1.42\ (10^4 \sim 10^5)$	Exp.

Note:
Exp. = Experimental work
Num. = Numerical work
Theor. = Theoretical work

Batchelor (1954) has theoretically determined that the effect of enclosure ends should extended along the heated surface for a distance approximately equal to the plate

spacing. This implies that the effect of aspect ratio decreases as aspect ratio increases. This idea is supported, e.g., by Elsherbiny et al. (1982) and Lee and Korpela (1983). The well-quoted experimental measurements of heat transfer by natural convection across vertical and inclined air layers are reported by Elsherbiny et al. (1982). This is an important experimental investigation carried out over very wide ranges of Ra ($10^2 \sim 2 \times 10^7$) and A ($5 \sim 110$). The data of Elsherbiny et al. (1982) (vertical cavity) are shown in Figure 1.10. The solid lines represent the approximate method of Raithby et al. (1977). It can be seen that (1) for large enough A, heat transfer in a laminar boundary layer regime would not be expected; (2) turbulence does not occur below a certain Ra ($\approx 6 \times 10^3$ from experimental data) even for very large aspect ratios; and (3) the critical value of Ra at which flow leaves the conduction regime is a function of A. The convective flow leaves the conduction regime at lower values of Ra in cavities with lower A values.

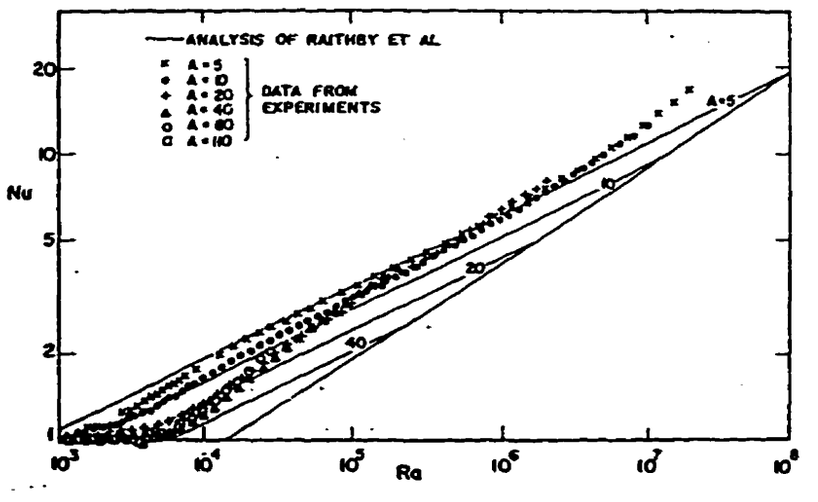

Figure 1.10 Nu vs. Ra and A, data of ElSherbiny et al. (1982) for air in a vertical cavity

Based on the experimental results, Elsherbiny et al. proposed correlation equations for vertical cavity as follows

$$Nu = [Nu_1, Nu_2, Nu_3]_{max} \tag{1.16}$$

where

$$Nu_1 = 0.0605 Ra^{1/3} \tag{1.17}$$

$$Nu_2 = \left[1 + \{0.104 Ra^{0.293} / (1 + (6310/Ra)^{1.36})\}^3\right]^{1/3} \tag{1.18}$$

$$Nu_3 = 0.242 (Ra/A)^{0.272} \tag{1.19}$$

Lee and Korpela (1983) numerically investigated the multicellular natural convection in a vertical enclosure and pointed out that increasing the aspect ratio only changes the number of cells and not the heat transfer across them. The following expression for the average Nusselt number was proposed:

$$Nu = \frac{10}{A} Nu_{10} + \left(1 - \frac{10}{A}\right) Nu_c \tag{1.20}$$

where Nu_1 represents the average Nusselt number for A=10 and Nu_c is the Nusselt number for a cell which is a function of Ra.

Equation (1.20) indicates that for sufficiently tall cavity, i.e., $A \to \infty$, the average Nusselt number Nu approaches the Nusselt number for a cell (Nu_c) which no longer depends on the aspect ratio A.

Raithby and Wong (1981) reported their numerical results for a wide range of Rayleigh numbers ($Ra = 10^3 \sim 10^5$) and aspect ratios ($A = 2 \sim 80$). Calculations were carried out for both perfectly conducting, i.e., a linear temperature profile (LTP), and

adiabatic, i.e., zero heat flux (ZHF), boundaries at the top and bottom ends of the cavity. The correlation equation was proposed as follows

$$Nu = \sqrt{1 + \left(\frac{0.334 (Ra^*)^{0.25}}{1 + 112/(Ra^*)^{0.87}} \right)^2} \tag{1.21}$$

where

$$Ra^* = \left(1 - \frac{1.02}{A^{0.44}}\right) \frac{Ra}{A} \text{ for LTP} \tag{1.22}$$

$$Ra^* = \left(0.89 - \frac{0.73}{A}\right) \frac{Ra}{A} \text{ for ZHF} \tag{1.23}$$

Their results showed that at small values of aspect ratio ($A < 10$), average Nusselt number at constant Rayleigh number for LTP boundary condition is significantly lower than that for ZHF case. Little difference can be found between the LTP and ZHF results when $A \geq 30$ (Wright and Sullivan 1994, Ramanan and Korpela 1989, and Novak and Nowak 1993).

1.3.3 The Effect of Venetian Blinds on Window Performance

Venetian blinds are a particularly versatile device, allowing selective control over window characteristics by means of adjusting blind height and the angles of the slats. Because of the high reflexivity of the blade surface, solar radiation to a room can be reduced in the summer and heat loss from the room, through thermal radiation, can also be reduced in the winter. Although the thermal performance of a window with a venetian blind is not equivalent to that of a wall, the blind when used properly can reduce undesirable heat gains and losses. Rubin et al. (1978) conducted a case study on the feasibility of energy saving operations dependent on the manipulation of interior venetian

blinds and pointed out that using a venetian blind to cover a south-facing window on a hot sunny day can cut the heat gain by at least one-half. The amount of heat gain into the room is partially dependent upon the angle of the slats. Slats set at a 45° angle can reduce the gain to about one-half, while fully closed slats can reduce it to almost one-quarter. The reduction in heat loss is not as great during the winter months, although fully closed venetian blinds can reduce the heat transmission of a single-glazed window by about 10-15%. Mills and McCluney (1993) concluded in their theoretical calculation that the use of interior shades and venetian blinds can exert a significant control over the solar radiant gain from windows in buildings. That control can be increased even further if the shades or blinds are adjusted several times a day.

The overall heat transfer coefficient for a window with an interior or between-the-panes venetian blind is important in analysis and design of an energy efficiency window. It is, however, not widely available in the literature. Among the few studies conducted are: the theoretical study of Rheault and Bilgen (1989), the experimental work of Fang and Ge (1993), Machin (1997), and Garnet et al. (1995).

Rheault and Bilgen (1989) give a theoretical radiation model to calculate the heat transfer through a window with a between-the-panes venetian blind. Results indicate that by using a blind system, the predicted auxiliary load for heating and cooling could be reduced by up to 36% and 47% for winter and summer, respectively.

Using a hot box, Fang and Ge (1993) measured the overall heat transfer coefficients of the single and double glazed windows with interior venetian blinds and some affecting factors. It was found that the blade angle has a significant effect on the overall heat transfer coefficient when the angle is below 50°(from vertical surface and the right-hand side of the louver surface). As the blade angle changes from 5° to 50°, the heat loss increases by about 20%.

An interferometer study of the effect of venetian blinds on free convection from a vertical surface has been carried out by Machin (1997), in which the vertical plate was heated to a temperature T_w above the ambient (room) temperature T_r. This experiment model is shown in fig. 1.11

The experimental results from Machin's work showed that venetian blinds have a strong influence on the local heat transfer characteristics. However, in general, the average convective heat transfer rate was only slightly lower than that for an isolated plate at the same Rayleigh number.

Garnet et al. (1995) used a guarded-heater-plate apparatus to obtain experimental results for between-the-panes venetian blinds, specially with respect to the effect of blind angle. The results reported indicate that the effect of blade angle on U-value is significant. As the blind is closed, the performance of the window improves, but in the open position, the effect of the blind is to reduce the thermal resistance of the window.

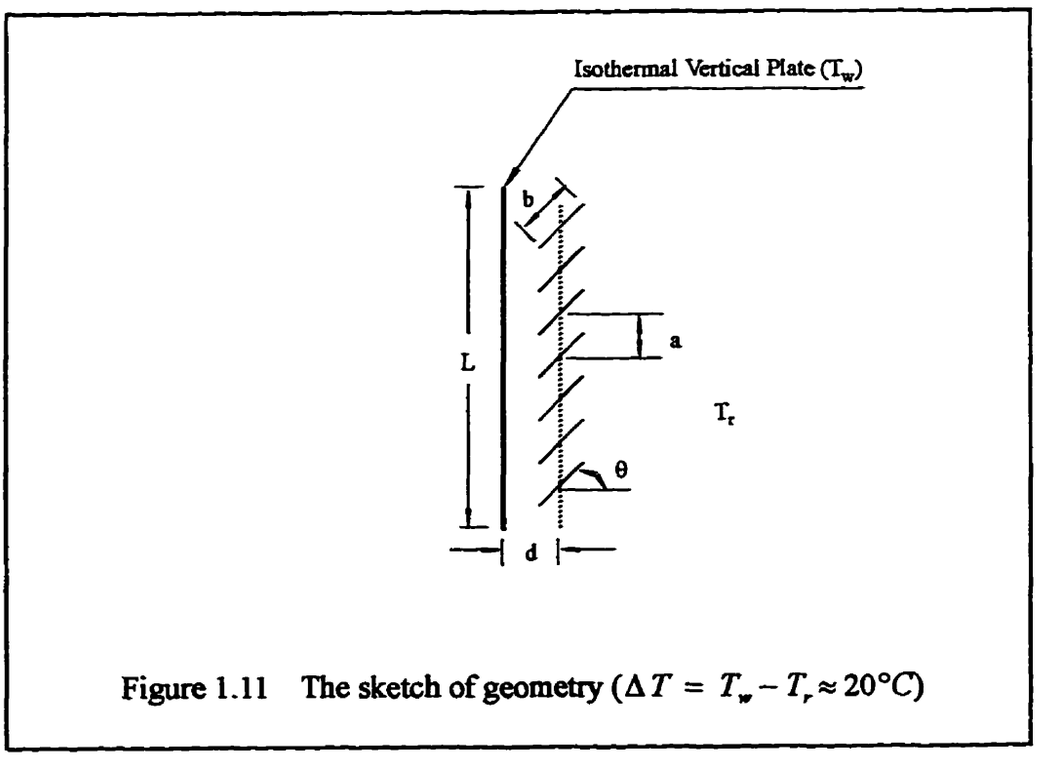

Figure 1.11 The sketch of geometry ($\Delta T = T_w - T_r \approx 20°C$)

1.3 PRESENT STUDY

The present numerical modeling work was motivated by the lack of information about the effects of venetian blinds on the flow pattern and heat transfer through glazing systems. As mentioned before, there is very little information available about the thermal performance of windows with venetian blinds. Fewer results reported to date are available from either experimental or theoretical work. There are very few numerical studies on this subject. Development of computer models of heat flow through glazing units is the next logical step towards a better understanding and better design of energy efficiency windows incorporating venetian blinds.

The main objective of this study was to numerically examine the influence of louvers (blade-to-plate spacing d and blade angle θ) on the natural convective heat transfer (local and overall) from an isothermal surface, and to model the combined heat transfer through IGU systems with internal venetian blinds (including combined convective and radiative heat transfer on an indoor glass pane and laminar natural convection in an IGU cavity). The modeling tool used was based on the finite element numerical method (FEM) incorporated into the FIDAP (1990) computer package.

The more specific aims of the present research are outlined below:

(1) Model the laminar natural convection heat transfer on an isothermal flat plate and compare the results of the present work with the well-accepted previous work in order to verify the basic finite element numerical model;

(2) Develop a two-dimensional finite element model of the laminar natural convection on an isothermal surface adjacent to a venetian blind to investigate the influence of the louvers on the flow pattern and heat transfer rate;

(3) Model the combined convection and radiation on the indoor glass pane surface and compare the present results with those used by the most popular window evaluation

computer programs, e.g., WINDOW3.1, VISION and ISOWIN04. Obtain the combined heat transfer coefficient for the indoor pane surface which will be used as a boundary condition on the indoor surface of the IGU systems;

(4) Simulate the free convection in an IGU cavity and compare the results of this work with those from the well-known work of Ramanan and Korpela (1989), Raithby and Wong (1981) and Korpela et al. (1982) in order to verify the basic finite element numerical model;

(5) Develop a two-dimensional finite element model of combined heat transfer through IGU systems with internal venetian blinds. Numerically examine the effects of louver angles on the local and overall heat flux.

1.4 AN INTRODUCTION TO THE PRESENT STUDY

The present numerical study involves several simulations of heat transfer through glazing systems, with the emphasis on determining the effects of venetian blinds on the flow patterns and heat transfer rates. The following problems have been considered:

(1) The effects of louvers (blade-to-plate spacing d and blade angle θ) on free convection from an isothermal vertical surface,

(2) The combined convective and radiative heat transfer on an indoor pane glass and natural laminar convection in an IGU cavity,

(3) The effects of internal venetian blinds on the combined heat transfer through IGU systems.

CHAPTER 2

MATHEMATICAL FORMULATION

2.1 PHYSICAL MODEL AND ASSUMPTIONS

In this chapter, the equations governing fluid flow, conduction in the solid portions of an IGU system and radiation between solid surfaces of the IGU cavity will be developed. Assumptions will be made to simplify the expressions, however, these should not significantly affect their generality. The simplifying assumptions are described below:

1) Two-dimensional flow is assumed to exist; any effects occurring in the third dimension (horizontal and parallel to the window panes) are neglected — this assumption is reasonable and acceptable for the problem under study and can be justified by the results of numerical work of Curcija (1992). It was found that the temperature contours for 3-D case show essentially the same distribution as in 2-D case, and compared to 2-D case the overall U-value for the 3-D numerical simulation increases by only 0.07%.

2) The fluid is assumed to be Newtonian; shear stress in a fluid is proportional to the time-rate-of-strain, i.e., velocity gradients — this assumption is well-acceptable because the dynamic viscosity, μ, for air and common gases-filled in window cavities is independent of shear rate.

3) The Boussinesq approximation is applicable; the fluid is incompressible with

constant density except for a linear variation of density with temperature in the buoyancy term of the momentum equation — the changes in the density of the fluid can occur due to: (1) pressure changes, and (2) thermal expansion. In the former case, if the flow is steady and laminar, therefore, the relation $(\partial\rho/\rho = V^2/C_s^2) \ll 1$ exists (where ρ is the fluid density, V is the velocity of the fluid flow, assumed to be less than 0.3 m/sec in present study, and C_s — the velocity of sound which for air at normal temperature and pressure is 300 m/sec). Thus, subsequent calculations can safely neglect density changes due to changes in pressure.

In contrast to the influence of pressure changes on density changes, the effect of differences in temperature are larger in magnitude. It is these density changes, due to thermal expansion, that give rise to the buoyancy forces that drive the flow. The Boussinesq approximation would not only eliminate one more variable, but would substantially simplify the form of the equations to be solved. Daly and Pracht (1968) have solved buoyancy problems on a computer both with and without the Boussinesq approximation. They conclude that so long as the value $\beta\Delta T$ remains less than 0.3 (i.e., the fluid expands less than 30% during the flow), the error introduced due to the Boussinesq approximation is less than 5% (in the present calculation, $\beta\Delta T_{max} \cong 0.07$).

4) The dissipation term in the energy equation is neglected. A measure of the importance of this term in a problem is given by the quantity (Gadgil 1980):

$$\frac{1/2\rho\,(V_{max}^2 - V_{min}^2)}{\rho c_p \Delta T}$$

For the flow of buoyant air in this study, the velocities encountered are very small, while $\Delta T \approx 13 \sim 22$°C. This leads to a very small value of the above ratio. This means that the pool of kinetic energy available for possible conversion into thermal energy is insignificant compared to the thermal energy flows arising due to the boundary conditions

on temperature, and this term in the energy equation can be neglected in the problem under consideration.

5) The properties of air and solid materials are assumed constant over the temperature range of interest — Over the range of 0-43°C, the variations in properties determined at mean temperature T_m for air, i.e., c_p, μ, ν, and k_f, are very small. Therefore, for a problem involving buoyancy-driven air flow, the error introduced into the calculations by using this constant property assumption is small.

Finally, the flow is assumed to be steady-state and there are no heat sources within the calculation domain. The walls are stationary, non-slip and impermeable.

2.2 MATHEMATICAL FORMULATION

To understand the behavior of air movement inside a computational domain, one must first formulate, in general, the laws of motion which govern the movement of air. Applying these laws of motion to air flow under the specific boundary conditions will, in principle, define the problem completely.

The basic equations governing the motion of air are those representing conservation of mass, conservation of momentum (Newton's Law) and conservation of energy (first law of Thermodynamics). Equations which govern convection, conduction and radiation heat transfer, together with the appropriate boundary conditions, are presented in this chapter.

2.2.1 Governing Equations for Natural Convective Heat Transfer

The full equations governing the flow of a fluid are known as the so-called continuity equation, Navier-Stokes equation and energy equation. Each of them is discussed below.

The notation and the choice of axes are shown in fig. 2.1.

Conservation of mass—Continuity Equation. Consider a flow of a fluid with velocity $\vec{V}$ having u, v, and w components in the three coordinate directions x, y, and z respectively. Application of the principle of mass conservation to a control volume of the fluid, from the viewpoint of a observer moving at $\vec{V}$, results in the general equation

$$\frac{d\rho}{dt} + div(\rho\vec{V}) = 0 \tag{2.1}$$

The physical significance of each of the two terms in the equation can be obtained by integrating this equation over a differentially small rectangular control volume with sides parallel to the three coordinate directions (see fig. 2.2). The first term gives the rate of change of mass within the control volume, while the second term, changed to a surface integral using Gauss's theorem, gives the net flow of mass out of boundaries enclosing the elementary volume. The two terms must always add to zero if no fluid mass is created or destroyed within the volume.

Since the total derivative can be expressed as:

$$\frac{d}{dt} = \frac{\partial}{\partial t} + \frac{dx}{dt}\frac{\partial}{\partial x} + \frac{dy}{dt}\frac{\partial}{\partial y} + \frac{dz}{dt}\frac{\partial}{\partial z} \tag{2.2}$$

where dx/dt, dy/dt and dz/dt are the three components of the fluid velocity at the point of interest, eq. (2.1) may be rearranged as follows:

$$\frac{\partial\rho}{\partial t} + u\frac{\partial\rho}{\partial x} + v\frac{\partial\rho}{\partial y} + w\frac{\partial\rho}{\partial z} + \rho\left(\frac{\partial u}{\partial x} + \frac{\partial v}{\partial y} + \frac{\partial w}{\partial z}\right) = 0 \tag{2.3}$$

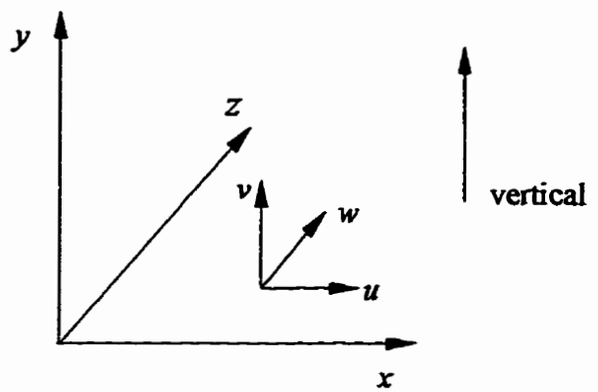

Figure 2.1 The coordinate axes and velocity components

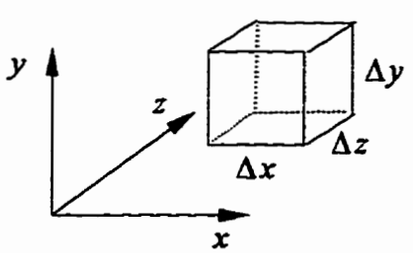

Figure 2.2 The control volume

In eq. (2.3) we note that since the flow is

(a) two-dimensional, then $w = 0, \frac{\partial}{\partial z} = 0$

(b) incompressible, then $\frac{\partial \rho}{\partial x} = 0, \frac{\partial \rho}{\partial y} = 0$

Therefore, eq. (2.2) reduces to:

$$\frac{\partial u}{\partial x}+\frac{\partial v}{\partial y}=0 \tag{2.4}$$

Which is known as the continuity equation for two-dimensional, steady and incompressible flow.

Conservation of momentum—Navier-Stokes Equation. The Navier-Stokes equation is obtained by the application of the conservation of momentum principle to the fluid flow. The same control volume shown in fig. 2.2 is considered.

Conservation of momentum is expressed by Newton's law

$$\vec{F}=\frac{d}{dt}(m\vec{V}) \tag{2.5}$$

where $\vec{F}$ is the force acting on the control volume in space and $\vec{V}$ is the instantaneous velocity of the fluid element.

In general, forces acting on a fluid system may be classified as body forces proportional to the volume or mass of the system, such as gravity and buoyancy force, and surface forces proportional to the area of surface on which they act, such as pressure and viscous forces.

For convenience, the conservation of momentum in each of the three coordinate directions is separately considered. Equation (2.5) for three directions can be written as

$$\frac{\partial}{\partial t}(\rho u)=-u\frac{\partial}{\partial x}(\rho u)-v\frac{\partial}{\partial y}(\rho u)-w\frac{\partial}{\partial z}(\rho u)+\frac{\partial \sigma_x}{\partial x}+\frac{\partial \tau_{yx}}{\partial y}+\frac{\partial \tau_{zx}}{\partial z}+F_x \tag{2.6a}$$

$$\frac{\partial}{\partial t}(\rho v) = -u\frac{\partial}{\partial x}(\rho v) - v\frac{\partial}{\partial y}(\rho v) - w\frac{\partial}{\partial z}(\rho v) + \frac{\partial \sigma_y}{\partial y} + \frac{\partial \tau_{xy}}{\partial x} + \frac{\partial \tau_{zy}}{\partial z} + F_Y \qquad (2.6b)$$

$$\frac{\partial}{\partial t}(\rho w) = -u\frac{\partial}{\partial x}(\rho w) - v\frac{\partial}{\partial y}(\rho w) - w\frac{\partial}{\partial z}(\rho w) + \frac{\partial \sigma_z}{\partial z} + \frac{\partial \tau_{xz}}{\partial x} + \frac{\partial \tau_{yz}}{\partial y} + F_Z \qquad (2.6c)$$

where F_X, F_Y, and F_Z are body forces per unit volume in the coordinate directions and for a Newtonian fluid. In addition

$$\sigma_x = -p + 2\mu\frac{\partial u}{\partial x} - \frac{2}{3}\mu\left(\frac{\partial u}{\partial x} + \frac{\partial v}{\partial y} + \frac{\partial w}{\partial z}\right) \qquad (2.7a)$$

$$\sigma_y = -p + 2\mu\frac{\partial v}{\partial y} - \frac{2}{3}\mu\left(\frac{\partial u}{\partial x} + \frac{\partial v}{\partial y} + \frac{\partial w}{\partial z}\right) \qquad (2.7b)$$

$$\sigma_z = -p + 2\mu\frac{\partial w}{\partial z} - \frac{2}{3}\mu\left(\frac{\partial u}{\partial x} + \frac{\partial v}{\partial y} + \frac{\partial w}{\partial z}\right) \qquad (2.7c)$$

$$\tau_{xy} = \mu\left(\frac{\partial u}{\partial y} + \frac{\partial v}{\partial x}\right) = \tau_{yx} \qquad (2.7d)$$

$$\tau_{yz} = \mu\left(\frac{\partial v}{\partial z} + \frac{\partial w}{\partial y}\right) = \tau_{zy} \qquad (2.7e)$$

$$\tau_{zx} = \mu\left(\frac{\partial w}{\partial x} + \frac{\partial u}{\partial z}\right) = \tau_{xz} \qquad (2.7f)$$

In these equations σ's are normal stresses, composed of non-viscous normal stresses or pressures, p, and viscous normal stresses. τ's are viscous shear stresses. μ is the dynamic viscosity.

Equation (2.6) states that the rate of change of momentum within a differential volume element fixed in space equals the net momentum influx due to fluid motion (first three terms on right), net surface forces (middle three terms on right), and body forces (last term on right).

With the assumptions that the flow is

(a) two-dimensional, then $w = 0, \frac{\partial}{\partial z} = 0, F_z = 0$

(b) steady, then $\frac{\partial}{\partial t} = 0$, and

(c) of constant properties, then $\frac{\partial \rho}{\partial x} = 0, \frac{\partial \rho}{\partial y} = 0, \frac{\partial \mu}{\partial x} = 0, \frac{\partial \mu}{\partial y} = 0$,

Further, if the Boussinesq approximation is applicable, in the coordinate system shown in fig. 2.1, the buoyancy forces caused by the density variation resulting from variations in temperature are

$$F_x = 0, \qquad F_y = -(\rho_T - \rho) g = \rho \beta g (T - T_\infty)$$

where β is the volumetric thermal expansion coefficient, ρ_T and ρ are the densities of the fluid at temperatures T and T_∞ respectively.

Equations (2.6) and (2.7) combined with the continuity equation (eq. 2.4) simplify to:

$$\rho \left(u \frac{\partial u}{\partial x} + v \frac{\partial v}{\partial y} \right) = \frac{\partial \sigma_x}{\partial x} + \frac{\partial \tau_{yx}}{\partial y} \tag{2.8a}$$

$$\rho \left(u \frac{\partial v}{\partial x} + v \frac{\partial v}{\partial y} \right) = \frac{\partial \sigma_y}{\partial y} + \frac{\partial \tau_{xy}}{\partial x} + \rho \beta g (T - T_\infty) \tag{2.8b}$$

and

where

$$\sigma_x = -p + 2\mu \frac{\partial u}{\partial x} \tag{2.9a}$$

$$\sigma_y = -p + 2\mu \frac{\partial v}{\partial y} \tag{2.9b}$$

$$\tau_{xy} = \mu\left(\frac{\partial u}{\partial y} + \frac{\partial v}{\partial x}\right) \tag{2.9c}$$

Substitution of eq. (2.9) into eq. (2.8) gives:

$$u\frac{\partial u}{\partial x} + v\frac{\partial u}{\partial y} = -\frac{1}{\rho}\frac{\partial p}{\partial x} + \nu\left(\frac{\partial^2 u}{\partial x^2} + \frac{\partial^2 u}{\partial y^2}\right) \tag{2.10a}$$

$$u\frac{\partial v}{\partial x} + v\frac{\partial v}{\partial y} = -\frac{1}{\rho}\frac{\partial p}{\partial y} + \nu\left(\frac{\partial^2 v}{\partial x^2} + \frac{\partial^2 v}{\partial y^2}\right) + \beta g(T - T_\infty) \tag{2.10b}$$

where $\nu = \mu/\rho$, is the kinematic viscosity.

Equation (2.10) is called the Navier-Stokes equations for two-dimensional, steady, and constant fluid property flow.

Energy Conservation. If the kinetic and potential energy changes are neglected, the principle of conservation of thermal energy within the control volume shown in fig. 2.2 is expressed by means of the following equation

$$\underbrace{\frac{\partial}{\partial t}(\rho c_p T)}_{\substack{\text{rate of energy increase} \\ \text{within the control volume}}} = \underbrace{\left(\frac{\partial}{\partial x}\left(k_f\frac{\partial T}{\partial x}\right) + \frac{\partial}{\partial y}\left(k_f\frac{\partial T}{\partial y}\right) + \frac{\partial}{\partial z}\left(k_f\frac{\partial T}{\partial z}\right)\right)}_{\substack{\text{net heat transfer by conduction} \\ \text{into the control volume}}}$$

$$+ \left(\underbrace{-\left(\frac{\partial}{\partial x}(\rho c_p u T) + \frac{\partial}{\partial y}(\rho c_p v T) + \frac{\partial}{\partial z}(\rho c_p w T)\right)}_{\substack{\text{net energy associated with fluid motion} \\ \text{transferred into the control volume}}}\right) + \mu\Phi + \dot{q} \tag{2.11}$$

where $\dot{q}$ is a general heat generation term, and Φ is termed the dissipation function

In this study, based on the assumptions mentioned before, i. e.,

(a) the flow is assumed two-dimensional, then $w = 0, \frac{\partial}{\partial z} = 0$

(b) the flow is assumed steady, i.e., $\frac{\partial T}{\partial t} = 0$, and

(c) the properties (k_f, ρ, μ and c_p) are assumed constant.

If dissipation is neglected (i.e., $\Phi = 0$) and there are no heat sources within the fluid ($\dot{q}$=0), then eq. (2.10) may be combined with the continuity equation (eq. 2.4) and reduced to

$$u\frac{\partial T}{\partial x} + v\frac{\partial T}{\partial y} = \frac{k_f}{\rho c_p}\left(\frac{\partial^2 T}{\partial x^2} + \frac{\partial^2 T}{\partial y^2}\right) \tag{2.12}$$

This is the energy equation for two-dimensional, steady, and constant property flow with negligible dissipation and no internal heat generation.

2.2.2 Non-dimensionalization of the Governing Equations

The variables appearing in the governing equations are dimensional variables (defined in terms of mass, length and time). This is a disadvantage if one were to attempt to bring out the similarity between two different physical situations that differ from each other only by a set of scaling factors. Under such situations, if the boundary conditions and the variables appearing in the equations are properly scaled, the two problems will appear identical in terms of the numerical solution required, if the equations were set up to deal with non-dimensional variables. Seen another way, if the equations are expressed in terms of non-dimensional variables, then a specific particular solution obtained for a given set of non-dimensionally expressed boundary conditions can be readily applied to several different physical situations, by dimensionalizing the particular numerical solution with appropriate dimensionalizing parameters.

In order to put the governing equations in dimensionless form, the following set of dimensionless variables are defined:

$$X = x/W, \qquad Y = y/W,$$

$$U = (u/U_{ref}), \qquad V = v/U_{ref} \tag{2.13}$$

$$\theta = (T - T_0)/\Delta T \quad P = (pW)/(\mu U_{ref})$$

where W is the length scale, $U_{ref} = (\alpha Pr Gr^{1/2})/W$, called characteristic velocity and T_0 is the reference temperature.

In terms of these dimensionless variables, the governing equations become:

Continuity Equation:

$$\frac{\partial U}{\partial X} + \frac{\partial V}{\partial Y} = 0 \tag{2.14a}$$

Navier-Stokes Equations:

$$Gr^{1/2}\left(U\frac{\partial U}{\partial X} + V\frac{\partial U}{\partial Y}\right) = -\frac{\partial P}{\partial X} + \frac{\partial^2 U}{\partial X^2} + \frac{\partial^2 U}{\partial Y^2} \tag{2.14b}$$

$$Gr^{1/2}\left(U\frac{\partial V}{\partial X} + V\frac{\partial V}{\partial Y}\right) = -\frac{\partial P}{\partial Y} + \frac{\partial^2 V}{\partial X^2} + \frac{\partial^2 V}{\partial Y^2} + Gr^{1/2}(\theta - \theta_\infty) \tag{2.14c}$$

Energy Equation:

$$Gr^{1/2}Pr\left(U\frac{\partial \theta}{\partial X} + V\frac{\partial \theta}{\partial Y}\right) = \frac{\partial^2 \theta}{\partial X^2} + \frac{\partial^2 \theta}{\partial Y^2} \tag{2.14d}$$

where $Gr = \rho\beta g\Delta T W^3/\nu^2$ is called Grashof number and $Pr = \nu/\alpha$, the Prandtl number.

Equations (2.14), together with the appropriate boundary conditions, define the problem completely.

2.2.3 Governing Equation for Conductive Heat Transfer

Conduction heat transfer through the solid portions of an IGU system

incorporating a blind (e.g., glass panes, blind blade and spacer) is governed by energy equation.

The control volume is shown in fig. 2.3. The surface is denoted as A and the volume as V. An element of the surface, dA, is identified and two vectors are shown on dA: one is the unit normal vector, $\vec{n}$ (with $|\vec{n}|=1$), and the other is the heat flux vector, $\vec{q} = -k_s\vec{\nabla}T$, at that point on the surface (where k_s is the conductivity of the solid material)

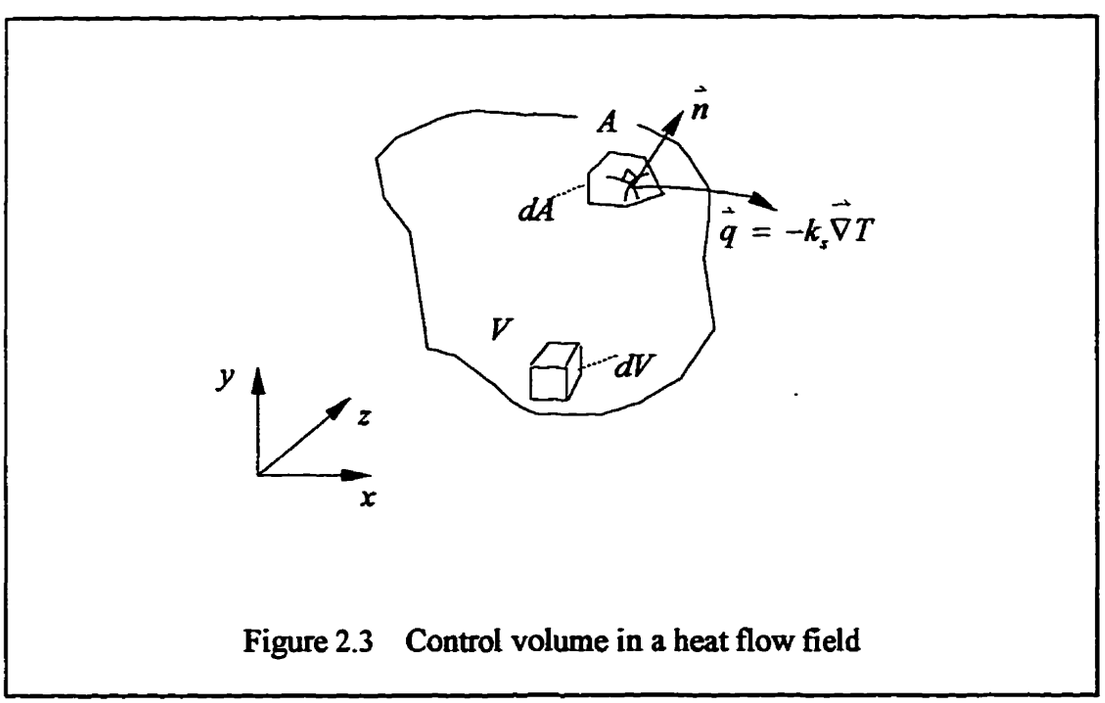

Figure 2.3 Control volume in a heat flow field

Application of the first law of thermodynamics to the above control volume results in the following energy equation:

$$\underbrace{\int_V \left(\rho c_p \frac{\partial T}{\partial t}\right) dV}_{\text{rate of energy increase of the control volume}} = \underbrace{-\int_A (-k_s\vec{\nabla}T)\cdot(\vec{n}dA)}_{\text{rate of heat conducted into the control volume}} + \underbrace{\int_V \dot{q}dV}_{\text{rate of heat generated within the control volume}} \qquad (2.15)$$

The two limitations on eq. (2.15) are:

It applies only to an incompressible medium. (This was implied when no expansion work term was included), and there can be no convection in the fluid i.e., the medium cannot undergo any relative motion.

The first term on the right-hand side can be changed to a volume integral using Gauss's theorem:

$$\int_A k_s \vec{\nabla} T \cdot \vec{n} dA = \int_V (\vec{\nabla} \cdot k_s \vec{\nabla} T) \, dV \tag{2.16}$$

Therefore, eq. (2.15) reduces to

$$\int_V \left(\vec{\nabla} \cdot k_s \vec{\nabla} T - \rho c_p \frac{\partial T}{\partial t} + \dot{q} \right) dV = 0 \tag{2.17}$$

Since the control volume is arbitrary, the terms in parentheses must be zero everywhere, i.e.,

$$\vec{\nabla} \cdot k_s \vec{\nabla} T + \dot{q} = \rho c_p \frac{\partial T}{\partial t} \tag{2.18}$$

Again, with the following assumptions for the problem being considered are:

(a) the problem is two-dimensional, $\frac{\partial}{\partial z} = 0$

(b) the heat flow field is steady, $\frac{\partial T}{\partial t} = 0$

(c) the solid materials are homogenous and isotropic, i.e., $k_s = constant$, and

(d) there are no internal heat sources in the system, i.e., $\dot{q} = 0$.

Therefore eq. (2.18) becomes:

$$\frac{\partial^2 T}{\partial x^2}+\frac{\partial^2 T}{\partial y^2}=0 \tag{2.19}$$

With the same dimensionless quantities defined in eq. (2.13), the non-dimensional form of eq. (2.19) is:

$$\frac{\partial^2 \theta}{\partial X^2}+\frac{\partial^2 \theta}{\partial Y^2}=0 \tag{2.20}$$

2.2.4 Boundary Conditions

In order to solve either the governing eq. (2.14) alone or eqs. (2.14) and (2.20) simultaneously, the velocity and temperature boundary conditions must be prescribed. In the problem under study, the following three kinds of dimensionless thermal and hydrodynamic boundary conditions will apply:

1) specification of the velocity components and temperature (in dimensionless form), i.e.,

$$U = U_\Gamma$$

$$V = V_\Gamma \text{ on } \Gamma, \text{ and} \tag{2.21}$$

$$\theta = \theta_\Gamma$$

2) insulated horizontal surface exists

$$\frac{\partial \theta}{\partial Y}=0 \tag{2.22}$$

3) a convective and radiative boundary exists such that

$$-k'_s\left(\frac{\partial\theta}{\partial X}l_X+\frac{\partial\theta}{\partial Y}l_Y\right) = q'_c+q'_r \tag{2.23}$$

where l_X and l_Y are defined by (see fig. 2.4)

$$l_X = cos\beta, \qquad l_Y = cos\alpha \tag{2.24}$$

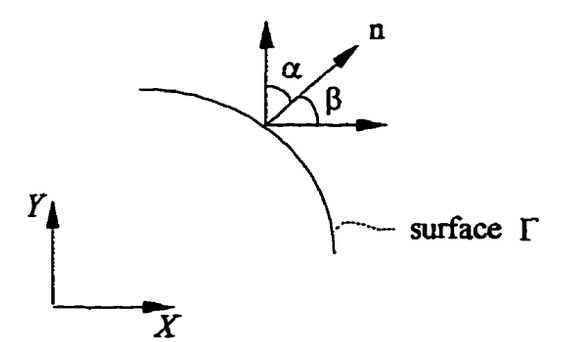

Figure 2.4 The direction of normal vector of a surface

$k'_s = k_s/k_f$ (k_f, k_s — dimensional conductivities of the fluid and solid respectively)

$q'_c = h'_c(\theta-\theta_\infty)$, $q'_r = h'_r(\theta-\theta_\infty)$, and $h' = hW/k_f$

2.2.5 Radiation Heat Transfer

Radiation is one of three modes of heat transfer. A major difference between radiation and either conduction or convection is that radiative heat transfer depends on the fourth power of absolute temperature whereas, for convection or conduction, the transfer of heat depends on a temperature gradient only.

For an conventional double glazed window, under standard winter design conditions, the radiation heat transfer is slightly larger than the natural convective heat transfer on the indoor glass surface ($h_{ir}/h_i \approx 55 \sim 59\%$) and within the glazing cavity($h_{gr}/h_g \approx 61\%$), while it is much lower than the forced convective heat transfer on the outdoor fenestration surface ($h_{or}/h_o \approx 11\%$).

There are two classes of radiation problems in this study. One, radiation from the indoor glass surface to room walls. Two, internal radiation exchange to a window cavity with or without a blind. The simulation of radiation exchange in this work has been carried out with the following assumptions:

1) all the elements are considered diffuse gray surfaces with prescribed emissivities.

2) the radiative exchange with the room walls are considered as if all the room surfaces are blackbodies at indoor air temperature.

3) each surface element is assumed to be isothermal.

The energy equation (eq. (2.20)) determines the temperature distribution in the solid. At the interface of the solid surface and the fluid, the following dimensionless relation exists:

$$-k'_s\left(\frac{\partial\theta}{\partial X}l_X+\frac{\partial\theta}{\partial Y}l_Y\right)_s = -\left(\frac{\partial\theta}{\partial X}l_X+\frac{\partial\theta}{\partial Y}l_Y\right)_f + q'_r \qquad (2.25)$$

where q'_r is the dimensionless radiative heat flux which can be written in terms of a reference heat flux

$$q'_r = q_r/q_{ref} \qquad (2.26)$$

where the reference heat flux can be found from,

$$q_{ref} = k_f \frac{\Delta T}{W}$$

The radiation heat transfer is described using the Net Radiation Method for determining radiation exchange in an enclosure. The dimensionless heat exchange relationship between the *i*'th surface and all other radiating boundaries is given by

$$\sum_{k=1}^{N} \left(\frac{\delta_{ik}}{\varepsilon_k} - F_{ik} \frac{1-\varepsilon_k}{\varepsilon_k} \right) q'^{k}_{r} = \sum_{k=1}^{N} (\delta_{ik} - F_{ik}) S' \left(\theta_k + \frac{T_0}{\Delta T} \right)^4 \qquad (2.27)$$

where δ_i is the Kronecker delta defined as

$$\delta_i = \begin{cases} 1, if \ \ i = k, \\ 0, if \ \ i \neq k, \end{cases}$$

ε_k is the emissivity of the *k*'th surface,

F_{ij} is view factor between surfaces *i* and *j*,

q'^{k}_{r} is the dimensionless radiative heat flux of *k*'th surface, and

S' is the dimensionless Stefan-Boltzman constant defined as

$$S' = \frac{w (\Delta T)^3 S}{k_f}, \qquad (2.28)$$

θ_k is the dimensionless temperature of *k*'th surface.

Thus the coupling between the energy equation (eq. (2.20)), with eq. (2.25), and eq. (2.27) is through the q'_r term. The derivation of eq. (2.27) and the expression of F_i are discussed in detail by Siegel and Howell (1972).

CHAPTER 3

NUMERICAL MODEL

As discussed before, the problem under study involves the combined conduction, convection and radiation heat transfer. Numerical methods are needed to solve this nonlinear problem. Frequently, the radiative heat transfer problem itself is fairly involved and demands a solution of the energy transfer between various neighboring surface and regions at different temperatures. Such problems are very difficult to solve analytically because of the non-linearity and coupling with other modes of energy transfer. As a consequence, the Finite Element Method based on the Galerkin Weighted Residual Method will be employed to solve the coupled conduction, convection and radiation problem. The modelling of the cases considered in this study were implemented though FIDAP, a commercially available finite element analysis package. The basis of the computation procedure used in the paper is described in this chapter.

3.1 AN INTRODUCTION TO THE GALERKIN WEIGHTED RESIDUAL METHOD

The weighted residual methods involve an integral. In these methods, an approximate solution is substituted into the differential equation. Since the approximate

solution does not satisfy the equation, a residual or error term results. Suppose that

$$\tilde{\phi}(x) = \sum_{i=1}^{N_H} N_i(x)\,\Phi_i \qquad i = 1, 2, \ldots, N_H \tag{3.1}$$

is an approximate solution to the following one-dimensional differential equation:

$$D\frac{d^2\phi}{dx^2} + Q = 0 \tag{3.2}$$

with the boundary conditions $\phi(0) = \Phi_1$ and $\phi(H) = \Phi_{N_H}$.

In eq. (3.1) the Φ_i are quantities defined at the node points. The $N_i(x)$ define the spatial form of the solution between node points and are called the shape or interpolation functions. Each term in the summation represents the contribution from a particular node i and contains a $N_i(x)$ and Φ_i defined for that node.

Since the approximate solution (eq. (3.1)) does not satisfy eq. (3.2), a residual or error term results:

$$D\frac{d^2\tilde{\phi}}{dx^2} + Q = D\left(\sum_{i=1}^{N_H}\frac{d^2N_i}{dx^2}\Phi_i\right) + Q = R(x) \neq 0 \tag{3.3}$$

The weighted residual methods require that

$$\int_0^H W_i(x)\,R(x)\,dx = 0 \qquad i = 1, 2, \ldots, N_H \tag{3.4}$$

The residual $R(x)$ is multiplied by a weighting function $W_i(x)$, and the integral of the product is required to be zero. There are several choices for the weighting functions

which lead to different numerical methods ($W_i(x) = \delta(x - X_i)$ for **Collocation Method**, $W_i(x) = 1$ for **Subdomain Method**, and $W_i(x) = R(x)$ for **Least Squares Method**). The most frequent choice for the weighting function is the interpolation function itself, that is, the $N_i(x)$ in eq. (3.1). This choice is known as **Galerkin's Method**. Eq. (3.4) then yields the global equations

$$\int_0^H N_i \left(D\frac{d^2\tilde{\phi}}{dx^2} + Q \right) dx = 0 \qquad i = 1, 2, \ldots, N_H \tag{3.5}$$

where the integration is over the entire solution domain.

3.2 THE FINITE ELEMENT METHOD

The finite element method is a numerical procedure for obtaining solutions to many of the problems encountered in engineering analysis. It has two characteristics that distinguish it from other numerical procedures:

— the method utilizes an integral formulation to generate a system of algebraic equations. (Finite difference methods approximate the derivatives in the governing differential equation using difference equations.)

— the method uses continuous piecewise smooth functions for approximating the unknown quantities. (Finite difference methods generally provide point-wise approximations.)

The finite element method can be subdivided into following five basic steps:

1) Divide the continuum region of interest into a number of simple shaped regions called elements. This includes locating and numbering the node points, as well as specifying their coordinates values.

2) Select interpolation or shape functions for the elements. The interpolation functions represent the assumed form of the spatial solution in the elements and are related to the elements.

3) Develop the system of algebraic equations. When using Galerkin's method, the weighting function for each unknown nodal value is defined and the weighted residual integral is evaluated. This generates one equation for each unknown nodal value.

4) Solve the system of equations.

5) Calculate quantities of interest. These quantities are usually related to derivative of the parameter and include stress components, heat flux and fluid velocities.

3.3 ELEMENT

Nine node quadratic and iso-parametric elements are used in this work. The shape functions are expressed in terms of the natural coordinates for the element, r and s, which vary from -1 to +1 as shown in fig. (3.1).

For this element, the velocity components and temperatures are approximated using the same biquadratic interpolation functions (shape function) given by,

$$\varphi = \vartheta \begin{bmatrix} (1/4)rs(1-r)(1-s) \\ -(1/4)rs(1+r)(1-s) \\ (1/4)rs(1+r)(1+s) \\ -(1/4)rs(1-r)(1+s) \\ -(1/2)s(1-r)(1-s) \\ (1/2)r(1+r)(1-s^2) \\ (1/2)s(1+s)(1-r^2) \\ -(1/2)r(1-r)(1-s^2) \\ (1-r^2)(1-s^2) \end{bmatrix} \tag{3.6}$$

The discontinuous pressure approximation employed in this work is a linear function. The three pressure degrees of freedom are not actual pressure values but are the coefficients of the linear polynomial approximating the pressure on the element. By default, the basis functions are based on the normalized coordinates *r* and *s*.

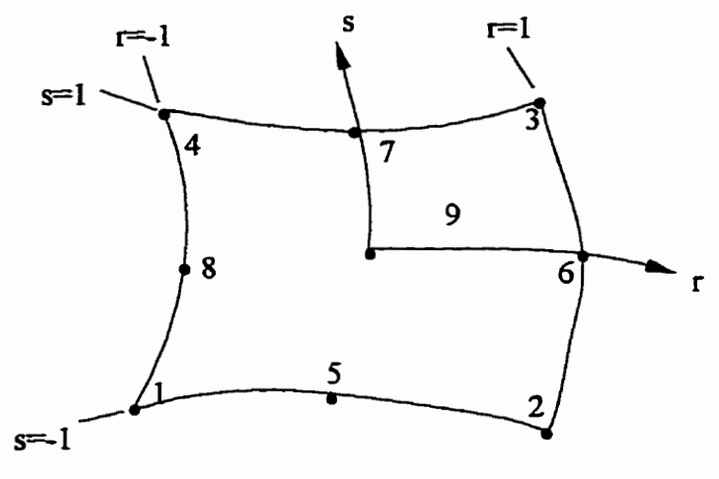

Figure 3.1 Nine node quadratic element

The coordinate transformation between the dimensionless physical coordinates *X*, *Y* and the natural coordinates *r*, *s* for an element is defined by

$$X = \varphi^T \boldsymbol{X} \ , \qquad Y = \varphi^T \boldsymbol{Y} \tag{3.7}$$

where φ is defined by eq. (3.6) and $\boldsymbol{X}$, $\boldsymbol{Y}$ are vectors of the nodal coordinates of the element.

In order to be able to evaluate the element matrices which will be defined in the

following section, it is necessary to convert the derivatives and integrals in physical coordinates to those in natural (normalized) coordinates.

$$\begin{bmatrix} \frac{\partial \varphi}{\partial r} \\ \frac{\partial \varphi}{\partial s} \end{bmatrix} = \begin{bmatrix} \frac{\partial X}{\partial r} & \frac{\partial Y}{\partial r} \\ \frac{\partial X}{\partial s} & \frac{\partial Y}{\partial s} \end{bmatrix} \begin{bmatrix} \frac{\partial \varphi}{\partial X} \\ \frac{\partial \varphi}{\partial Y} \end{bmatrix} = \begin{bmatrix} \frac{\partial \varphi^T}{\partial r} X & \frac{\partial \varphi^T}{\partial r} Y \\ \frac{\partial \varphi^T}{\partial s} X & \frac{\partial \varphi^T}{\partial s} Y \end{bmatrix} \begin{bmatrix} \frac{\partial \varphi}{\partial X} \\ \frac{\partial \varphi}{\partial Y} \end{bmatrix} \quad J \begin{bmatrix} \frac{\partial \varphi}{\partial X} \\ \frac{\partial \varphi}{\partial Y} \end{bmatrix} \tag{3.8}$$

Hence, the derivatives in physical coordinates can be expressed as:

$$\begin{bmatrix} \frac{\partial \varphi}{\partial X} \\ \frac{\partial \varphi}{\partial Y} \end{bmatrix} = J^{-1} \begin{bmatrix} \frac{\partial \varphi}{\partial r} \\ \frac{\partial \varphi}{\partial s} \end{bmatrix} \tag{3.9}$$

where J is called the Jacobian matrix.

In the case of integral evaluation, to complete the transformation from physical coordinates to normalized coordinates, the expression for an elemental area is required. Thus,

$$dXdY = |J| drds, \quad |J| = \text{determinant of } J \tag{3.10}$$

3.4 NUMERICAL APPROXIMATION OF THE GOVERNING EQUATIONS

Natural Convection of the Fluid

Within each element, the two-dimensional velocity, pressure and temperature fields (in non-dimensional form) are approximated by,

$$\tilde{U} = \varphi^T U \text{ and } \tilde{V} = \varphi^T V \tag{3.11a}$$

$$\tilde{P} = \psi^T \boldsymbol{P} \tag{3.11b}$$

$$\tilde{\theta} = \vartheta^T \Theta \tag{3.11c}$$

where $\boldsymbol{U}$, $\boldsymbol{V}$, $\boldsymbol{P}$, and Θ are column vectors of element nodal point unknowns and φ, ψ, and ϑ are column vectors of the interpolation functions. In this study the same basis functions are employed for the velocity and temperature, i.e., $\varphi = \vartheta$. Substitution of these approximations into the non-dimensional governing eq. (2.14) yields a set of equations:

$$\frac{\partial \varphi^T}{\partial X}\boldsymbol{U} + \frac{\partial \varphi^T}{\partial Y}\boldsymbol{V} = R_1 \tag{3.12a}$$

$$Gr^{1/2}\left(\tilde{U}\frac{\partial \varphi^T}{\partial X} + \tilde{V}\frac{\partial \varphi^T}{\partial Y}\right)\boldsymbol{U} + \frac{\partial \psi^T}{\partial X}\boldsymbol{P} - \left(\frac{\partial^2 \varphi^T}{\partial X^2} + \frac{\partial^2 \varphi^T}{\partial Y^2}\right)\boldsymbol{U} = R_2 \tag{3.12b}$$

$$Gr^{1/2}\left(\tilde{U}\frac{\partial \varphi^T}{\partial X} + \tilde{V}\frac{\partial \varphi^T}{\partial Y}\right)\boldsymbol{V} + \frac{\partial \psi^T}{\partial Y}\boldsymbol{P} - \left(\frac{\partial^2 \varphi^T}{\partial X^2} + \frac{\partial^2 \varphi^T}{\partial Y^2}\right)\boldsymbol{V} - Gr^{1/2}(\vartheta^T\Theta - \theta_\infty) = R_3 \tag{3.12c}$$

$$Gr^{1/2}Pr\left(\tilde{U}\frac{\partial \vartheta^T}{\partial X} + \tilde{V}\frac{\partial \vartheta^T}{\partial Y}\right)\Theta - \left(\frac{\partial^2 \vartheta^T}{\partial X^2} + \frac{\partial^2 \vartheta^T}{\partial Y^2}\right)\Theta = R_4 \tag{3.12d}$$

where R_1, R_2, R_3, and R_4 are the residuals (errors) resulting from the use of the approximations of eq. (3.12).

The Galerkin form of the Method of Weighted Residuals seeks to reduce these errors to zero, in a weighted sense, by making the residuals orthogonal to the interpolation functions of each element (i.e., φ, ψ, and ϑ). These orthogonality conditions are expressed by

$$\int_{A_e} (R_1 \cdot \psi)\, dA_e = 0 \tag{3.13a}$$

$$\int_{A_e} (R_2 \cdot \varphi)\, dA_e = 0 \tag{3.13b}$$

$$\int_{A_e} (R_3 \cdot \varphi)\, dA_e = 0 \tag{3.13c}$$

$$\int_{A_e} (R_4 \cdot \vartheta)\, dA_e = 0 \tag{3.13d}$$

where A_e is the area of the element.

Substitution of eq. (3.12) into eq. (3.13) gives:

Continuity Equation

$$\left(\int_{A_e} \psi \frac{\partial \varphi^T}{\partial X} dA_e\right) U + \left(\int_{A_e} \psi \frac{\partial \varphi^T}{\partial Y} dA_e\right) V = 0 \tag{3.14a}$$

X-Momentum

$$\int_{A_e} Gr^{1/2} \varphi \left(\tilde{U} \frac{\partial \varphi^T}{\partial X} + \tilde{V} \frac{\partial \varphi^T}{\partial Y}\right) U dA_e$$

$$+ \int_{A_e} \varphi \frac{\partial \psi^T}{\partial X} P dA_e - \int_{A_e} \varphi \left(\tilde{U} \frac{\partial^2 \varphi^T}{\partial X^2} + \tilde{V} \frac{\partial^2 \varphi^T}{\partial y^2}\right) U dA_e = 0 \tag{3.14b}$$

Y-Momentum

$$\int_{A_e} Gr^{1/2} \varphi \left(\tilde{U} \frac{\partial \varphi^T}{\partial X} + \tilde{V} \frac{\partial \varphi^T}{\partial Y}\right) V dA_e + \int_{A_e} \varphi \frac{\partial \psi^T}{\partial Y} P dA_e - \int_{A_e} \varphi \left(\tilde{U} \frac{\partial^2 \varphi^T}{\partial X^2} + \tilde{V} \frac{\partial^2 \varphi^T}{\partial y^2}\right) V dA_e$$

$$- \left(\int_{A_e} Gr^{1/2} \varphi \vartheta^T dA_e\right) \Theta - \int_{A_e} Gr^{1/2} \varphi \theta_\infty dA_e = 0 \tag{3.14c}$$

Energy Equation

$$\left(\int_{A_e} Gr^{1/2} Pr \vartheta \left(\tilde{U} \frac{\partial \vartheta^T}{\partial X} + \tilde{V} \frac{\partial \vartheta^T}{\partial Y}\right) dA_e\right) \Theta - \left(\int_{A_e} \vartheta \left(\frac{\partial^2 \vartheta^T}{\partial X^2} + \frac{\partial^2 \vartheta^T}{\partial Y^2}\right) dA_e\right) \Theta = 0 \tag{3.14d}$$

The second-order diffusion terms in the momentum and energy equations and the pressure terms can be reduced to first-order terms plus a line integral by using the Green-Gauss theorem expressed as follows:

$$\int_A f\frac{\partial g}{\partial x_i}dA = -\int_A \frac{\partial f}{\partial x_i}g dA + \oint_\Gamma f g l_{x_i} d\Gamma \tag{3.15}$$

where f and g are functions of x and y and l_{x_i} is defined by eq. (2.24).

Hence, eq. (3.14) can be rearranged as follows:

Continuity Equation

$$\left(\int_{A_e} \psi \frac{\partial \varphi^T}{\partial X} dA_e\right) U + \left(\int_{A_e} \psi \frac{\partial \varphi^T}{\partial Y} dA_e\right) V = 0 \tag{3.16a}$$

X-Momentum

$$\left(\int_{A_e} Gr^{1/2} \varphi \left(\tilde{U}\frac{\partial \varphi^T}{\partial X} + \tilde{V}\frac{\partial \varphi^T}{\partial Y}\right) dA_e\right) U - \left(\int_{A_e} \frac{\partial \varphi}{\partial X}\psi^T dA_e\right) P$$

$$+ \left(2\int_{A_e} \frac{\partial \varphi}{\partial X}\frac{\partial \varphi^T}{\partial X} dA_e + \int_{A_e} \frac{\partial \varphi}{\partial Y}\frac{\partial \varphi^T}{\partial Y} dA_e\right) U + \left(\int_{A_e} \frac{\partial \varphi}{\partial Y}\frac{\partial \varphi^T}{\partial X} dA_e\right) V$$

$$= \oint_\Gamma \varphi \left(\sigma'_X l_X + \tau'_{XY} l_Y\right) d\Gamma \tag{3.16b}$$

Y-Momentum

$$\left(\int_{A_e} Gr^{1/2} \varphi \left(\tilde{U}\frac{\partial \varphi^T}{\partial X} + \tilde{V}\frac{\partial \varphi^T}{\partial Y}\right) dA_e\right) V - \left(\int_{A_e} \psi^T \frac{\partial \varphi}{\partial Y} dA_e\right) P + \left(\int_{A_e} \frac{\partial \varphi}{\partial X}\frac{\partial \varphi^T}{\partial Y} dA_e\right) U$$

$$+ \left(\int_{A_e} \frac{\partial \varphi}{\partial X}\frac{\partial \varphi^T}{\partial X} dA_e + 2\int_{A_e} \frac{\partial \varphi}{\partial Y}\frac{\partial \varphi^T}{\partial Y} dA_e\right) V - \left(\int_{A_e} Gr^{1/2} \varphi \vartheta^T dA_e\right) \Theta$$

$$= \oint_\Gamma \varphi \left(\sigma'_Y l_Y + \tau'_{YX} l_X\right) d\Gamma + \int_{A_e} Gr^{1/2} \varphi \theta_\infty dA_e \tag{3.16c}$$

Energy Equation

$$\left(\int_{A_e} Gr^{1/2} Pr \vartheta \left(\tilde{U}\frac{\partial \vartheta^T}{\partial X} + \tilde{V}\frac{\partial \vartheta^T}{\partial Y}\right) dA_e\right) \Theta + \left(\int_A \left(\frac{\partial \vartheta}{\partial X}\frac{\partial \vartheta^T}{\partial X} + \frac{\partial \vartheta}{\partial Y}\frac{\partial \vartheta^T}{\partial Y}\right) dA_e\right) \Theta$$

$$= -\oint_{\Gamma} (q'_c + q'_r)\, \vartheta\, d\Gamma \tag{3.16d}$$

where q'_c, q'_r, σ'_i, and τ'_i $(i,j = 1,2)$ are dimensionless quantities and

$$(q'_c + q'_r) = -k'_f\left(\frac{\partial\theta}{\partial X} l_X + \frac{\partial\theta}{\partial Y} l_Y\right) \qquad (k'_f = 1)$$

$$\sigma'_i = \frac{\sigma_i}{(\mu U_{ref}/w)} = -\tilde{P} + 2\frac{\partial \tilde{U}_i}{\partial X_i}$$

$$\tau'_{XY} = \frac{\tau_{xy}}{(\mu U_{ref}/w)} = \frac{\partial \tilde{U}}{\partial Y} + \frac{\partial \tilde{V}}{\partial X} = \tau'_{YX}$$

Once the form of the interpolation functions φ, ψ, and ϑ is specified, the integrals defined in eq. (3.16) may be evaluated to produce the required coefficient matrices.

Equation (3.16) can be written in a matrix form:

$$\begin{bmatrix} 2K_{11}+K_{22} & K_{12} & 0 & -C_1 \\ K_{21} & K_{11}+2K_{22} & B & -C_2 \\ 0 & 0 & L_{11}+L_{22} & 0 \\ -C_1^T & -C_2^T & 0 & 0 \end{bmatrix} \begin{bmatrix} U \\ V \\ \Theta \\ P \end{bmatrix}$$

$$+ \begin{bmatrix} A_1(U)+A_2(V) & 0 & 0 & 0 \\ 0 & A_1(U)+A_2(V) & 0 & 0 \\ 0 & 0 & D_1(U)+D_2(V) & 0 \\ 0 & 0 & 0 & 0 \end{bmatrix} \begin{bmatrix} U \\ V \\ \Theta \\ P \end{bmatrix} = \begin{bmatrix} F_1 \\ F_2 \\ G \\ 0 \end{bmatrix} \tag{3.17}$$

The coefficient matrices shown in eq. (3.17) are defined by,

$$K_{ij} = \int_{A_e} \frac{\partial\varphi}{\partial X_j} \frac{\partial\varphi^T}{\partial X_i} dA_e \tag{3.18a}$$

$$C_i = \int_{A_e} \frac{\partial\varphi}{\partial X_i} \psi^T dA_e \tag{3.18b}$$

$$C_i^T = \int_{A_e} \frac{\partial \varphi^T}{\partial X_i} \psi dA_e \tag{3.18c}$$

$$L_{ij} = \int_{A_e} \frac{\partial \vartheta \, \partial \vartheta^T}{\partial X_i \partial X_j} dA_e \tag{3.18d}$$

$$A_i(U_j) = \int_{A_e} Gr^{1/2} \varphi \tilde{U}_j \frac{\partial \varphi^T}{\partial X_i} dA_e \tag{3.18e}$$

$$D_i(U_j) = \int_{A_e} Gr^{1/2} Pr \varphi \tilde{U}_j \frac{\partial \vartheta^T}{\partial X_i} dA_e \tag{3.18f}$$

$$B = \int_{A_e} Gr \varphi \vartheta^T dA_e \tag{3.18g}$$

$$F_1 = \oint_\Gamma \varphi \, (\sigma'_X l_X + \tau'_{XY} l_Y) \, d\Gamma \tag{3.18h}$$

$$F_2 = \oint_\Gamma \varphi \, (\sigma'_Y l_Y + \tau'_{YX} l_X) \, d\Gamma + \int_{A_e} Gr^{1/2} \varphi \theta_\infty dA_e \tag{3.18i}$$

$$G = -\oint_\Gamma (q'_c + q'_r) \, \vartheta d\Gamma \tag{3.18j}$$

where $i = 1, 2$; $j = 1, 2$, and the subscripts 1 and 2 denote the X and Y components respectively.

When a penalty formulation is used, the row and column corresponding to the pressure unknowns **P** are deleted in the matrices of eq. (3.17) (see Appendix A).

Conduction in the solid portion

The same approximate function $\tilde{\theta} = \vartheta^T \Theta$ is considered to replace the unknown function θ in the energy eq. (2.20). Applying the Galerkin weighted residual method to each element in the solid portion yields the following equation:

$$\left(\int_{A_e} \vartheta \left(\frac{\partial^2 \vartheta^T}{\partial X^2} + \frac{\partial^2 \vartheta^T}{\partial Y^2} \right) dA_e \right) \Theta = 0 \tag{3.19}$$

Again, the Green-Gauss theorem (eq. 3.15) is used to reduce the second-order terms to first-order terms plus a line integral. Equation (3.20) can be expressed as:

$$-\left(\int_{A_e}\left(\frac{\partial \vartheta}{\partial X}\frac{\partial \vartheta^T}{\partial X}+\frac{\partial \vartheta}{\partial Y}\frac{\partial \vartheta^T}{\partial Y}\right)dA_e\right)\Theta+\left(\oint_\Gamma \vartheta\left(\frac{\partial \vartheta^T}{\partial X}l_X+\frac{\partial \vartheta^T}{\partial Y}l_Y\right)d\Gamma\right)\Theta=0 \qquad (3.20)$$

Substitution of eq. (2.23) into above equation gives:

$$\left(\int_{A_e}k'_s\left(\frac{\partial \vartheta}{\partial X}\frac{\partial \vartheta^T}{\partial X}+\frac{\partial \vartheta}{\partial Y}\frac{\partial \vartheta^T}{\partial Y}\right)dA_e\right)\Theta=-\left(\oint_S \vartheta\,(q'_c+q'_r)\,dS\right) \qquad (3.21)$$

The above derivation has focused on a single finite element. The discrete representation of the entire continuum region of interest is obtained through an assemblage of elements such that inter-element continuity of velocity and temperature is enforced. This continuity requirement is met through the appropriate summation of equations for nodes common to adjacent elements - the direct stiffness approach. The result of such an assembly process is a system of matrix equations of the form given by eq. (3.17)

Boundary Conditions

As mentioned before, there are three kinds of dimensionless thermal and hydrodynamic boundary conditions used in this study. The finite element implementation of these boundary conditions will be discussed separately.

Specification of velocity components and temperature. The specification of particular constant values for velocity components and temperatures at a boundary node results in the field equation for that particular degree of freedom being deleted and the specified value being imposed for that degree of freedom in the other equations.

Insulated horizontal surface. On the insulated horizontal boundary, zero heat flux will apply. This yields a zero line integral for the coefficient matrix G:

$$G = \left(\oint_\Gamma \vartheta k' \frac{\partial \vartheta^T}{\partial Y} l_y d\Gamma\right)\Theta = -\oint_\Gamma \vartheta \,(q'_c + q'_r)\, d\Gamma = 0 \tag{3.22}$$

Convective and radiative boundary. The combined convective and radiative heat transfer boundary condition

$$q'_c + q'_r = (h'_c + h'_r)\,(\theta - \theta_\infty) \tag{3.23}$$

is different from boundary conditions discussed above. It contributes both to the element stiffness matrix and to the element forcing vector. This is due to the presence of the dependent variable θ in the boundary condition.

Substitution of eq. (3.23) into eq. (3.18i) gives

$$G = \left(-\oint_\Gamma (h'_c + h'_r)\,\vartheta^T \vartheta d\Gamma\right)\Theta + \oint_\Gamma (h'_c + h'_r)\,\theta_\infty \vartheta d\Gamma \tag{3.24}$$

The first integral contributes the matrix,

$$H = \oint_\Gamma (h'_c + h'_r)\,\vartheta^T \vartheta d\Gamma \tag{3.25}$$

to the global element stiffness matrix.

The radiation exchange in an enclosure, given by eq. (2.27), is already a discrete equation which can be written

$$\boldsymbol{Eq} = \boldsymbol{I}\left(\Theta + \frac{T_0}{\Delta T}\right) \tag{3.26}$$

where

$$\boldsymbol{E} = (E_{ij});\ E_{ij} = \frac{\delta_{ij}}{\varepsilon_j} - F_{ij}\frac{1-\varepsilon_j}{\varepsilon_j} \quad \text{(no summation on } j\text{)}$$

$$\boldsymbol{I} = (I_{ij});\ I_{ij} = (\delta_{ij} - F_{ij})\, S\left(\theta_j + \frac{T_0}{\Delta T}\right)^3 \quad \text{(no summation on } j\text{)}$$

$\boldsymbol{q}$ is a column vector of radiative heat flux which is coupled with the main system of eqs. (3.17) and (3.20) through the boundary radiation flux term in eq. (2.25).

In order to reduce the size of the $\boldsymbol{E}$ and $\boldsymbol{I}$ matrices and the number of view factors, a simplified approach is employed in this work which is to "lump" together elements on the boundary and consider this group of element sides as a "macro surface" for radiation exchange. Equation (3.26) is solved first (for a given temperature field) and then the resultant heat flux values are used as applied boundary conditions.

3.5 SOLUTION PROCEDURE

In this work, two different iteration methods (Picard iteration and Broyden's update) have been utilized for solving the nonlinear and coupled equation systems described above.

Picard iteration procedure is a particularly simple scheme which may be written as:

$$\boldsymbol{K}(\boldsymbol{u}_i)\,\boldsymbol{u}_{i+1} = \boldsymbol{F} \tag{3.27}$$

where $\boldsymbol{K}$ is the global system matrix, $\boldsymbol{u}$ is the global vector of unknowns (velocities,

pressures, and temperatures) and $\boldsymbol{F}$ is a vector which includes the effects of body forces and boundary conditions.

The nonlinearity is evaluated at the known $\boldsymbol{u}_i$ taken from the previous iteration, and a non-symmetric linear system must be formed and solved at each iteration.

The rate of convergence of the basic iterative procedure of eq. (3.27) can often be improved by the use of an acceleration or scaling factor α as detailed below, i.e.

$$\boldsymbol{K}(\boldsymbol{u}_i)\,\boldsymbol{u}^* = \boldsymbol{F}$$

$$\boldsymbol{u}_{i+1} = \alpha \boldsymbol{u}_i + (1-\alpha)\,\boldsymbol{u}^* \quad ; \quad 0 \le \alpha \le 1 \tag{3.28}$$

Broyden's update is one of the Quasi-Newton update formulas which can be written as

$$\boldsymbol{u}_{i+1} = \boldsymbol{u}_i - s_i \boldsymbol{A}_i^{-1} \boldsymbol{R}_i \tag{3.29}$$

$$\boldsymbol{A}_{i+1} = \boldsymbol{A}_i + \Delta \boldsymbol{A}_i \tag{3.30}$$

where $\boldsymbol{A}_i$ is an $n \times n$ matrix and s_i is a scaling (or acceleration) factor ($0 \le s_i$ 1). $\boldsymbol{R}_i$ (=$\boldsymbol{R}(\boldsymbol{u}_i)$) is the residual defined by

$$\boldsymbol{R}(\boldsymbol{u}_i) = \boldsymbol{K}(\boldsymbol{u}_i)\,\boldsymbol{u}_i - \boldsymbol{F} \tag{3.31}$$

It is required that the $\boldsymbol{A}_i$ satisfy the "quasi-Newton equation"

$$\boldsymbol{A}_i(\boldsymbol{u}_i - \boldsymbol{u}_{i-1}) = \boldsymbol{R}_i - \boldsymbol{R}_{i-1} \tag{3.32}$$

This equation simply requires that A_i is a first order approximation to the Jacobian matrix $J(u_i)$ $(=\partial R_i/\partial u)$, $A_i = J(u_i) + O(\Delta u_i)$; hence the name quasi-Newton.

The aim of quasi-Newton updates is to update the A_i^{-1} (in eq. (3.29)) in a computationally efficient and simple manner rather than recompute it entirely (Newton-Raphson Method) or leave it unchanged (Modified Newton-Raphson).

The rank one update of Broyden in inverse form is

$$\Delta A_i^{-1} = \frac{(\delta_{i+1} - A_i^{-1}\gamma_{i+1})\,\delta_{i+1}^T}{\delta_{i+1}^T A_i^{-1}\gamma_{i+1}} A_i^{-1} \tag{3.33}$$

where $\delta_i = u_i - u_{i-1}$ and $\gamma_i = R_i - R_{i-1}$. The derivation of above equation can be found in FDI (1990).

In the cases corresponding to problems with heat transfer involving natural convection only, the solution procedure proposed is a combination of Picard iteration and Broyden's update. Two iterations of Picard iteration method which has a larger radius of convergence but slower convergence rate are followed by m (varying from 2 to 100 depending on the Grashof number imposed) iterations of Broyden's update method which has a faster convergence rate.

In the situations involving radiation exchange, only the robust Picard iteration scheme is used.

3.6 CONVERGENCE CRITERIA

The convergence criterion used in FIDAP is a combination of the termination criteria based on solution vector u_i (at iteration i) and the residual vector $R(u_i$ respectively. It is desired that the solution vector at the end of each iteration be within a

certain tolerance, ε_u, of the true solution vector $\boldsymbol{u}$. Hence, the termination criterion for solution vector, based on relative error, is

$$\frac{\|\boldsymbol{u}_i - \boldsymbol{u}\|}{\|\boldsymbol{u}\|} \leq \varepsilon_u \tag{3.34}$$

where $\|\bullet\|$ is an appropriate norm. $\|\boldsymbol{u}\|$ and $\boldsymbol{u}$ are approximated by $\|\boldsymbol{u}_i\|$ and $\boldsymbol{u}_{i-1}$ respectively.

The other suitable convergence criterion based on the residual vector which must tend to zero as $\boldsymbol{u}_i$ tends to $\boldsymbol{u}$ requires that

$$\frac{\|\boldsymbol{R}(\boldsymbol{u}_i)\|}{\|\boldsymbol{R}_0\|} \leq \varepsilon_F \tag{3.35}$$

where $\boldsymbol{R}_0 = \boldsymbol{R}(\boldsymbol{u}_0)$, a reference vector.

It is found that the combination of these two checks provides an effective overall convergence criterion for all possible situations, since both $\Delta \boldsymbol{u}_i$ and $\boldsymbol{R}(\boldsymbol{u}_i)$ tend to zero near the true solution.

CHAPTER 4

2-D CONVECTIVE HEAT TRANSFER FROM AN ISOTHERMAL VERTICAL FLAT PLATE ADJACENT TO A VENETIAN BLIND

4.1 INTRODUCTION

In this chapter, the flow over and convective heat transfer rate from an isothermal vertical flat plate adjacent to a venetian blind has been studied. This investigation was undertaken to determine the effects of blade-to-plate spacing, d, and blade angle, θ, on the flow pattern and convective heat transfer coefficients. Results are presented for values of d=15, 20, 25, 30, and 40 *mm*, and at each of these spacings, blade angle was varied, i.e., θ=0°, 45°, -45°, 80°. To increase confidence in the computer results, both local heat flux and flow distribution for d=15 *mm* were compared to the experimental results measured by Machin (1997).

As an additional verification of the modelling, a commonly studied base-case was also investigated, i.e., the simulation of laminar natural convection on an isothermal, vertical flat plate has been performed first.

4.2 FLOW OVER AN ISOLATED, VERTICAL, ISOTHERMAL FLAT PLATE

As discussed in chapter 1, natural convection on a vertical flat plate has been

extensively studied either theoretically or experimentally. The heat transfer coefficient for natural convection between room air and an indoor glass surface can usually be obtained from the average Nusselt number for natural convection over an isothermal, vertical flat plate. Results produced by the current model were compared with the well-accepted results from the work of Ostrach (1952), Le Fevre (1956), Ede (1967), Churchill and Chu (1975), and the experimental results of Machin (1997).

4.2.1 Geometry and Boundary Conditions

The case considered is shown in fig. 4.1. The inflow and outflow regions, C_o, is assumed to be 1 inch long, and it is introduced into the model to avoid any inaccuracy resulting from the boundary conditions on the horizontal surfaces. The natural convective flow over a heated vertical flat plate is governed by the dimensionless equation (2.14). The fluid is assumed to be of infinite extent and devoid of any motion or temperature variations other than those associated with the free convection. The system of coordinates is also displayed in fig. 4.1. T represents the dimensional temperature of the fluid, and was assumed to equal to $43°C$ at the wall and $21°C$ in the bulk fluid to duplicate the conditions used in the experiments of Machin. The quantities in parentheses denote the dimensionless terms defined by equation (2.13) (in which W=0.0762 m (3 $in.$), T_0=T_r=21°C, and $\Delta T = T_w - T_r = 22\,°C$).

Fluid properties evaluated at the mean film temperature of $305K$ were taken from Lienhard (1981) and were shown in table 4.1. The resulting dimensionless Grashof number based on L was obtained: $Gr_L = g\beta\Delta TL^3/\nu^2 = 1.508 \times 10^8$

Table 4.1 Fluid properties evaluated at T=305K

c_p (J/kg-K)	ρ (kg/m^3)	β (1/K)	ν (m^2/s)	μ (kg/m-s)	k_f (W/m-K)
1003.5	1.1656	0.0033	1.6156×10^{-5}	1.876×10^{-5}	0.0265

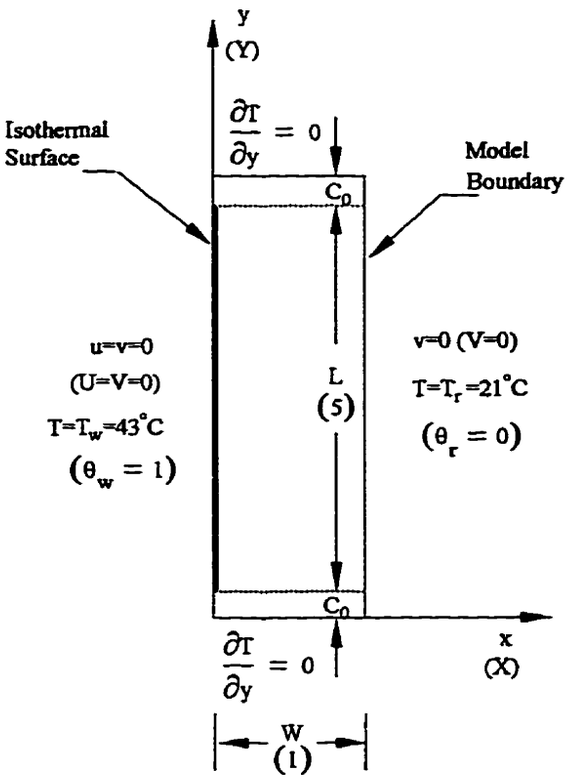

Figure 4.1 Geometry and boundary conditions for laminar natural convection on a flat plate

4.2.2 Mesh Development

The mesh density required is dependent upon the thermal loading of the problem, as represented by the Grashof number. The mesh density near the isothermal wall must be able to resolve both the thermal and velocity boundary layers developing on the wall, which requires that at least one node be located within the boundary layers.

For this problem, an estimate of the non-dimensional thickness δ of the boundary layers is given by Gill (1966) as,

$$\delta = (A/PrGr)^{0.25} = 0.04914 \qquad (4.1)$$

where $A = L/W = 5$, the aspect ratio

In formulating the computer model, it was decided to vary the spacing in the x-direction. Specifically, the mesh spacing in the region near the wall was reduced. In addition, the spacing was varied in the y-direction to improve the modelling of the inflow and outflow regions. The final mesh grid was produced by the FIDAP mesh generation module FIMESH (1990). The generated mesh is shown in fig. 4.2 which shows that there are three full elements (X_1=0.0115108, X_2=0.0122595, X_3=0.0130569, and X_4=0.0139061) contained within the velocity and temperature boundary layers as estimated by equation (4.1). It is reasonable to expect, therefore, good resolution with this mesh for the flow under consideration.

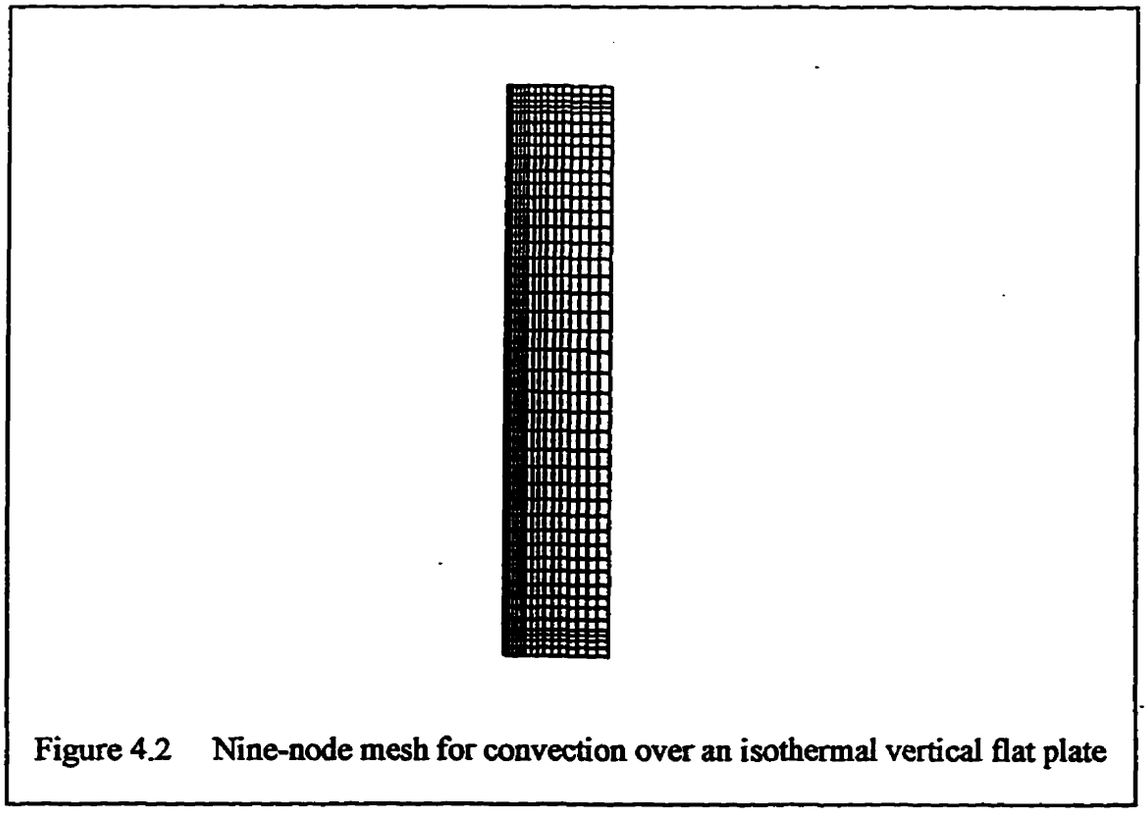

Figure 4.2 Nine-node mesh for convection over an isothermal vertical flat plate

4.2.3 Comparisons of Results

Simulation results produced for the above case are shown in figs. 4.3 through 4.5 and table 4.2. These results are presented in terms of: isotherms, streamline plots; velocity vector field; temperature and vertical velocity distributions at half height of the plate; local and average heat transfer coefficients.

The temperature and velocity fields are best illustrated by the use of velocity vectors and temperature contour plots. The isothermal, streamline plots and velocity vectors are shown in fig. 4.3. The isotherms and velocity vectors given in (a) and (c) of fig. 4.3 show the development and growth of the thermal and velocity boundary layer, respectively.

The vertical velocity profile and temperature distribution from this work are compared with those of Ostrach (1952) at half height of the plate in fig. 4.4.

It can be seen from fig. 4.4 that the curves representing this numerical results follow the exact solutions of Ostrach (1952) very closely. The velocity and temperature profiles (both from this work and Ostrach 1952) display the same trend that velocity changes from zero through a maximum to zero again, whereas temperature varies monotonically from maximum wall temperature to the room temperature and at about X=0.3 (x=2.3 *cm*) and X=0.25 (x=1.9 *cm*) the vertical velocity and the temperature gradient approach zero, respectively (i.e. $v \to 0$ and $\partial T/\partial x \to 0$). The predicated local heat transfer coefficient, h_y, was calculated from dimensionless heat fluxes, q'_y, using the following equation:

$$h_y = \frac{k_f}{W} q'_y \qquad (4.2)$$

and is shown in fig. 4.5. The calculated local heat transfer coefficient, h_y, shows excellent

agreement between this work and the work of Ostrach (1952) and Le Fevre (1956), as well as the experimental work of Machin (1997).

The average heat transfer coefficient, $\bar{h}_l$, for the surface of some distance, l, is also of interest, and can be used to form a average Nusselt number $\overline{Nu}_l = \bar{h}_l l / k_f$. Comparisons of the average values determined over a distance of 265 *mm* from the leading edge (i.e., the Nusselt number $\overline{Nu}_{265}$ and the convection coefficient $\bar{h}_{265}$) are summarized in table 4.2. These also show excellent agreement between this work and the work of Ostrach (1952), Le Fevre (1956), Ede (1967), Churchill and Chu (1975) and the experimental work of Machin (1997). These results indicate that the basic finite element model developed in this study is technically sound.

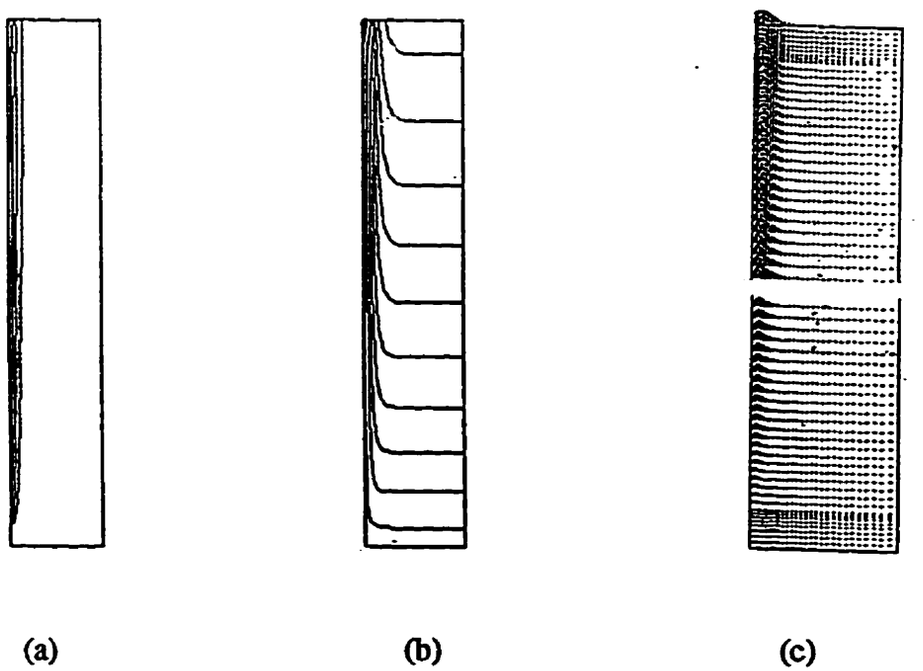

Figure 4.3 (a) Temperature, (b) Streamline contours and (c) Velocity vector field

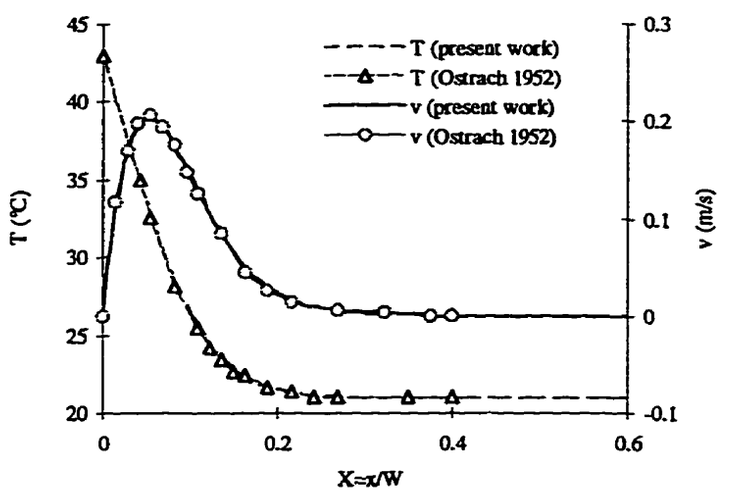

Figure 4.4 Comparison of temperature and vertical velocity distributions at Y=L/2

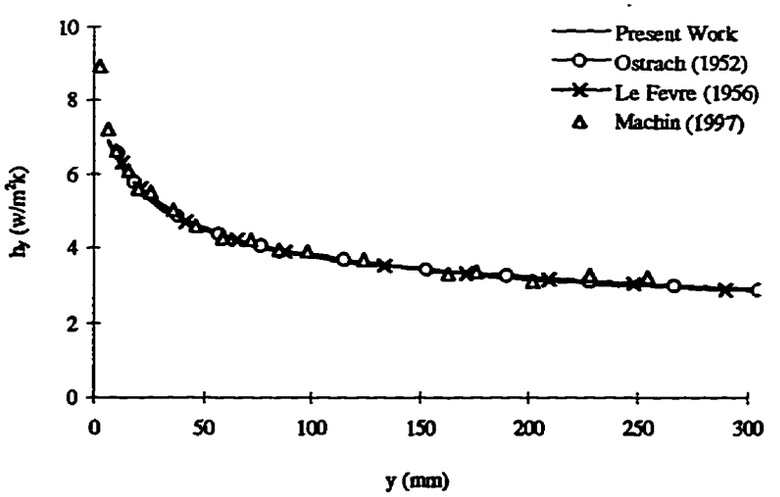

Figure 4.5 Comparison of local heat transfer coefficient for natural convection over a flat plate

Table 4.2 Comparison of average Nusselt number $\overline{Nu}_{265}$ and heat transfer coefficient h_{265}

Method	$\overline{Nu}_{265}$	$\bar{h}_{265}$ (W/m^2.K)
Analytical Work of Ostrach (1952)	39.932	3.993
Empirical Correlation of Le Fevre (1956)	39.943	3.994
Correlation of Ede (1967)	40.026	4.003
Experimental Correlation of Churchill and Chu (1975)	40.366	4.037
Experimental Measurement of Machin (1996)	39.137	3.935
Present work	40.007	4.001

Note: $Ra_l = Prg\beta\Delta Tl^3/\nu^2$

$Ra_{265} = 3.10 \times 10^7$ used by Machin (1997)

$Ra_{265} = 3.606 \times 10^7$ for present work

4.3 FLOW OVER AN ISOTHERMAL VERTICAL FLAT PLATE ADJACENT TO A VENETIAN BLIND

4.3.1 Geometry and Boundary Conditions

Based on the validated model, a model was developed to investigate the effect of shade louvers on the free convection from an isothermal vertical surface, a major focus of the study was on the determination of the influence of blade-to-plate spacing, d, and blade angle, θ, on the flow pattern and convective heat transfer coefficients. Fig. 4.6 illustrates the computational domain. Because the louvers were assumed to be made of some material with very low conductivities (such as plastic), they were treated as zero-thickness baffles. An equal value of louver width and pitch was used. On all the solid surfaces,

including the louver surfaces, a no slip velocity boundary conditions was applied. The heat flux on both sides of the louver was assumed to be equal. The same thermal boundary conditions as used for the isolated plate case (see section 4.2) were used, resulting in the same Grashof number: $Gr_L = g\beta\Delta TL^3/\nu^2 = 1.508 \times 10^8$.

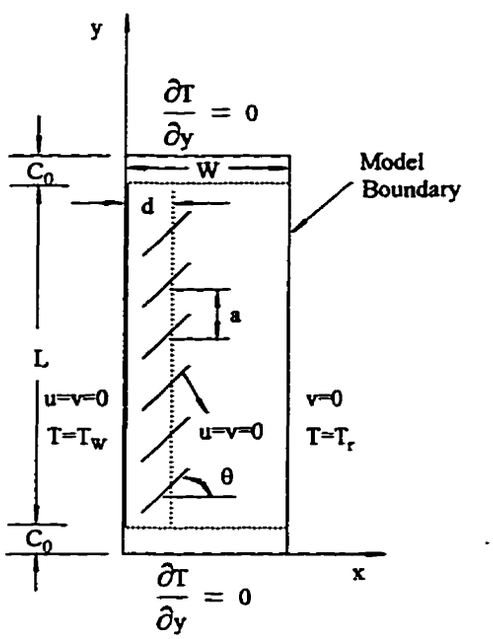

Figure 4.6 Computational domain for laminar flow over an isothermal surface adjacent to a Venetian blind

(L=15 in. W=3 in. a=1 in. C_0=1 in. T_W=43°C T_r=21°C)

4.3.2 Results and Discussions

In this section it will be shown how the two parameters, the plate-to-blade spacing, d, and the blade angle, θ, influence the convective flow in the computational domain by comparing the isotherms; the streamlines; the velocity vectors; the distributions of local heat transfer coefficient h_y; and integrated (average) Nusselt number $\overline{Nu}_t$ and heat transfer coefficient $\overline{h}_t$.

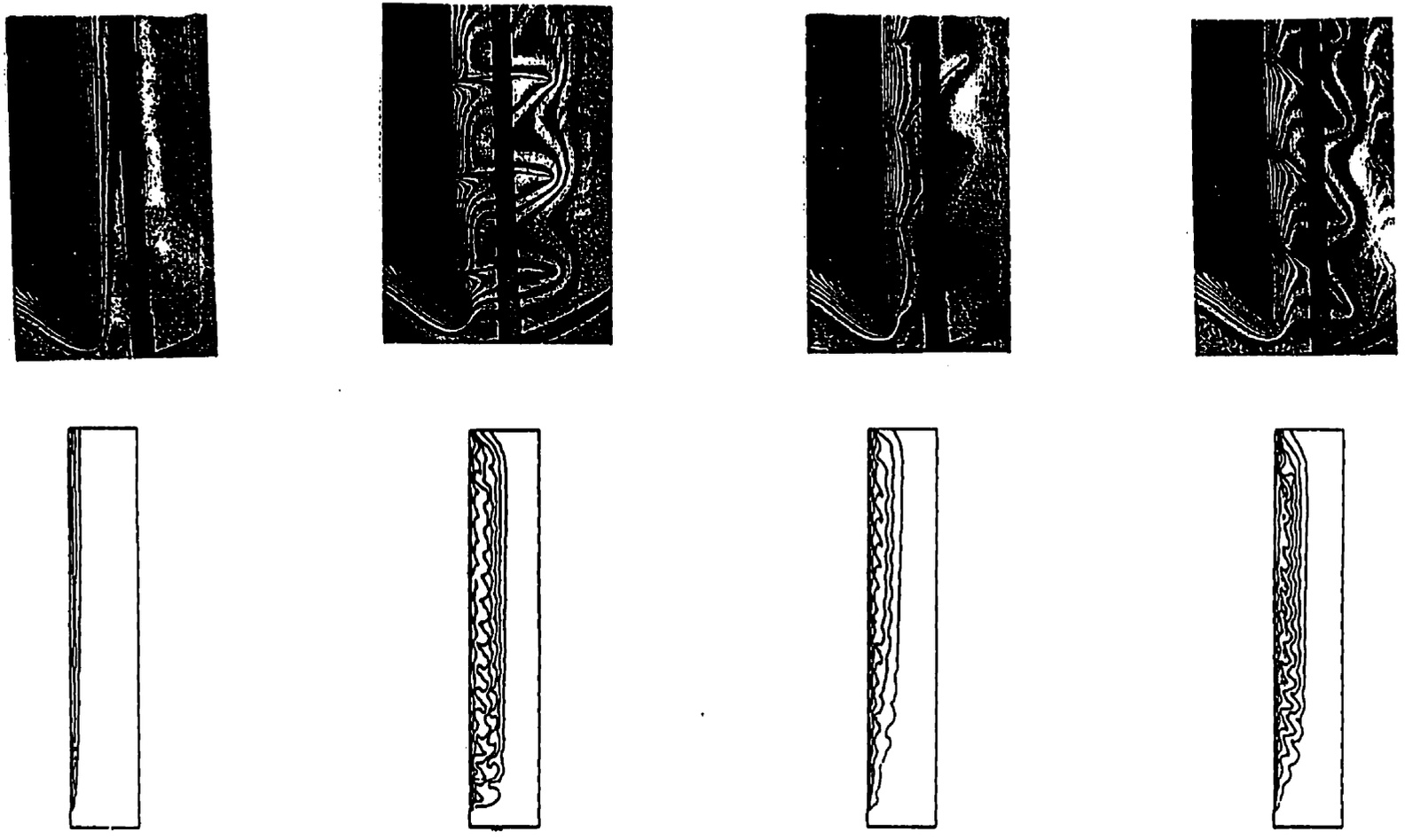

(a) No blind (b) $\theta = 0^{\circ}$ (c) $\theta = 45^{\circ}$ (d) $\theta = -45^{\circ}$

Figure 4.7 Comparison of isotherms for various θ

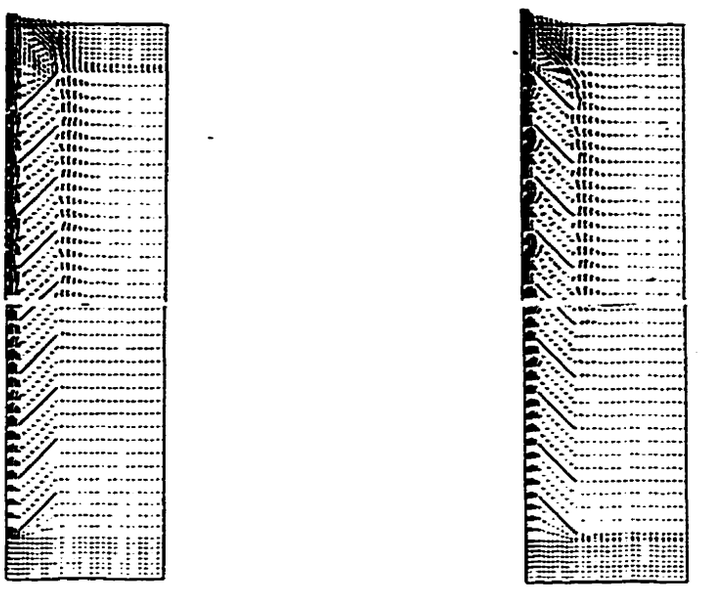

(a) $\theta = 45^{\circ}$ (b) $\theta = -45^{\circ}$

Figure 4.8 Velocity vectors for θ=-45° and θ=+45° at d=15 mm, (as produced from the current simulation)

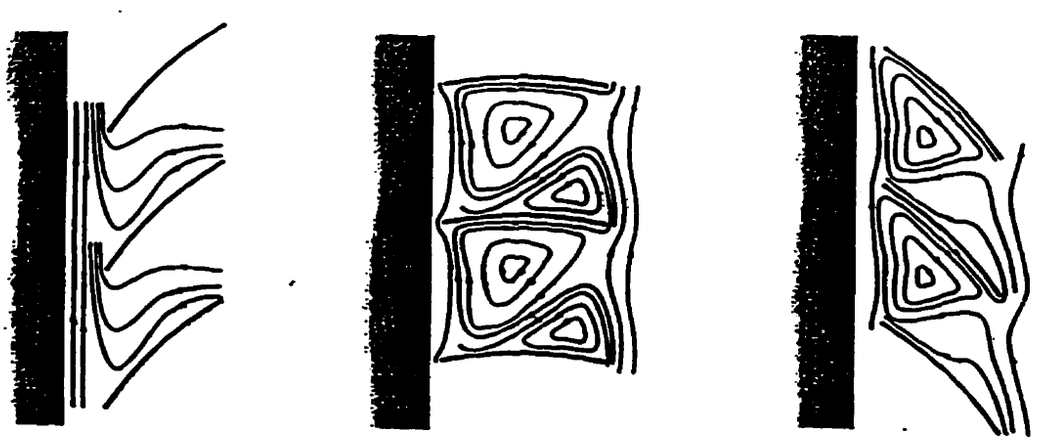

(a) $\theta = 45^{\circ}$ (b) $\theta = 0^{\circ}$ (c) $\theta = -45^{\circ}$

Figure 4.9 Flow visualization results from experimental work of Machin (1997)

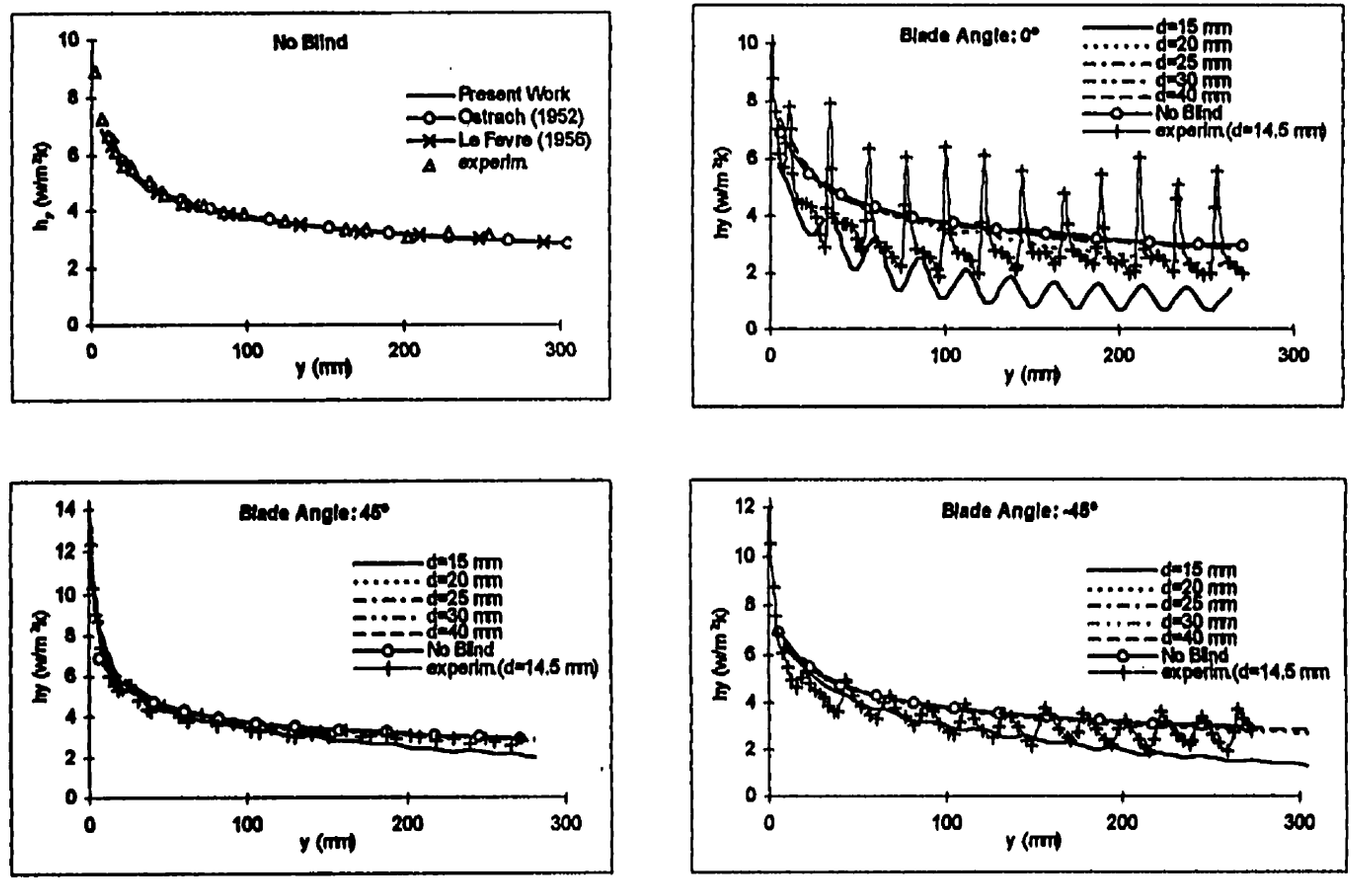

Figure 4.10 Comparison of local heat transfer coefficients

The effects of the blade angle on the flow are shown in fig. 4.7. Predicted isotherms for the case, d=15 *mm*, are compared with experimentally obtained interferometer photographs (d=14.5 *mm*) from Machin's (1997) work for various θ. Both the numerical simulation and the experimental results indicate that when the blind is in the open position (at θ=0°), the flow is seen to be mostly disturbed. The disturbance decreases as the blind closes. It is also worth noting that the orientation also affects the flow. For example, the effect for θ=-45° is stronger than that for θ=+45°. This can be explained from the flow shown in fig. 4.8 (from the numerical simulation) and fig. 4.9 (from experiment). The flow velocity near the wall is higher at θ=-45° than that at θ=45° because the flow resistance is lower for the former case (θ=-45°) than that for the latter case (θ=45°). As a result of the higher velocity, strong vortices are formed between blades near the upper wall at θ=-45°(figs. 4.8 and 4.9). These vortices essentially prevent the cooler fluid outside the blades from flowing into the main stream near the heated wall, this resulting in a lower temperature gradient near the wall and therefore the lower local heat transfer rate (fig. 4.10).

Attention is now given to the effect of plate-to-blade spacing, d, on the flow. In fig. 4.11 and fig. 4.12, the effects of plate-to-blade spacing d on the isotherms and streamline contours for a constant value of θ=0° are illustrated. It can be seen that plate-to-blade spacing, d, has very strong effect on the flow pattern at a small value of d, but when the blind is located far enough away from the surface, there is almost no effect observed. A closer inspection of fig. 4.12 shows that the flow changes from three flow regions to one with an increasing value of d from 15 to 40 *mm*. For example, at d=20 *mm*, there is a strong inner flow between the surface and the louver-tips, in addition to vortices in the region between the louvers, and a weaker flow stream outside the blind. As previously discussed, it is these vortices, formed in the region between the louvers, that decreases the local convective heat transfer and creates a periodic variation in local heat transfer coefficient, h, with a spatial frequency equal to the blade pitch (fig. 4.10).

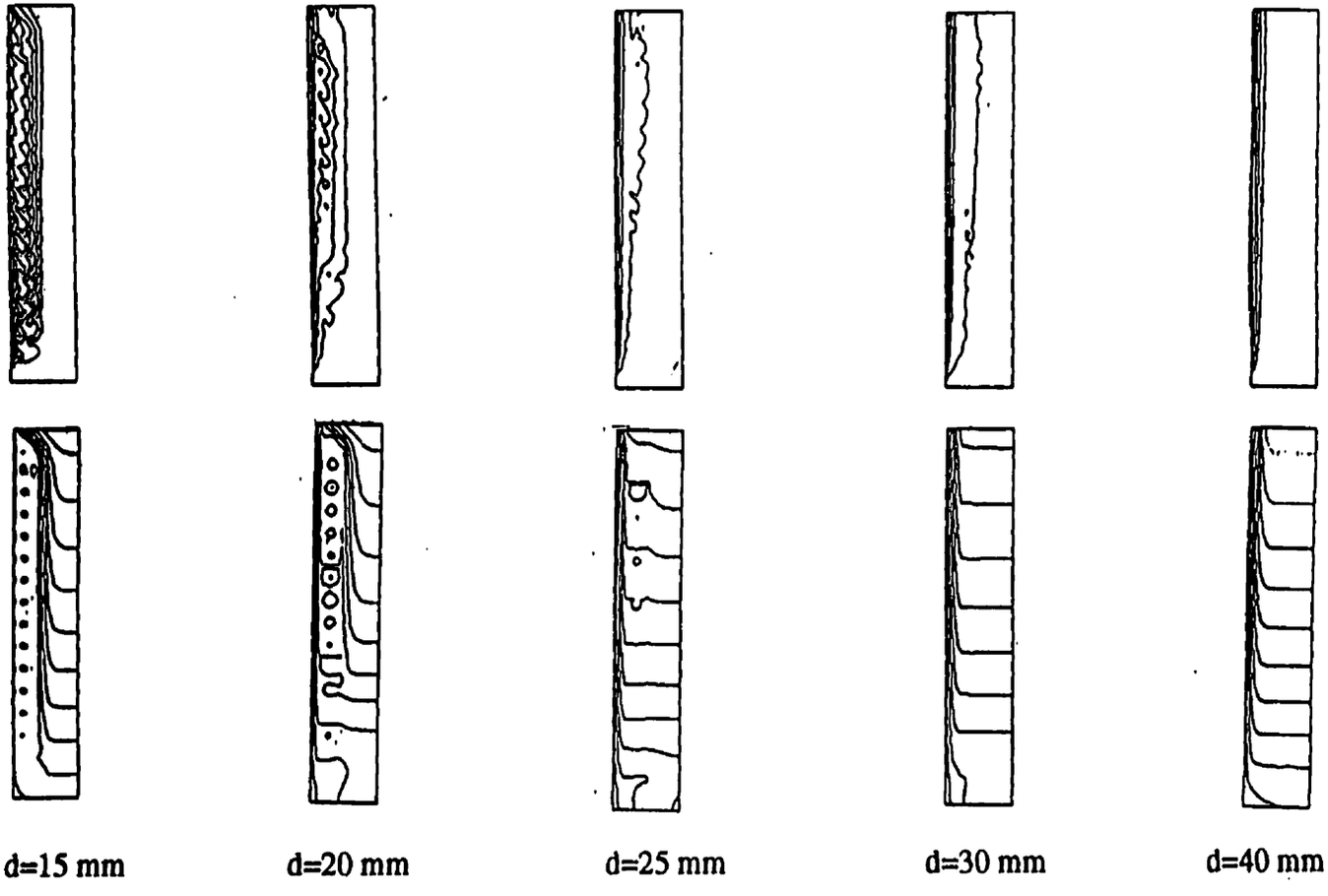

Figure 4.11 Isotherms and streamline contours for various d (θ=0°)

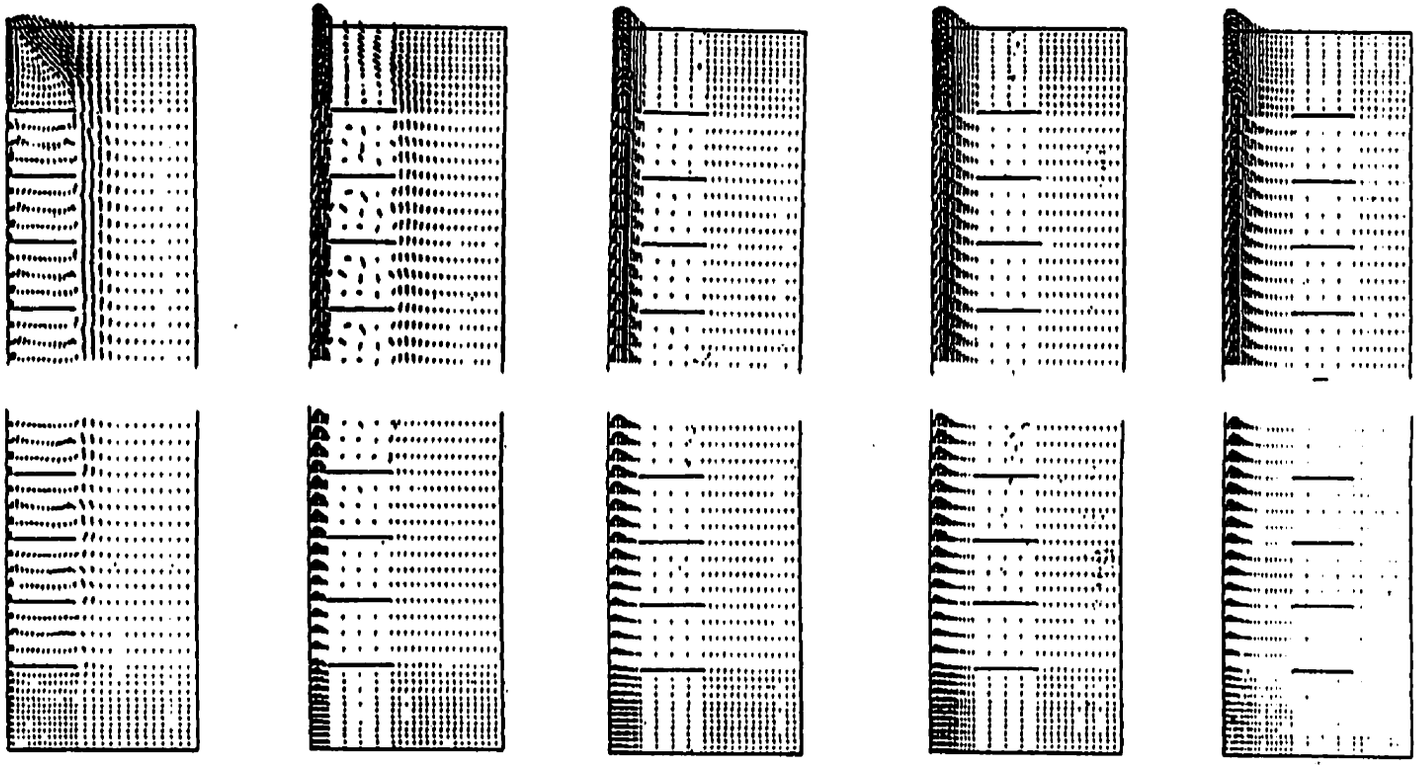

Figure 4.12 Velocity vectors for different d (θ=0°)

These three distinct flow regions disappear as d is increased. The closer the blind is located to the surface, the weaker the inner flow is and the stronger the effect of the cellular flow. This results in a further decrease in local heat transfer rate (see fig. 4.10). It may be observed that, only one main flow stream exists for the larger value of d (e.g., d=40 *mm*). The isotherm and streamline contours for d=40 *mm* presented in fig. 4.12 are similar to the case with no blind (fig. 4.3). The decreasingly effect of blind for a large value of d is seen to be applicable for all blade angles (shown in fig. 4.10).

Finally, the effects of d and θ on average Nusselt number $\overline{Nu}_t$ and heat transfer coefficient $\overline{h}_t$ are summarized in table 4.3 and fig. 4.13. It can be seen from table 4.3 that both experimental results (d=14.5 *mm*) and numerical results (d=15 *mm*) show the same trend for the effect of blade angle θ. In every case (except for θ=80° or 90°, for the cases of θ=80° or 90°, the predicted and measured values are a little higher than those of no blind case), the average values are lower than those of an isolated plate with lowest values for θ=0°. The results shown in fig. 4.13 indicate that the closer the blind is located to the plate, the stronger the effect of the louvers will be; in the case of θ=0° this effect is the most pronounced. As the blind is moved far enough away from the surface, the effects of the blind are minimal and the average heat transfer coefficients approach that of the isolated flat plate without blind, regardless of blade angles.

It should be pointed out that the average heat transfer coefficients from the experimental work are consistently higher than the corresponding values of this work. This is probably due to the different boundary conditions on the louver surfaces between the experiment work and the present numerical work. In the experiment, commercially available aluminum blinds were used, which have high conductivity (120 W/m · K.), resulting in a higher local heat transfer rate at the location of the blades (experimental results shown in fig. 4.10). Therefore, the temperature on each louver in the experiment was efficiently constant (see fig. 4.7), while in the numerical study, temperature varies along each louver.

Table 4.3 The summary of average Nusselt number and heat transfer coefficient

Method	d (mm)	Blade Angle θ							
		0°		45°		-45°		80°	
		$\overline{Nu}_{265}$	h_{265}	$\overline{Nu}_{265}$	h_{265}	$\overline{Nu}_{265}$	h_{265}	$\overline{Nu}_{265}$	h_{265}
present work	40	39.913	3.991	40.077	4.008	39.982	3.998		
	30	39.559	3.956	39.957	3.996	39.841	3.984		
	25	39.203	3.920	39.667	3.967	39.685	3.969		
	20	36.102	3.610	38.230	3.823	38.928	3.893	40.085	4.009
	15	20.084	2.008	34.302	3.430	30.408	3.041	40.331	4.033
experimental results	14.5	33.398	3.360	36.864	3.710	33.878	3.41	42.073 (θ=-90°)	4.230 (θ=-90°)

Note:

without blind: $\overline{Nu}_{265}$ =40.007, $\bar{h}_{265}$ =4.001 (W/m^2-K)

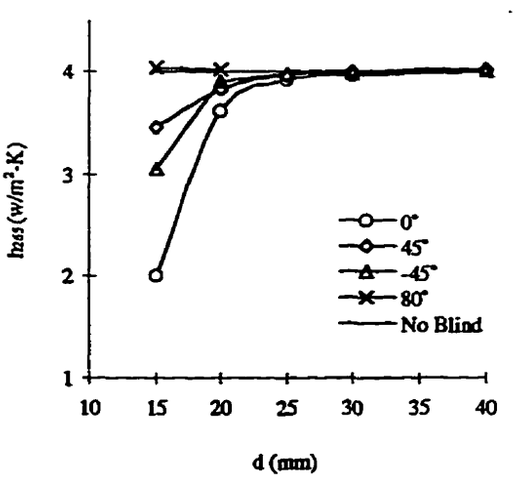

Figure 4.13 Average heat transfer coefficients $\bar{h}_{265}$

CHAPTER 5

COMBINED HEAT TRANSFER THROUGH IGU SYSTEMS WITH INTERNAL VENETIAN BLINDS

5.1 INTRODUCTION

In this chapter, the combined convection, conduction, and radiation heat transfer through IGU systems with between-the-panes venetian blinds have been studied. The combined heat transfer on an indoor pane surface was investigated first to obtain the indoor combined heat transfer coefficient, h_i. This was subsequently used as an indoor pane boundary condition for the evaluation of the 2-D combined heat transfer through the IGU systems studied.

To provided a benchmark verification of the model, the simulation of laminar natural convection in an IGU cavity was also performed. Finally, the combined heat transfer through IGU systems for five different blind blade angles (0°, 45°, -45°, 75°, and -75°) was investigated.

5.2 COMBINED HEAT TRANSFER ON AN INDOOR GLASS SURFACE

The choice of appropriate indoor thermal resistance has been the topic of a long-standing debate. The convective and radiative modes are often combined to form the

indoor heat transfer coefficient, $h_i=h_{ic}+h_{ir}$, which is usually called "film coefficient". Typical values of h_i used in well-known window evaluation computer programs, (i.e., *WINDOW3.1* developed in the U.S., *VISION* developed in Canada, and *ISOWIN04* developed by the International Standards Organization (ISO)) are tabulated in table 5.2 for winter or nighttime U-values. Comparisons of vertical velocity profiles and temperature distributions at three characteristic locations along the flat plate between this work and some published work show excellent agreement. Comparisons of the flat plate local heat transfer coefficient and integrated heat transfer coefficient also show excellent agreement.

5.2.1 Geometry and Boundary Conditions

Fig. 5.1 shows the geometry and boundary conditions assumed for the case of a natural convection flow on an indoor surface of a glass pane. This case is governed by the dimensionless equation (2.14). The thickness of the glass pane, $t_g = 3$ *mm*, was considered in order to be able to model the effect of radiation heat transfer. The convective and radiative boundary conditions on the indoor surface are given in eq. (2.23), in which the non-dimensional conductivity of glass $k'_s = k_s/k_f$ (k_s=0.88 $W/m \cdot K$) and the non-dimensional radiative heat flux q'_r can be expressed as

$$q'_r = S'\varepsilon_g(\theta^4 - \theta_{ref}^4) \tag{5.1}$$

where S' — the non-dimensional Stefan-Boltzmann constant defined by equation (2.28).

ε_g — emissivity of glass surface which is equal to 0.84.

θ_{ref} — the non-dimensional reference temperature (in this problem $\theta_{ref} = \theta_r = 1.0$).

The system of coordinates is also displayed in fig. 5.1. T represents the

dimensional temperature of the fluid, and set to T_w=279.8K (6.8°C) at the isothermal surface (calculated based on Curcija's result (Curcija 1992) in which he assumed the temperature of the indoor surface to be 7.2°C) and T_r=294K (21°C) in the bulk fluid. The quantities in parentheses denote the dimensionless variables defined by eq. (2.13) (in which W=0.05 m, T_0=0K, and $\Delta T = T_r = 294K$).

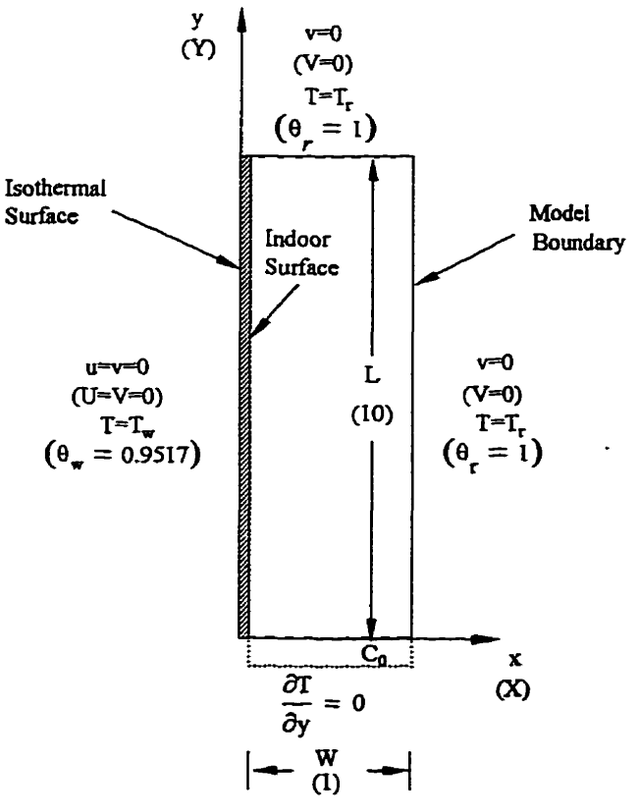

Figure 5.1 Geometry and boundary conditions for indoor pane glass surface

Table 5.1 Fluid properties evaluated at T=294K

c_p (J/kg-K)	ρ (kg/m^3)	β (1/K)	ν (m^2/s)	μ (kg/m-s)	k_f (W/m-K)
1003	1.2126	0.0034	1.5128×10^{-5}	1.8234×10^{-5}	0.02567

Fluid properties evaluated at the room temperature of $294K$ were taken from Lienhard (1981) and shown in table 5.1. The resulting dimensionless Grashof number based on L was obtained: $Gr_L = g\beta (T_r - T_w) L^3/\nu^2 = 2.584 \times 10^8$

5.2.2 Mesh Development

As discussed in chapter 4, the mesh density required is dependent upon the thermal loading of the problem.

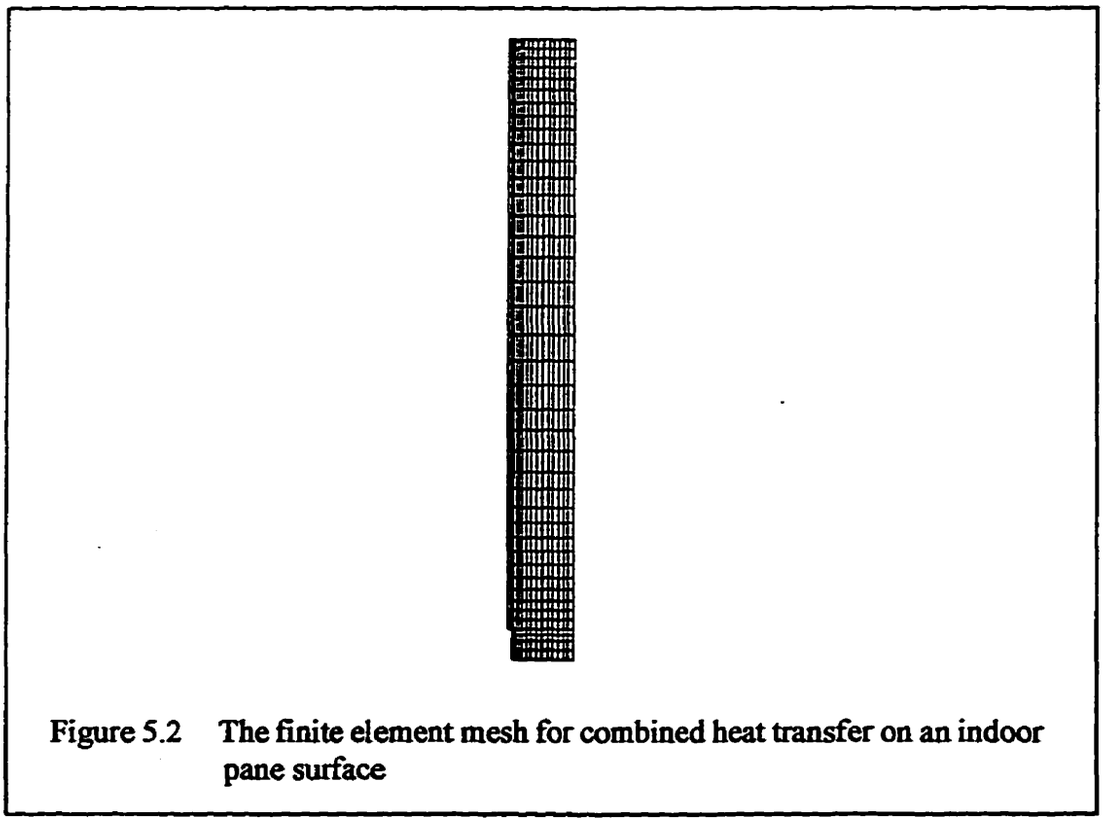

Figure 5.2 The finite element mesh for combined heat transfer on an indoor pane surface

The finite element mesh generated with the FIDAP mesh generation module FIMESH (1990) for this problem employed gradual (nonuniform) meshing in order to provide the finest mesh near the surface (in the boundary layer region). The size of the elements next to the surface were again determined with respect to the constraint that at least one node must lie within the boundary layer. Using eq. (4.1), the non-dimensional thickness of the boundary layer was estimated to be $\delta \approx 0.08539$ (in which,

$Gr_W = g\beta (T_w - T_r) W^3/\nu^2 = 2.5843\times10^5$). The generated mesh is tabulated in fig. 5.2 and shows that there are two full elements (X_1=0.03385, X_2=0.03961, and X_3=0.04634) contained within the velocity and temperature boundary layers as estimated by eq. (4.1).

5.2.3 Comparisons of Results

In order to examine the effect of radiation on the flow pattern, simulations were performed for two cases. In the first case, no radiation effects was included, the no radiation case (referred to as "NRD") and in the second case, radiation was included, (referred to as the "RD" case).

Results, expressed in form of isotherms and streamlines, are shown in fig. 5.3. These results indicate similar patterns. Velocities, however, are slightly lower in RD case than those in NRD case. The reason for this is that the temperature on the inner surface is seen to increase slightly due to the thermal radiation from the room air, resulting in a smaller temperature difference between the room air and the inner surface, producing a lower Rayleigh number. As a result, the flow is slightly slower in the RD case than in the NRD case.

Attention is now given to the temperature and velocity distributions at three typical locations. Fig. 5.4 through fig. 5.6 show the comparisons of the velocity profiles between this work and that of Ostrach (1952) and Curcija (1992) and the temperature distributions between this work and that of Ostrach (1952) at $Y=L/4$, $Y=L/2$, and $Y=3L/4$ respectively. A detailed view of the local temperature distribution around the glazing surface is also shown as an inset in each figure. It may be noted that the radiation does not affect the flow pattern and it only slightly increases the temperature on the indoor surface. The temperature gradients near the glass surface for both RD and NRD cases are almost the same (see the zoomed temperature distributions for the three locations shown in figs. 5.4 through 5.6). This indicates that the convective heat transfer is not affected by the

radiation.

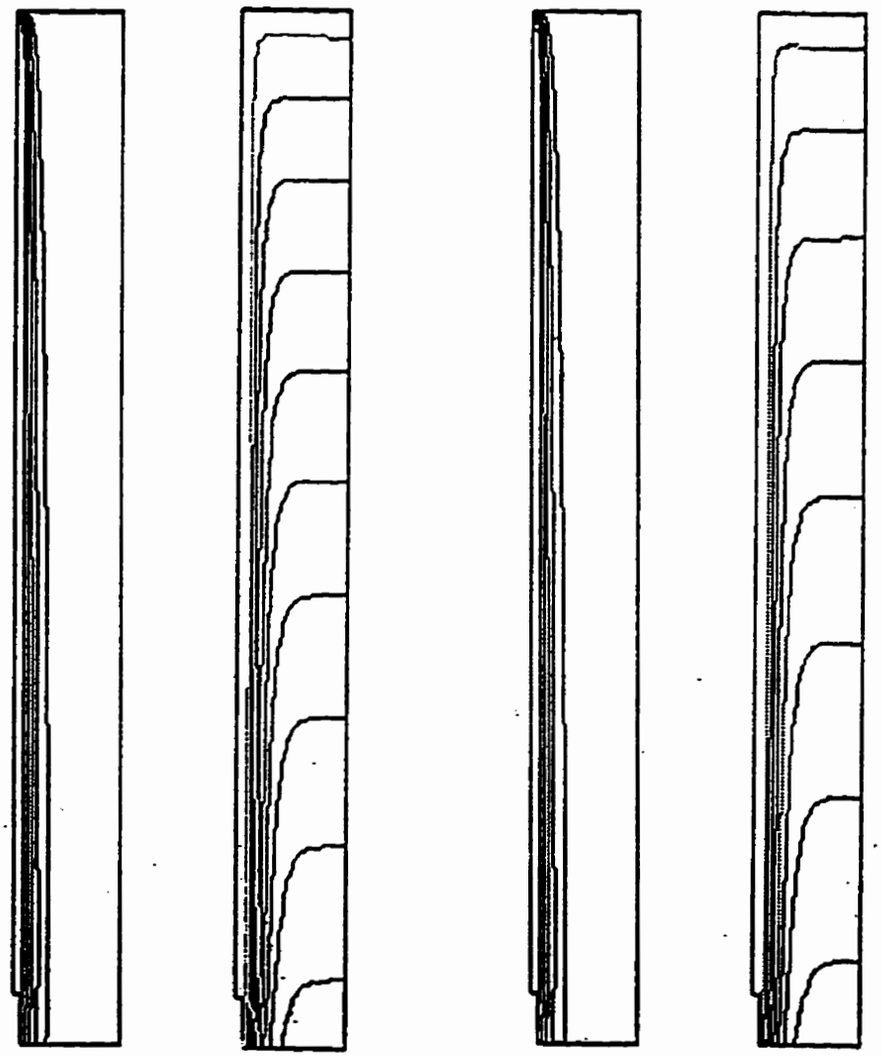

(a) NRD (b) RD

Figure 5.3 Isotherms (left) and streamlines (right) for indoor pane glass surfaces.

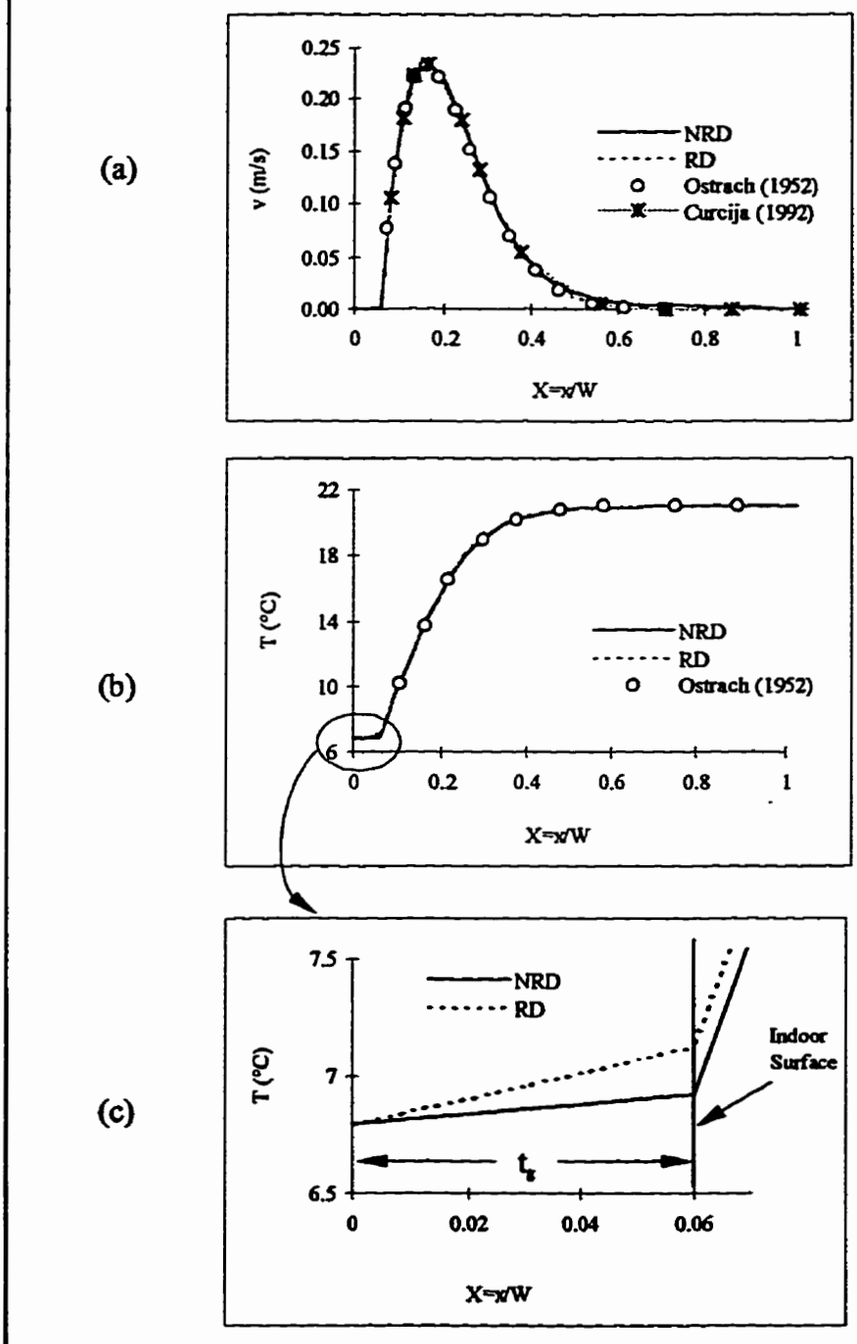

Figure 5.4 Comparisons of velocity profile and temperature distribution at $Y=L/4$ for indoor pane glass surface

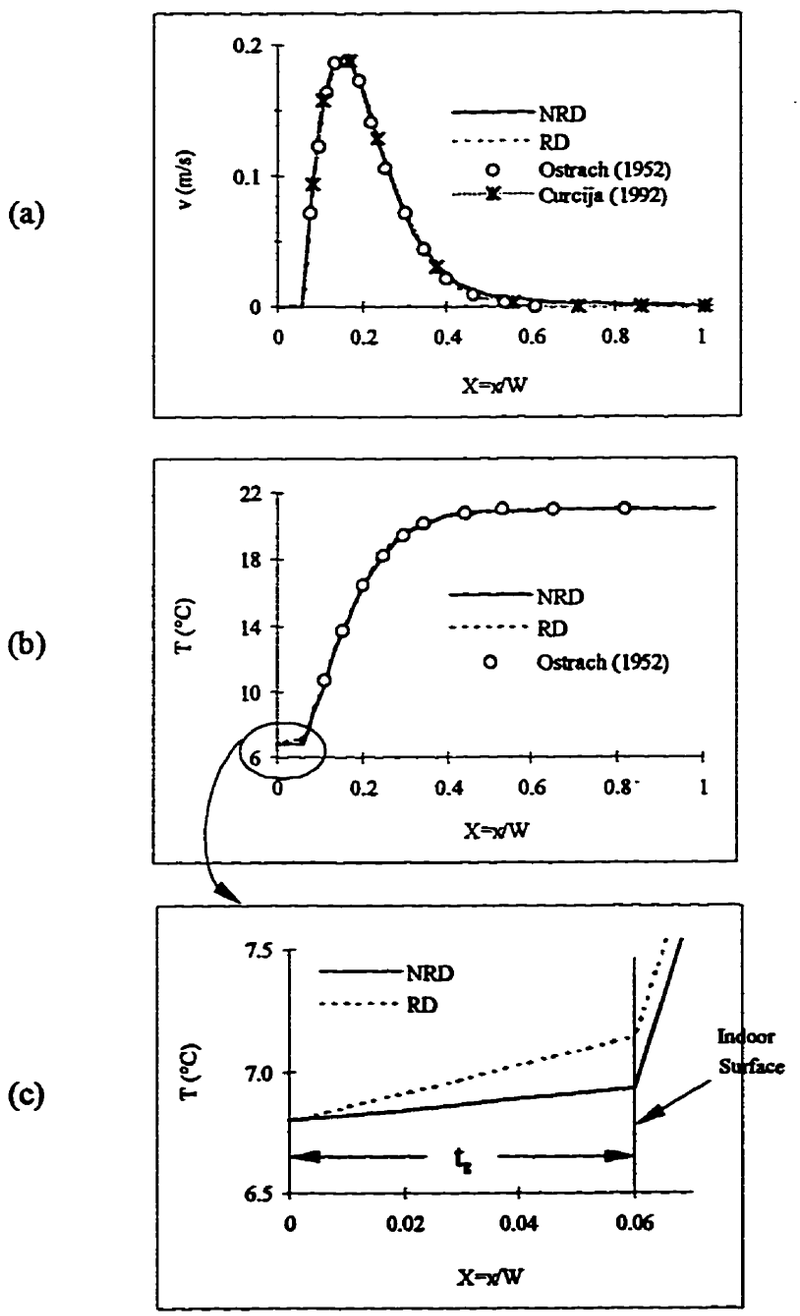

Figure 5.5 Comparisons of velocity profile and temperature distribution at $Y=L/2$ for indoor pane glass surface

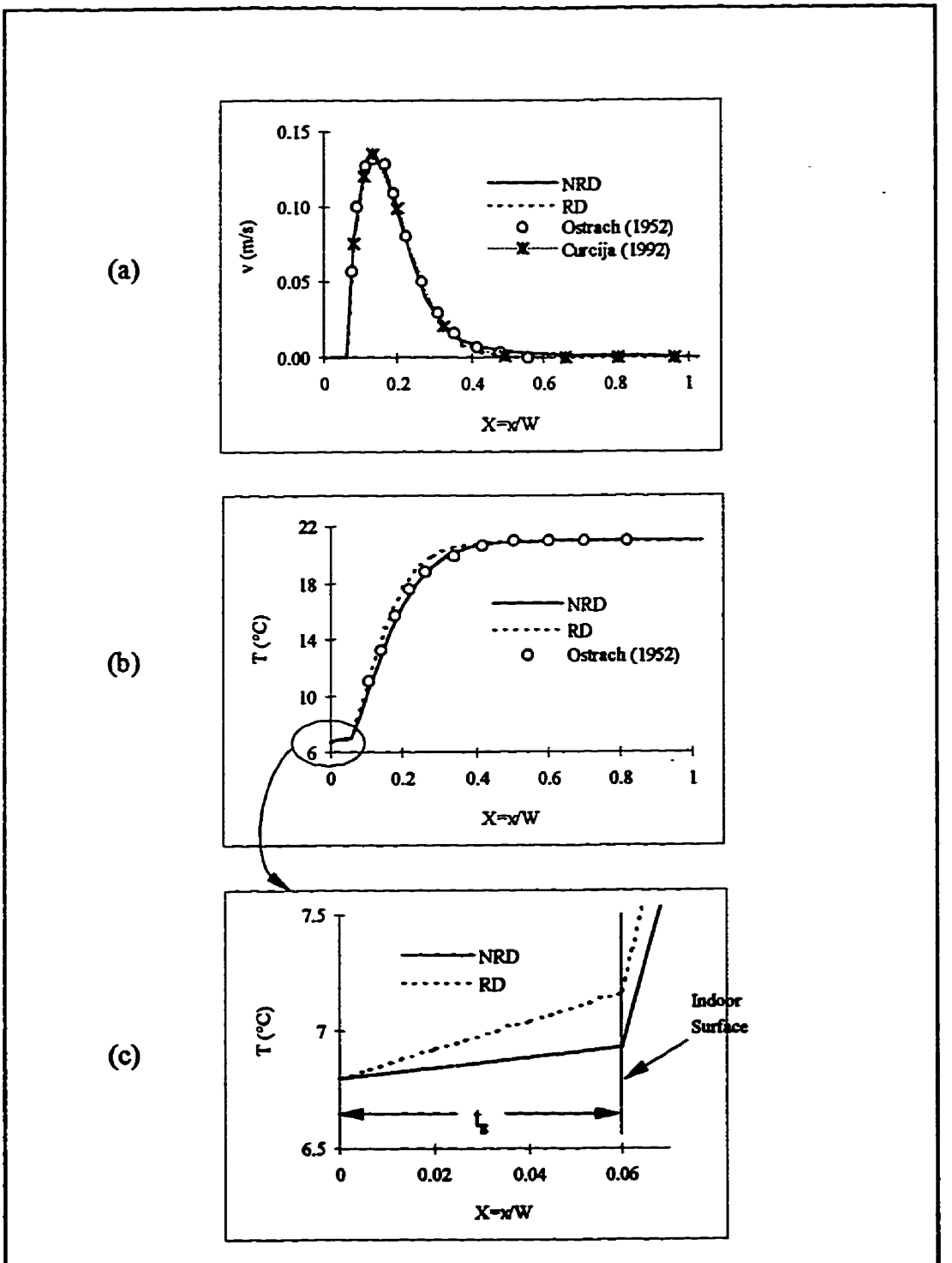

Figure 5.6 Comparisons of velocity profile and temperature distribution at $Y=3L/4$ for indoor pane glass surface

Finally, comparisons of the local and overall heat transfer coefficients between this work and the published work of Ostrach (1952) and Curcija and Goss (1993) are given in fig. 5.7 and table 5.2 respectively. The local and integrated heat transfer coefficients of Ostrach (1952) are calculated using the following equations:

$$h_Y = \frac{k_f Nu_Y}{Y} \tag{5.2}$$

and

$$h_{ic} = \frac{Nu_L k_f}{W} \tag{5.3}$$

where Y is non-dimensional distance from the top of the indoor pane of glass and, Nu_Y and Nu_L are defined by eqs. (1.6) and (1.7), respectively.

In the present study, the value of $h(Y)$ was calculated from non-dimensional heat flux, q'_Y, on the isothermal surface of the indoor glass pane, using the following equation:

$$\frac{1}{h_L} = \frac{(T_r - T_w)}{q'_Y \cdot q_{ref}} - \frac{t_g}{k_s} \tag{5.4}$$

and the integrated heat transfer coefficient, h_i or h_i, is calculated as follows:

$$h = \frac{1}{Y_L}\int_0^{Y_L} h(Y)\, dY \tag{5.5}$$

where $Y_L = L/W$.

It can be seen from fig. 5.7 that the local heat transfer coefficient for NRD case

compares very well with those of Ostrach (1952) and Curcija and Goss (1993).

Results indicate, for the RD case, that although convection and radiation occur simultaneously, they are almost independent with each other. This can be proven by the fact that the difference in corresponding values of h_Y between these two cases is a constant value of **4.584** which is defined as radiative heat transfer coefficient calculated by FIDAP, h_{ir}. The comparisons of integrated convective heat transfer coefficients, h_{ic}, in table 5.2 again show excellent agreement between this work and the published work of Ostrach (1952) and Curcija and Goss (1993). Comparisons of average heat transfer coefficients, h_{ic}, h_{ir}, and h_i, from this work with the typical values used by the well known computer programs WINDOW3.1, VISION and ISOWIN04 also indicate that the values predicted by FIDAP are reasonable and acceptable. A value of 7.708 for the overall heat transfer coefficient, h_i, will be used as a convective boundary condition on the indoor surface of an IGU system in the following modeling.

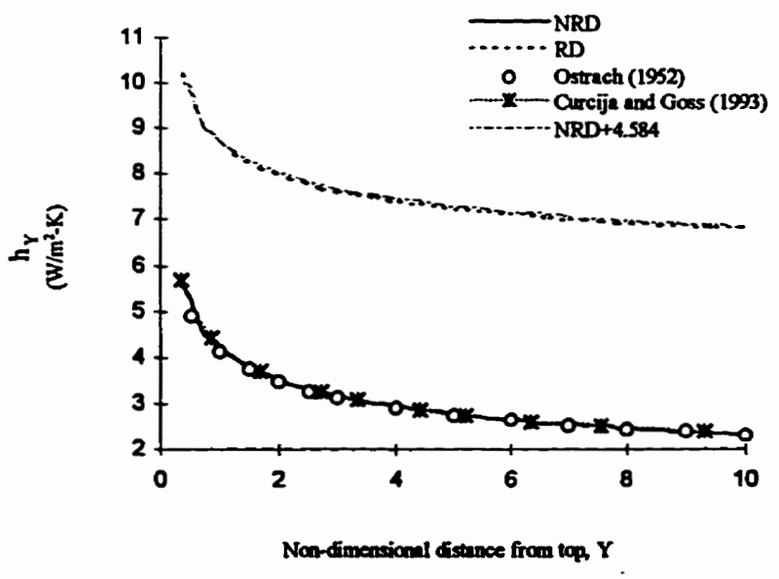

Figure 5.7 Comparison of local heat transfer coefficient

Table 5.2 Comparison of integrated heat transfer coefficient

h (W/m^2K)	Method					
	WINDOW3.1	ISOWIN04	VISION	Present work	Ostrach (1952)	Curcija and Goss (1993)
h_{ic}	3.41	3.6	3.04	3.124	3.09	3.13
h_{ir}	4.52	4.4	4.49	4.584 (FID) 4.511 (Cal)	N.A.	N.A.
h_i	7.93	8.0	7.53	7.708*	N.A.	N.A.

h_{ic}— convective heat transfer coefficient
h_{ir}— radiative heat transfer coefficient
$h_i=h_{ic}+h_{ir}$

N.A.— not available
FID— calculated by FIDAP
Cal— calculated using equation:

$$h_{ir}=S\varepsilon(T_w^2+T_r^2)(T_w+T_r)\ (T_w=7.2°C)$$

*— This value will be used as boundary conditions on the indoor surfaces of IGU systems.

5.3 LAMINAR NATURAL CONVECTION IN AN IGU CAVITY

The combined heat transfer through an IGU with a between-the-panes venetian blind is a complex, highly non-linear process and the accuracy with which this process is solved will significantly affect the accuracy of the whole model. For the purpose of validating the basic finite element model, numerical simulation of natural convection in an IGU cavity was performed first.

As discussed in chapter 1, over the past eighty years, numerous studies have been conducted either analytically, numerically or experimentally for natural convection in rectangular cavities with isothermal vertical surfaces and adiabatic horizontal surfaces as shown in fig. 5.8, in which the dimensionless quantities in parentheses are defined by eq. (2.13). In the present study, a constant value of aspect ratio A=10 is adopted and four Grashof numbers, Gr_w = 4×10^4, 6×1^4, 8×1^4 and 10^5 are investigated.

The results of the present numerical simulation are compared to appropriate results

to verify the model.

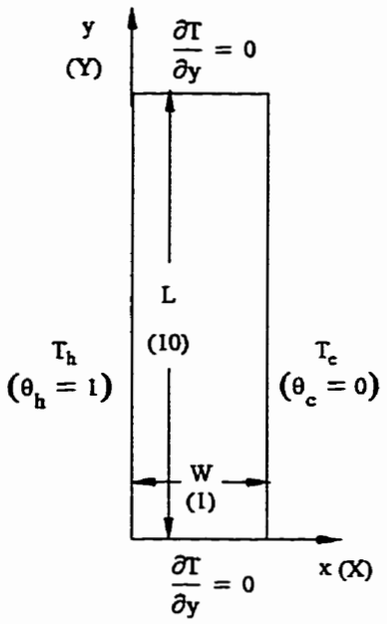

Figure 5.8 2-D laminar natural convection in a rectangular cavity

$$Gr = g\beta\Delta TW^3/\nu^2 = f(\Delta T) \;;\; (\Delta T = T_h - T_c)$$

5.3.1 Nodes and Mesh Development

Again, eq. (4.1) is used to estimate the thickness of thermal and velocity boundary layers. The smallest size of the boundary layers for $Gr_W = 10^5$ is 0.1089. As previously discussed, a non-uniform mesh with high density near the cavity boundaries was employed. The generated finite element mesh is given in fig. 5.10 which shows that there are at least two full elements (X_1=0.0373428, X_2=0.0492741, and X_3=0.0650175) contained within the velocity and temperature boundary layers as estimated by equation (4.1). To confirm the suitability of the grid spacing, a finer mesh for this calculation was tested, which demonstrated that the average running time increased about 3 times and the

overall accuracy improved less than 0.1%.

Figure 5.9 2-D finite element mesh for laminar natural convection in an IGU cavity

5.3.2 Comparisons of Results

The dimensionless heat flux can be evaluated by calculating the temperature gradients at the integration point of the elements bounding the hot wall or cold wall, which is given by,

$$q' = \frac{q}{q_{ref}} = \frac{\partial \theta}{\partial X} \tag{5.6}$$

The Nusselt number is defined as,

$$Nu = \frac{hW}{k_f} \tag{5.7}$$

where $h = q/\Delta T$, therefore

$$Nu = \frac{qW}{k_f \Delta T} = \frac{q}{q_{ref}} = q' \tag{5.8}$$

which means that in this case, the Nusselt number and dimensionless heat flux are equivalent.

Results from the numerical prediction are reported in terms of contour plots of the stream function and temperature, local heat flux (Nusselt number) along the hot wall and average (integrated over the vertical hot wall) Nusselt number. The effect of Grashof number, Gr_W, on the isotherms and streamlines are shown in fig. 5.10. As expected, for all cases, the flow is skew-symmetric about the cavity mid-point. Even at the relatively low Grashof number of 4×1^{4}, the isotherms in the central region tend toward the horizontal, indicating that the flow is in the transitional regime which is characterized by the presence of the boundary layer on the vertical surface, but only to the point where the two boundary layers have merged together. As Grashof number is increased, the flow regime changes from a transition flow to a boundary layer regime, in which two boundary layers grow in the temperature field, one growing up the hot wall and the other growing down the cold wall. In the central region, however, the isotherms have extended past the horizontal, indicating that the transport of energy must be purely by convection. A further increase in the Grashof number caused the distortion of the isotherms in the central region to become more severe.

The effect of local heat flux distribution along the hot wall was also investigated. Local Nusselt numbers occurring along the hot wall, for various values of Grashof number, are plotted in fig. 5.11. These results show an excellent agreement with the work

of Ramanan and Korpela (1989). Both results show the cold fluid sweeping across the bottom of the cavity, picking up heat. The local Nusselt number near this corner was found to be the largest, which is to be expected since as this represents the region of the greatest temperature gradient. As the fluid rises up the hot wall, its temperature rises and the heat transfer rate decreases continuously with height. For $Gr_w = 10^5$ there is a small bulge in the local Nusselt number near the bottom. A small dip in Nusselt number near the top end can also be seen.

The flow evidently changes its character in the ends as the Grashof number is increased to this value. This has also been observed by Laurit and Desrayaud (see Ramanan and Korpela 1989).

Finally, a comparison of integrated heat flux (Nusselt number) with the available results is summarized in table 5.3. Again as can be seen from the results, the present study compares quite well with the other results for the range of Grashof numbers considered in this work.

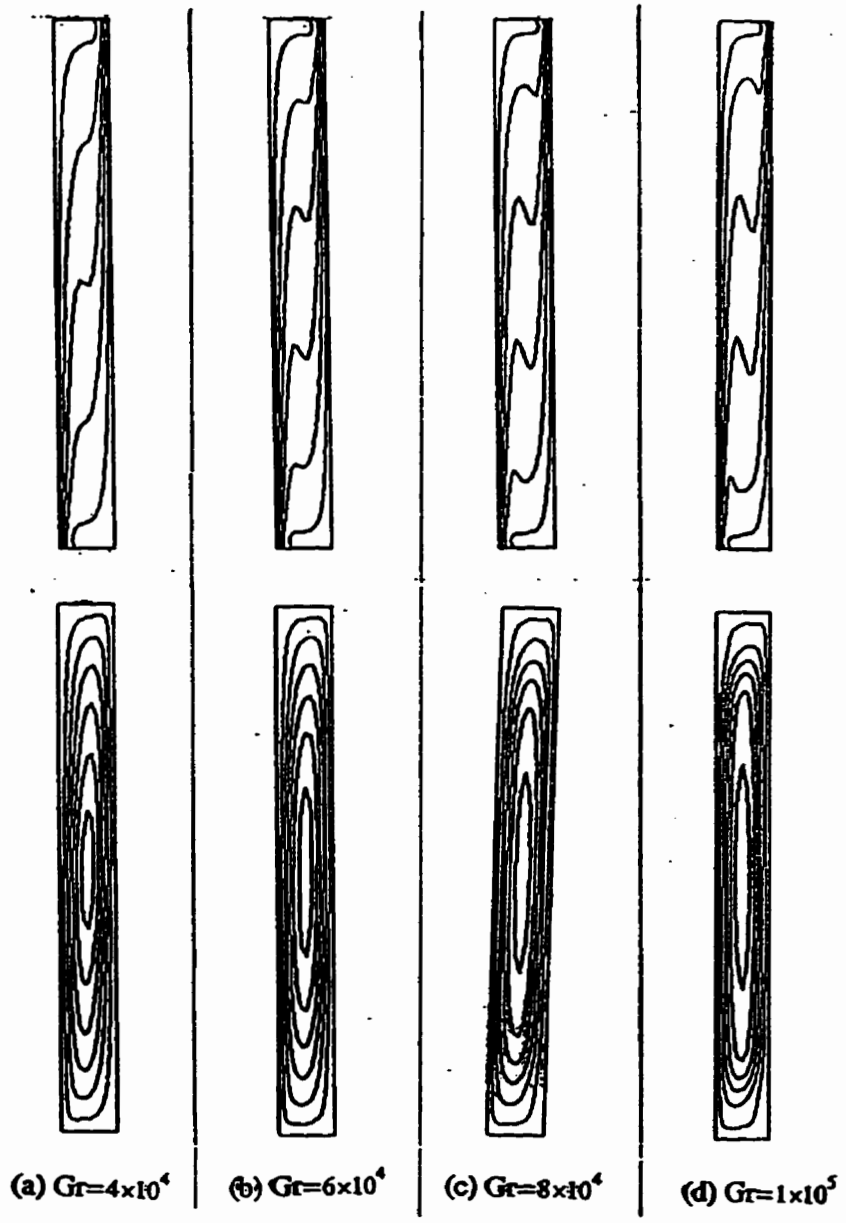

Figure 5.10 Isotherms and streamlines for natural convection in cavities

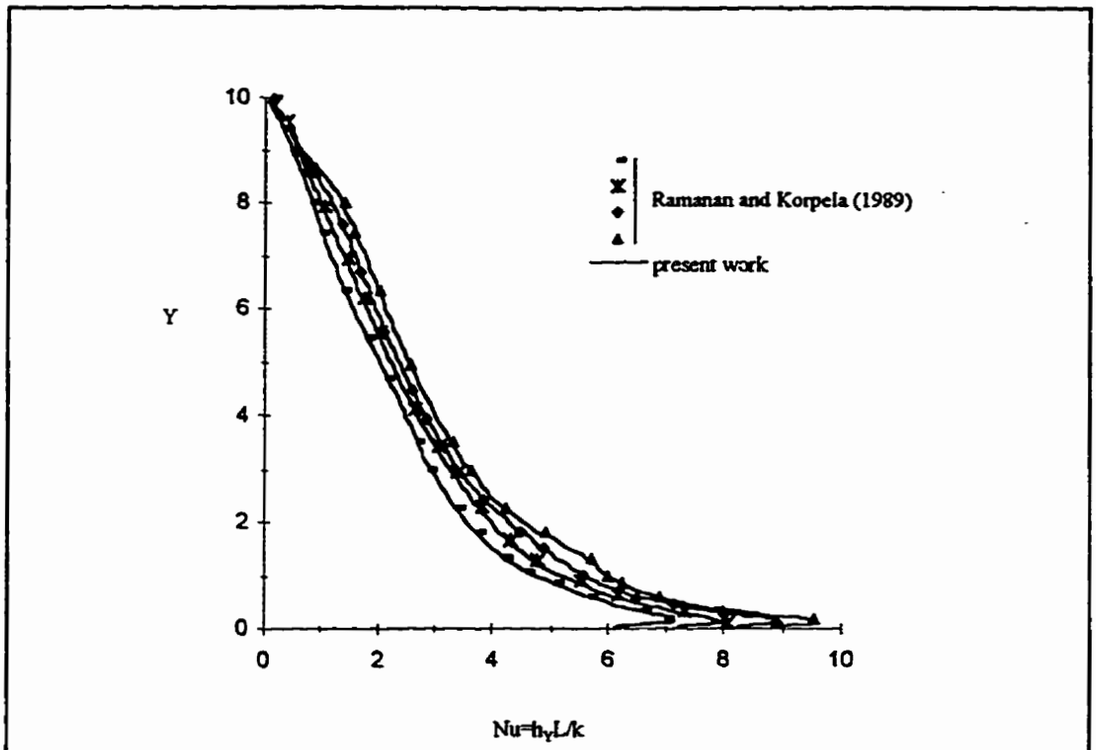

Figure 5.11 Comparison of local Nusselt number along the hot wall (A=10, Gr_W = 4×10^4, 6×10^4, 8×10^4, 10^5, with Gr_W increasing from left to right).

Table 5.3 Comparison of the average Nusselt number for an IGU cavity

Method	Gr			
	4×10^4	6×10^4	8×10^4	10^5
Ramanan and Korpela (1989) (numerical)	23.12	25.99	28.11	29.75
Raithby and Wong (1981) (numerical correlation)	22.79	25.52	27.58	29.27
Korpela et al (1982) (numerical)	22.00 ($Gr=3.9\times10^4$)	25.50 ($Gr=6.4\times10^4$)	N.A.	N.A.
Present work	23.09	25.85	27.89	29.47

5.4 COMBINED HEAT TRANSFER THROUGH IGU SYSTEMS WITH INTERNAL VENETIAN BLINDS

Based on the validated models for combined heat transfer on an indoor glass pane and natural convection in an IGU cavity, a model was developed for the combined heat transfer through an entire IGU system with a between-the-panes venetian blind. Fig. 5.12 gives the geometry and the problem's computational domain. Seven cases were considered in this study and are summarized in the following table:

Table 5.4 Summary of cases investigated in this study

Case	Venetian Blind	Louver Angle	Radiation
1	No		Not included
2	No		included
3	Between-the-panes	0°	included
4	Between-the-panes	45°	included
5	Between-the-panes	-45°	included
6	Between-the-panes	75°	included
7	Between-the-panes	-75°	included
Positive Louver Angle — indoor side up Negative Louver Angle — outdoor side up			

The venetian blind modeled consists of 19 louvers and was located in the center of the IGU cavity. The aspect ratio ($A=L/W$) of the IGU cavity was set to 10 and the following geometric dimensions were assumed:

L_s — the thickness of spacer, L_s=25.4 *mm* (1.0 *in.*)

a — the louver width and pitch, a=25.4 *mm* (1.0 *in.*)

t_g — the thickness of glass pane, t_g=3.0 *mm*

t_b — the thickness of blind louver, t_b=0.5 *mm*

The air flow in the IGU cavity and the heat conduction in the solid portion are governed by equations (2.14) and (2.20) respectively. Radiative heat transfer was considered through the boundary condition. The dimensionless variables are still defined by eq. (2.13), in which the length scale W=0.05 *m*, and $\Delta T = T_r = 294K$ (21°C).

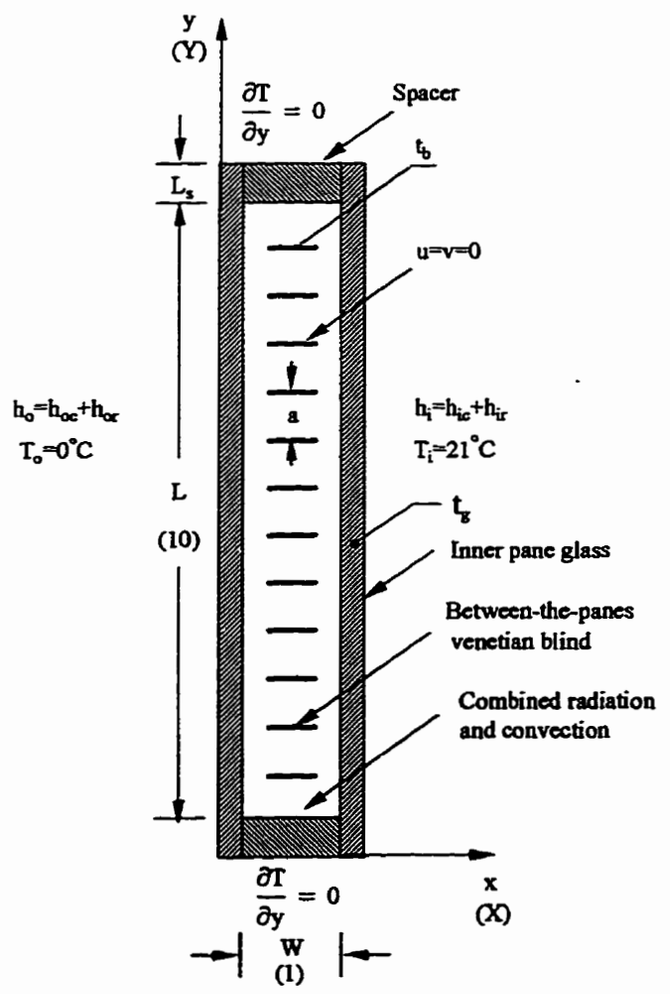

Figure 5.12 A sketch of the IGU system with a between-the-panes venetian blind

5.4.1 Boundary Conditions and Material Properties

The assumed non-dimensional boundary conditions are:

(1) Hydrodynamic boundary conditions:

On all solid surfaces, including the surfaces of the blind blades, a no slip velocity boundary condition is applied, i.e., U=V=0 on all solid surfaces.

(2) Thermal boundary conditions:

a) Convective boundaries (indoor and outdoor surfaces):

$$-k'_s\left(\frac{\partial\theta}{\partial X}\right)_s = h'_i(\theta-\theta_i) \qquad \text{for indoor surface} \tag{5.9}$$

$$-k'_s\left(\frac{\partial\theta}{\partial X}\right)_s = h'_o(\theta-\theta_o) \qquad \text{for outdoor surface} \tag{5.10}$$

where the dimensionless heat transfer coefficients, h_i and h_o, are defined as:

$$h'_{i(o)} = h_{i(o)}W/k_f \tag{5.11}$$

and $h_i = 7.708\ W/m^2\cdot K$, (as determined in Section 5.2), and $h_o = 23\ W/m^2\cdot K$

b) Convective and radiative boundaries:

On all surfaces of the IGU cavity, including the surfaces of the blind blades, a convective and radiative boundary condition defined by eq. (2.25) is applied.

c) insulated horizontal surfaces:

On the horizontal ends of the computational domain, i.e., at Y=0.0 and Y=11.016

respectively, the adiabatic boundary condition defined in eq. (2.22) is applied.

The materials selected and their properties are tabulated in the following Table.

Table 5.5 Materials and their properties

Element	**Material**	**emissivity** ε	**Conductivity** k $(W/m \cdot K)$
Glass panes	Clear glass	0.84	0.88
Spacers	corrugated-strip	0.827	0.80
Blind louvers	Aluminum with coatings	0.45	169

Note: 1) k_{seal} was calculated using the following equation:

$k_{seal} = k_{lin}\frac{W}{L_s}$, where $k_{lin} = 0.41 \ W/m \cdot K$ called linear conductance (Wright and Sullivan 1989).

2) Emissivity of seal, ε_{sea}, was taken from Wright and Sullivan (1995)

5.4.2 Mesh Development

The mesh for cases 1 and 2 was generated first. A coarser mesh was used to perform a preliminary numerical study in order to obtain the average temperatures on each vertical surface of the IGU cavity, which were found to be 2 and 13°C respectively. The thermophysical properties of air were evaluated at the average of these values, 7.5°C. The resulting Groshof number used to evaluated the boundary layer thickness was then obtained, i.e., $Gr_W = g\beta\Delta TW^3/\nu^2 = 2.4783\times10^5$. The non-dimensional boundary layer thickness calculated from eq. (4.1) was found to be 0.08667. The final mesh was shown in fig. 5.13(a) for cases 1 and 2. The size of the first line of elements from the vertical surfaces of the IGU cavity is 0.0573, which satisfies the constraint that at least one node is located within the boundary layers.

Based on the generated mesh for cases 1 and 2, the meshes for the subsequent cases were developed. For all the cases considered, a finer, non-uniform mesh was employed in the region between the cavity surfaces and the louver tips where the gradient of the flow variables were expected to be great. A coarser, uniform mesh was used in the center region of the IGU cavity. Several runs were repeated using finer meshes, with no appreciable difference in the internal flow field and heat transfer results. Examples of finite element meshes for cases 3, 4, and 6 are shown in fig. 5.13.

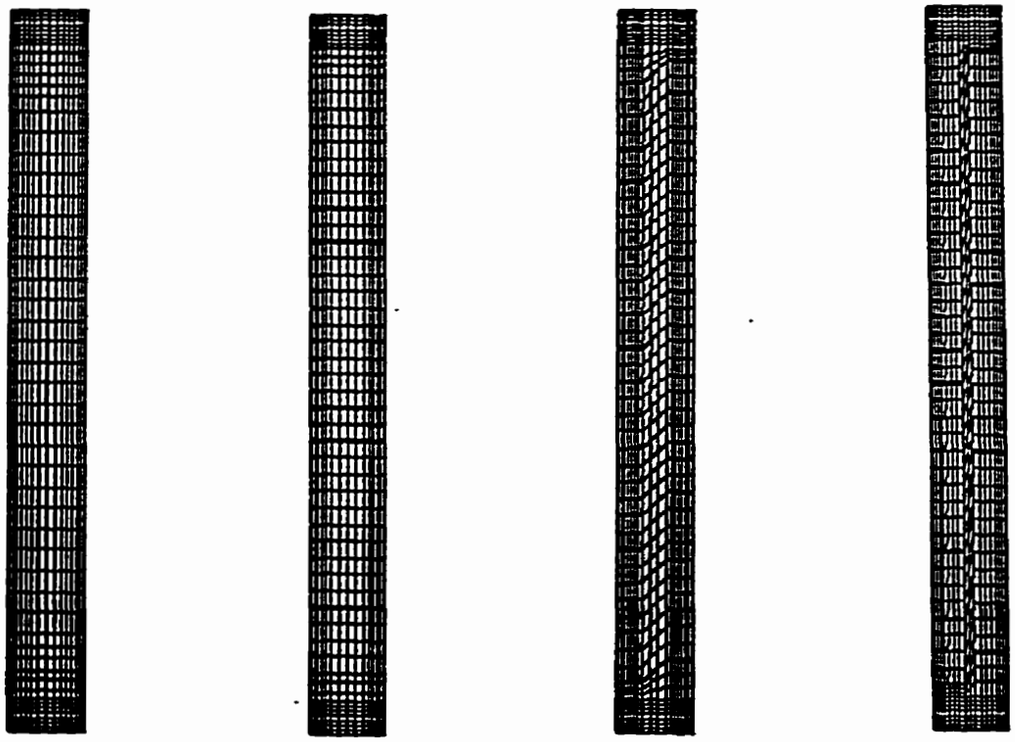

(a) cases 1 and 2 (b) case3 (c) case 4 (d) case 6

Figure 5.13 Examples of finite element meshes generated for combined heat transfer through IGU systems

5.4.3 Results and Discussions

As mentioned before, the numerical study examined the effects of the internal venetian blinds on the flow fields and combined heat transfer rates through IGU systems. Solutions were obtained for all 7 cases described in table 5.4. The numerical results are presented in terms of temperature contours, velocity vector plots, local heat flux and temperature distributions along the indoor surface, and the overall heat transfer coefficients.

Temperature contours and velocity vector plots for cases 2 through 7 are given in fig. 5.14 and fig. 5.15. The effects of blind louvers on the local heat flux and temperature distributions along indoor surfaces are presented in figs 5.16 and 5.17 respectively. It may be seen from these figures that the louvers reduce the local heat flux and increase the local temperature in the central portions of the indoor surface. The larger blade angle (approaching the closed position) produces lower local heat fluxes and higher local temperatures. In addition, although the average heat transfer rates are about the same (shown in table 5.6), the local heat transfer distributions are quite different for positive and negative blade angles (figs. 5.16 (b) and (c)). Near the lower end, the local heat flux is higher for negative blade angles than for positive blade angles. In the upper region, however, the local heat flux is lower for negative blade angles than for positive blade angles. This can be explained by the fact that with the negative blade angle, the lowest blade and the bottom wall (spacer) form a "nozzle" which accelerates the flow, impinging on the indoor surface. This larger flow velocity will result in larger local heat transfer coefficient and therefore the higher local heat flux. Alternatively, if the blade angle is positive, the lowest blade and the bottom wall (spacer) will form a "diffuser" which slows down flow.

Finally, table 5.6 shows the effects of louver angles on the average heat transfer rate and the calculated overall heat transfer coefficient, namely, U-value. The U-values

calculated from experimental measurement of Garnet et al. (1995) are also given in the same table. As can be seen that by using between-the-panes venetian blinds, the numerically predicted U-value is reduced for all the cases where the louver angles are different. This indicates that the thermal performance of windows with between-the-panes venetian blinds is improved. Since the louvers block the direct exchange of long wave radiation between the panes, as the blind closes the U-values decrease. However the way in which the blind closes (indoor side up or outdoor side up) seems not to influence the overall results significantly, which does not agree with the experimental results. It can be seen from the experimental results that the U-values for positive angles are consistently lower than the corresponding values for negative angles. The reason for this is probably due to the different geometry of the cross section of the louver. A rectangular cross section of the louver is adopted in the numerical prediction while a louver with a curved top side is used in the experimental study. It is interesting to note that although the experimental results show the same tread that the U-values decrease with increasing louver angles, the experimental study also shows that when the louvers are in the open positions ($\theta = 0°$), the U-value is even greater than that for case 2. This difference between the experimental study and this work can be explained as follows: the gap between the louver-tip and the vertical surfaces of the IGU cavity is much smaller (1.524 *mm* in the experimental study) than that used in this work (12.3 *mm*), therefore the effect of the louver conduction is more significant in the measurement, resulting in a consistently higher experimental U-value for the same louver angle. However, as blind closes, i.e., the gap increases, the difference of the U-values between the experimental work and present numerical study decreases.

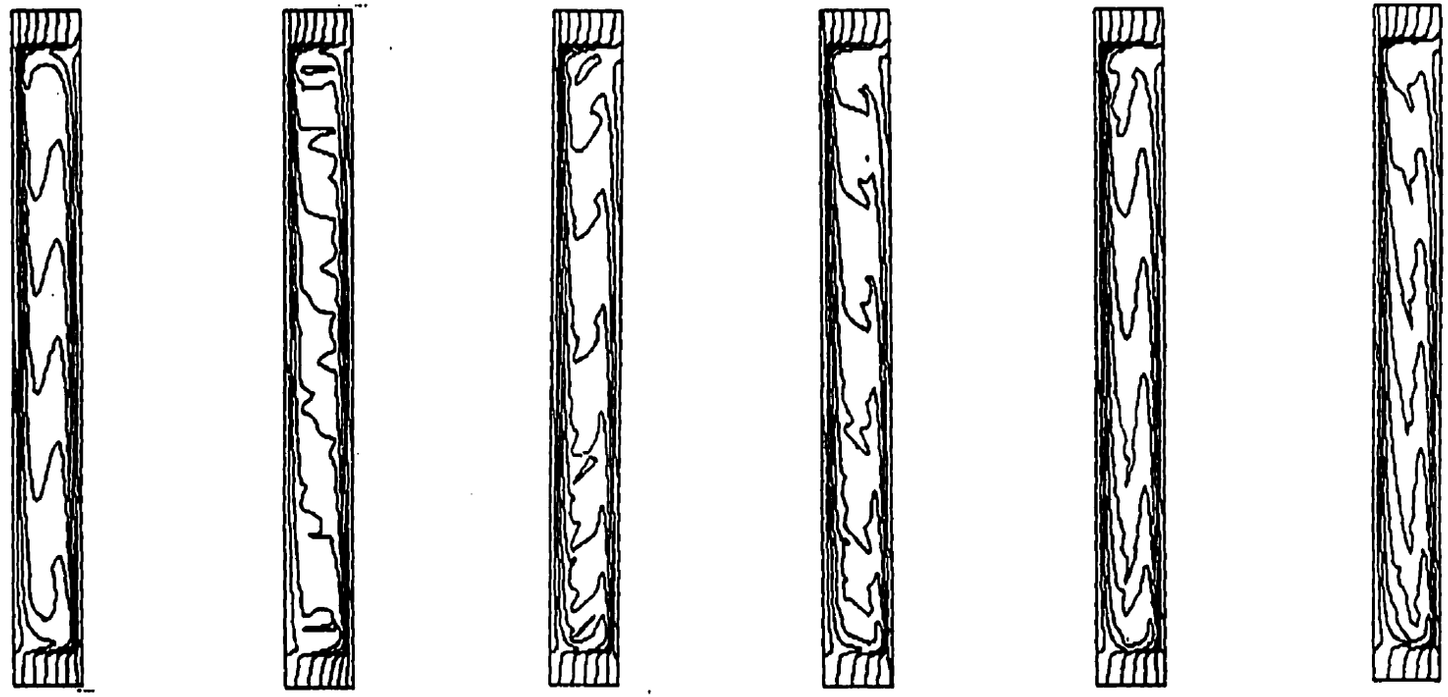

(a) case 2 (b) case 3 (c) case 4 (d) case 5 (e) case 6 (f) case 7

Figure 5.14 Temperature contours for case 2 through case 7

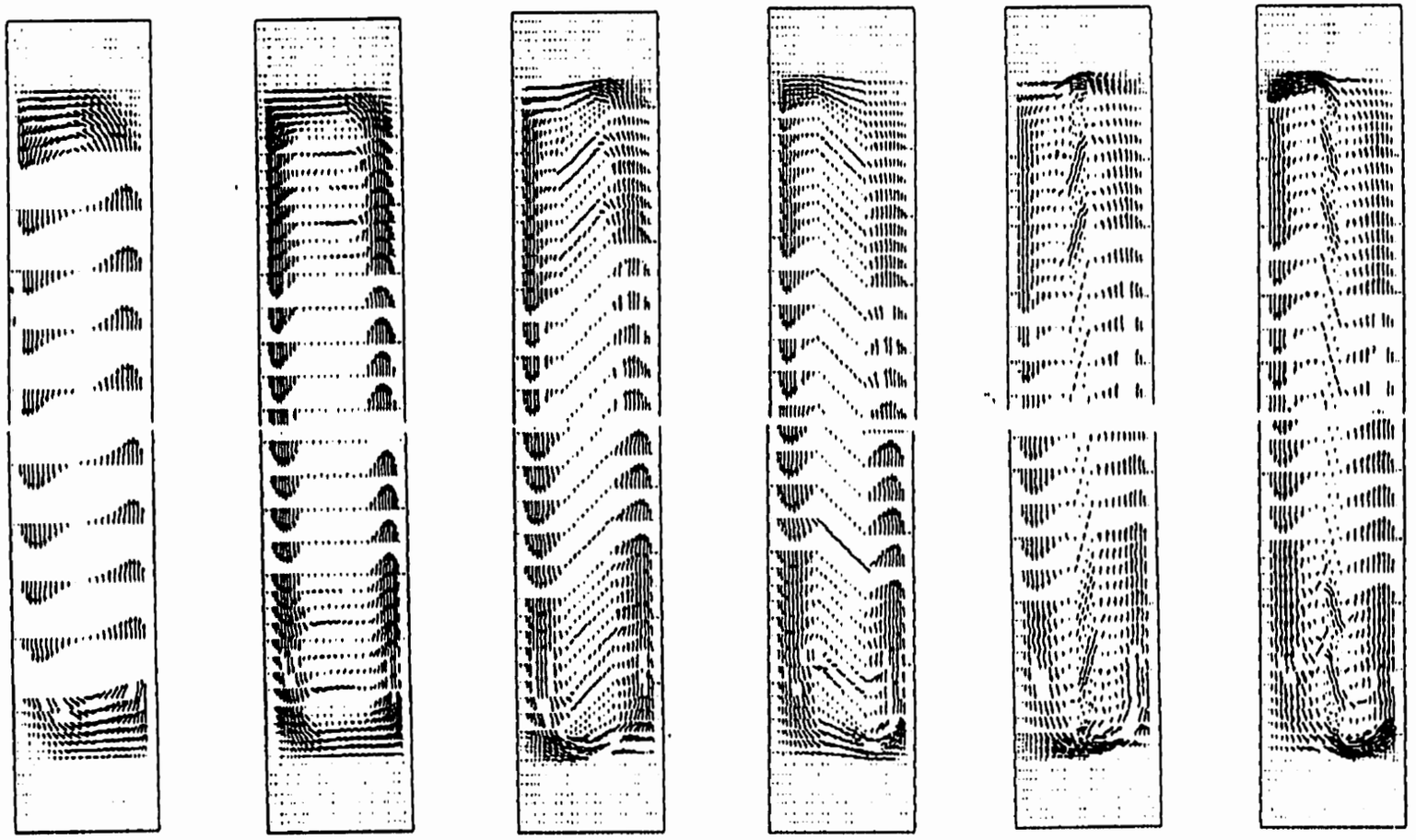

(a) case 2 (b) case 3 (c) case 4 (d) case 5 (e) case 6 (f) case 7

Figure 5.15 Velocity vector plots for case 2 through case 7

(a)

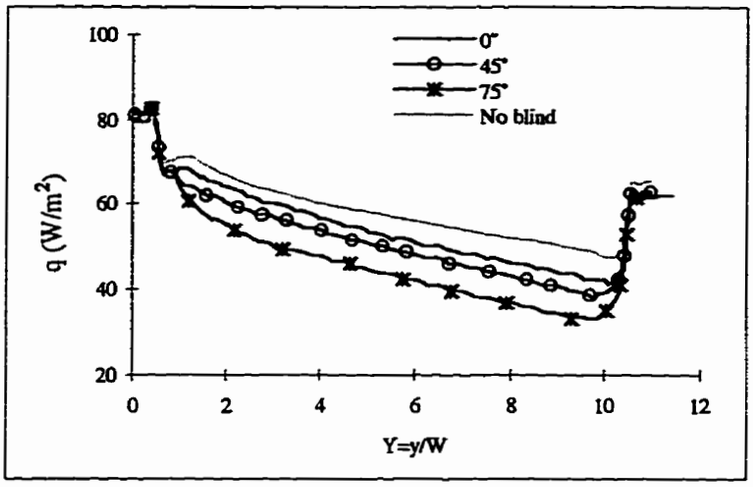

(b)

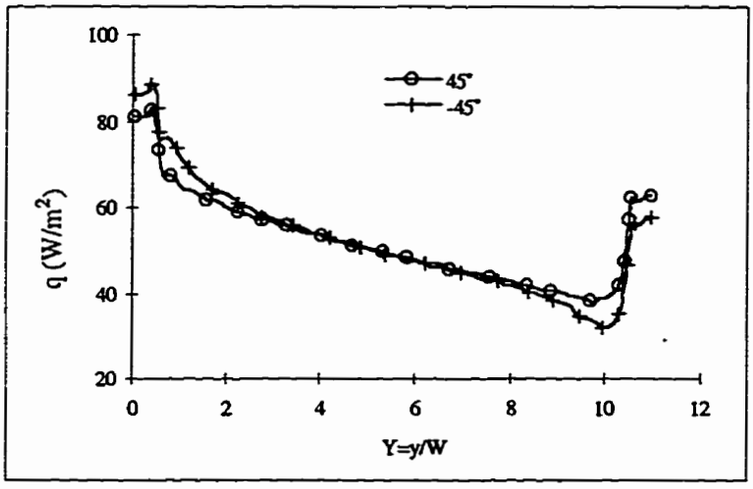

(c)

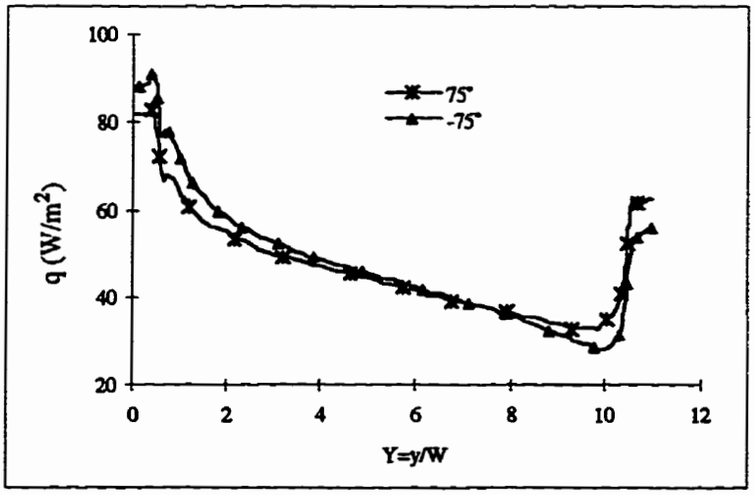

Figure 5.16 Local heat flux distributions on indoor pane surface for three cases corresponding to (a) blade angle θ = 0°, 45°, 75°, and no blind cases, (b) θ = 45° and -45°, and (c) θ = 75° and -75°

(a)

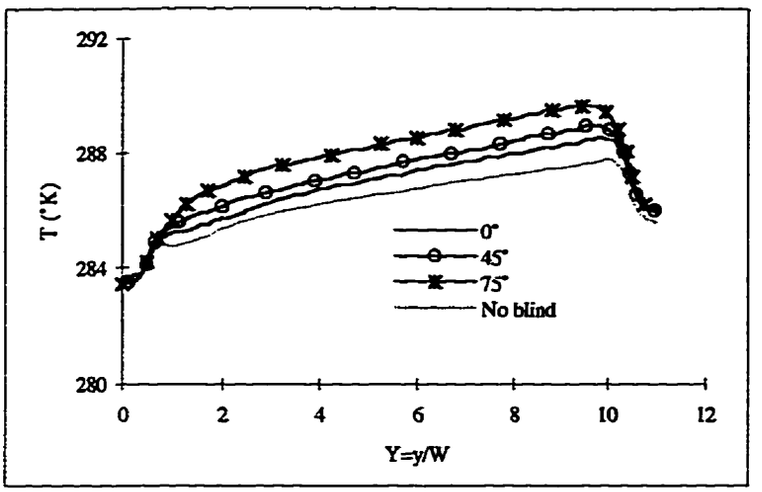

(b)

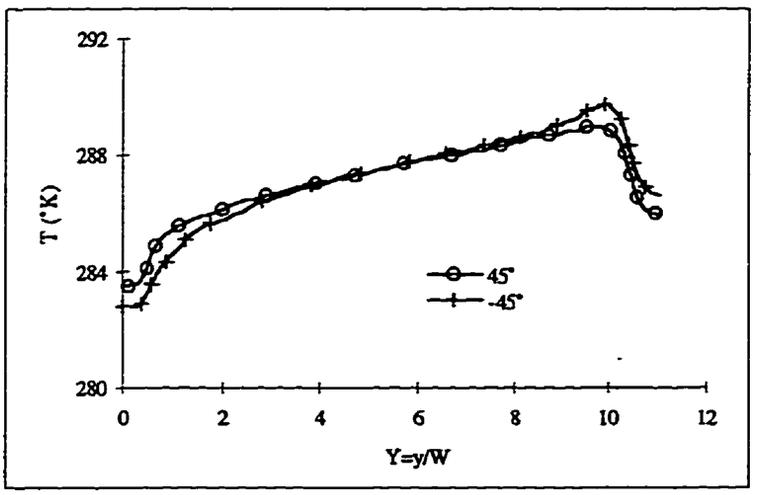

(c)

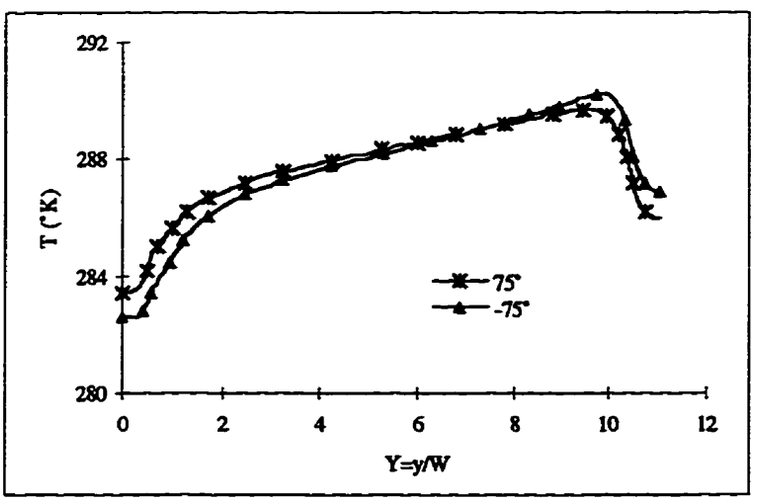

Figure 5.17 Temperature distributions on indoor surfaces for three cases corresponding to (a) blade angle θ = 0°, 45°, 75°, and no blind cases, (b) θ = 45° and -45°, and (c) θ = 75° and -75°

Table 5.6 Integrated heat transfer rate and U-value as a function of blind angle

Case	Blade Angle	q (W/m^2)	U-value ($W/m^2 \cdot K$)	
			Present work	Garnet (1995)
1	—	35.736	1.702	N.A.
2	—	59.148	2.817	2.789
3	0°	53.941	2.569	3.065
4	45°	52.808	2.515	2.579
5	-45°	52.645	2.507	2.712
6	75°	47.869	2.279	2.221
7	-75°	47.549	2.264	2.358

CHAPTER 6

CONCLUSIONS AND RECOMMENDATIONS

6.1 CONCLUSIONS

The numerical modeling of 2-D heat transfer through fenestration systems conducted in this study consists of the following two major parts: (A) modeling of natural convection from an isothermal vertical flat plate adjacent to a venetian blind; and (B) modeling of combined conductive, convective and radiative heat transfer through an IGU system with an internal venetian blind. Conclusions are presented for each of the above cases.

6.1.1 Numerical Modeling of Natural Convection Over an Isothermal Vertical Flat Plate Adjacent to a Venetian Blind

(1) A numerical model for 2-D natural convection from an isothermal flat plate adjacent to a venetian blind has been developed. It was found that, in general, the flow pattern is strongly influenced by the presence of a nearby venetian blind.

(2) The blade-to-plate spacing d has a strong effect on the flow and heat transfer. The smaller d is, the stronger the effect of the blind. When the blind is located far

enough away from the surface, there is almost no effect.

(3) For the same blade-to-plate spacing *d*, the flow structure varies with the louver angle θ. In the horizontal position (θ=0°), the flow is seen to be mostly disturbed. As the blind rotates towards the closed orientation (i.e., θ=90°), the disturbance decreases.

(4) There is little difference in the performance between negative angles (e.g. θ=-45°) and positive angles (e.g., θ=+45°) when the blind is located far away from the surface (*d*>2 *cm*). At a small blade-to-plate spacing *d* (*e.g.*, *d*=15 *mm*), however, a strong effect of the orientation was observed. The average heat transfer coefficient for the negative angle case is 13% lower than that for the corresponding positive angle.

6.1.2 Numerical Modeling of Combined Heat Transfer Through an IGU System With a Between-the -panes Venetian Blind

(1) A model has been developed for the simulation of combined heat transfer through an IGU system with an internal blind. The results indicated that the thermal performance of an IGU system can be improved by using a venetian blind.

(2) For the single pane case, the radiation does not affect the flow pattern. It only slightly increases the indoor surface temperature and does not alter the temperature gradient near the indoor surface. The convective heat transfer is, therefore, not affected by the radiation.

(3) For the IGU system, louver angle affects the thermal performance. As a blind closes, it blocks more direct exchange of long-wave radiation between panes, reducing heat transfer.

(4) Although the distributions of local heat transfer and temperature along the glass pane for positive and negative louver angles are different, the overall U-values for the two cases are very close.

6.2 RECOMMANDATIONS

(1) For the single pane case, the heat conduction of louvers should be considered in simulations conducted in the future This can be accomplished based on the present study with some modifications. Experimental studies indicate that the conduction may offset the convection suppression and these effects should be further investigated.

(2) For the IGU system, the effect of the gap between a vertical surface of an IGU cavity and blade tip on thermal performance should be studied. This can also be accomplished by modifying the input files.

(3) The effects of solar radiation striking the surface of the blind should also be considered in the future.

REFERENCE

Batchelor, G.K., 1954. "Heat Transfer by Free Convection Across a Closed Cavity Between Vertical Boundaries at Different Temperatures", Quarterly Journal of Applied Mathematics, Vol. 12, pp. 209-233.

Bejan, A., 1979. "Note on Gill's Solution for Free Convection in a Vertical Enclosure", J. of Fluid Mechanics, Vol. 90, Part 3, pp. 561-568.

Bergholtz, R.F., 1978. "Instability of Steady Natural Convection in a Vertical Fluid Layer", J. of Fluid Mechanics, Vol. 84, Part 4, pp.743-768.

Carpenter, S.C. and McGowan, A.G., 1989. "Frame and Spacer Effects on Window U-Value", ASHRAE Transaction, 95 (1), pp. 604-608.

Churchill, S.W. and Usagi, R., 1972. "A General Expression for the Correlation of Rates of Transfer and Other Phenomena", AIChE Journal, Vol. 18, pp. 1121-1128

Churchill, S.W. and Chu, H.S., 1975. "Correlation Equations For Laminar and Turbulent Free Convection from a Vertical Plate", I.J. Heat Transfer, Vol. 18, pp. 1323-1329.

Curciji, D., 1992. "Three-Dimensional Finite Element Model of Overall, Nighttime Heat Transfer Through Fenestration System", Ph.D. Dissertation, University of Massachusetts, pp. 62-79.

Curciji, D. and Goss.W.P., 1993. "Two-Dimensional Natural Convection Over the Isothermal Indoor Fenestration Surfac — Finite Element Numerical Solution", ASHRAE Transactions, 99(1), pp.274-287.

Daly and Pracht, 1968. phys. of Fluids 11(1), pp15.

Dropkin, D. and Somerscales, Z., 1965. "Heat Transfer By Natural Convection in Liquids Confined By Two Parallel Plates Which Are Inclined at Various Angles With Respect to the Horizontal", J. of Heat Transfer, Series C, Vol. 87, pp. 77-84.

Eckert, E.R.G. and Soehnghen, E., 1948. USAF Tech. Rept. 5747, Dec.

Eckert, E.R.G. and Carlson, W.O., 1961. "Natural Convection in an Air Layer Enclosed Between Two Vertical Plates With Different Temperatures", I. J. Heat and Mass Transfer, Vol. 2, pp. 106-120.

Ede, A.J., 1967. "Advances in Free Convection", Advances in Heat Transfer, Vol. 4, Academic Press, New York, London, pp. 1-62.

Elder, J.W., 1965. "Laminar Free Convection in a Vertical Slot", J. of Fluid Mechanics, Vol. 23, Part 1, pp. 77-98.

Elder, J.W., 1966. "Numerical Experiments With Free Convection in a Vertical Slot", J. of Fluid and Mechanics, Vol. 24, Part 4, pp. 823-843.

ElSherbiny, S.M.; Raithby, G.D. and Hollands, K.G.T., Februry 1982. "Heat Transfer By Natural Convection Across Vertical And Inclined Air Layers", J. of Heat Transfer, Vol. 104, pp.96-102.

ElSherbiny, S.M.; Raithby, G.D. and Hollands, K.G.T., August 1982. "Effect of Thermal Boundary Conditions on Natural Convection in Vertical and Inclined Air Layers", J. of Heat Transfer, Vol. 104, pp.515-520.

Falkner, V.M. and Skan, S.W., 1931. "Solutions of the Boundary Layer Equations", Philosophical Magazine and Journal of Science, Vol. 12, No. 80, pp.865-896.

Fang, X.D. and Ge, X.S., April 1993. "Experimental Study of Overall Heat Transfer Coefficients of the Glass Window with a Venetian Blind", Journal of Solar Energy (in Chinese), Vol. 14, pp138-142.

FDI 1990. "FIDAP 5.01 - Users and Reference Manual", Fluid Dynamics International, Evanston, IL.

Gadgil, A.J., 1980. "On Convective Heat Transfer In Building Energy Analysis", Ph.D. Dissertation, University of California, Berkeley, pp. 25.

Garnet,J.M.; Fraser,R.A.; Sullivan,H.F. and Wright,J.L., 1995. "Effect of Internal Venetian Blinds on Window Center-Glass U-Values", Conference Proceedings, WINDOW INNOVATIONS'95, 5&6 June 1995, TORONTO, PP273-279.

Gill, A.E., 1966. "The Boundary-Layer Regime for Convection in a Rectangular Cavity", J. of Fluid Mechanics, Vol. 26, Part 3, pp. 515-536.

Graebel, W.P., 1981. "The Influence of Prandtl Number on Free Convection in a Rectangular Cavity", I. J. of Heat and Mass Transfer, Vol. 24, pp. 125 131.

Hollands, K.G.T.; Unny, T.E.; Raithby, G.D. and Konicek, L., May 1976. "Free Convective Heat Tansfer Across Inclined Air Layers", Transactions of the ASME, J. of Heat Transfer, pp189-193.

Jones, I.P., 1979. "A Numerical Study of Natural Convection in an Air-Filled Cavity: Comparison With Experiment", Numerical Heat Transfer, Vol. 2, pp. 193-213.

Korpela, S.A.; Lee, Y. and Drummond, J.E., 1982. "Heat Transfer Through a Double Pane Window", J. of Heat Transfer, Vol. 104, pp. 539-544.

Landis, F. and Yanowitz, H., 1966. "Transient Natural Convection in a Narrow Vertical Cell", Transaction, International Heat Transfer Conference, pp. 139-151.

LeFevre, E.J., 1956. "Laminar Free Convection from a Vertical Plate Surface", Proc. 9th Intern. Congr. Appl. Mech., Vol. 4, Brussels, Belgium, pp. 168-174.

Lee, Y. and Korpela, S.A., 1983. "Multicellular Natural Convection in a Vertical Slot", J. of Fluid Mechanics, Vol. 126, pp. 91-121.

Lienhard, J.H., 1981. "A Heat Transfer Text Book", PRENTICE-HALL, INC., Englewood Cliffs, New Jersey 07632, pp. 346-358.

Lorenz, L., 1881. Ann. Phys. Chem., Vol. 13, pp. 582

Machin, A., 1997. "An Experimental Study of the Effect of Louvers on Free Convection from a Vertical Surface", M.Sc.Eng. Dissertation, University of Western Ontario, London, Canada.

Machin, A.; Naylor, D.; Harrison, S.J.; Oosthuizen, P.H. and Tarasuk, J.D., 1996. "An Interferometric Study of the Effect of Louvers on Free Convection from an Isothermal Vertical Surface", 4th Annual Great Lakes Region V Graduate Student Technical Conference.

Mills, A.F., 1992. "Heat Transfer" (Text Book), IRWIN, Homewood, IL 60430, Boston, MA 02116, pp. 293-294

Mills, L.R. and McCluney, W.R., November 1993. "The benefits of using window shades", ASHRAE Journal, pp20-27.

Newell, M.E. and Schmidt, F.W., 1970. "Heat Transfer By Natural Convection Within Rectangular Enclosures", J. of Heat Transfer, Series C, Vol. 92, pp. 159-168.

Novak, M.H. and Nowak, E.S., 1993. "Natural Convection Heat Transfer in Slender Window Cavities", J. of Heat Transfer, Vol.115, pp. 476-479.

Ostrach, S., 1952. "An Analysis of Laminar Free-Convection Flow and Heat Transfer About a Flat Plate Parallel to the Direction of the Generating Body Force", NACA TN 2635 (National Advisory Comm. Aeronaut, Tech. Note).

Ostrach, S., 1972. "Natural Convection in Enclosures", Advances in Heat Transfer, Vol. 8, Academic Press, New York, pp. 161-227.

Raithby, G.D.; Hollands, K.G.T. and Unny, T.E., 1977. "Analysis of Heat Transfer By Natural Convection Across Vertical Fluid Layer", J. of Heat Transfer, Vol. 99, pp. 287-293.

Raithby, G.D. and Wong, H.H., 1981. "Heat Transfer By Natural Convection Across Vertical Air Layer", Numerical Heat Transfer, Vol. 4, pp. 447-457.

Ramanan, N. and Korpela, S.A., 1989. "Multigrid Solution of Natural Convection in a Vertical Slot", Numerical Heat Transfer, Part A, Vol. 15, pp. 323-339.

Randall, K.R.; Mitchell, J.W. and El-Wakil, M.M., 1979. "Natural Convection Heat Transfer Characteristics of Flat Plate Enclosure", J. of Heat Transfer, Vol. 101, pp. 120-125.

Reilly, M.S., 1994. "Spacer Effects on Edge-of-Glass and Frame Heat Transfer", ASHRAE Transaction, 100 (1), pp. 1718-1723.

Rheault, S. and Bilgen, N., 1989. "Heat Transfer Analysis in an Automated Venetian Blind Window System", J. of Solar Energy Engineering, Vol. 111, pp89-95.

Rohsenow, W.M. and Choi, H., 1961. "Heat, Mass, and Momentum Transfer", PRENTICE-HALL, INC., Englewood Cliffs, New Jersey, pp. 153-163.

Rubin, I.; Collins, L. and Tibbott, L., May 1978. "Window Blinds as a Potential Energy Saver–A Case Study", NBS BUILDING SCIENCE SERIES 112.

Schmidt, E. and Beckmann, W., 1930. "Das Temperatur-und Geschwindigkeitsfeld vor einer Warme abgebenden senkrechter Platte bei naturlichen Konvektion", Tech. Mech. Thermo-Dynam, Berlin 1, pp. 341- 391

Seki, N., Fukusako, S. and Inaba, H., 1978. "Visual Observation of Natural Convective Flow in a Narrow Vertical Cavity", J. of Fluid Mechanics, Vol. 84, pp. 695-704.

Shewen, E.C., 1986. "A Peltier-Effect Technique for Natural Convection Heat Flux Measurement Applied to the Rectangular open Cavity", Ph.D. Thesis, Waterloo, On., Department of Mechanical Engineering, University of Waterloo.

Siegel, R. and Howell, J.R., 1972. "Thermal Radiation Heat Transfer", McGraw-Hill Book Company, pp238-245.

Sparrow, E.M., 1956. Ph.D. Thesis, Mech. Engrg. Dept., Harvar Univ..

Spradley,L.W. and Churchill, S.W., 1975. "Pressure and Buoyancy-Driven Thermal Convection in a Rectangular Enclosure", J. of Fluid Mechanics, Vol. 70, Part 4, pp. 705-720.

Squire, H.B., 1938. "Modern Developments in Fluid Dynamics", Oxford Univ. Press, London and New York.

Vest, C.M. and Aparci, V.S., 1969. "Stability of Natural Convection in a Vertical Slot", J. of Fluid Mechanics, Vol. 36, pp. 1-15.

Wilkes, J.O. and Churchill, S.W., 1966. "The Finite-Difference Computation of Natural Convection in a Rectangular Enclosure", AIChE Journal, Vol. 12 (1), pp. 161-166.

Wright, J.L., P.F. de Abreu, R.A. Fraser and H.F. Sullivan, 1994. "Heat Transfer in Glazing System Edge-Seals: Calculations Regarding Various Design Options", ASHRAE Transaction, 100 (1), pp. 1705-1717.

Wright, J.L. and Sullivan, H.F., 1989. "Natural Convection in Sealed Glazing Units: A Review", ASHRAE Transactions, Vol. 95 (2), pp. 592-603.

Wright, J.L. and Sullivan, H.F., 1994. 'A Two-Dimensional Numerical Model For Natural Convection in a Vertical, Rectangular Window Cavity", ASHRAE Transactions, Vol. 100(2), pp. 1193-1206.

Yazdanian, M. and Klems, J.H., 1994. "Measurement of the Exterior Convective Film Coefficient for Windows in Low-rise Buildings", ASHRAE Transaction, 100 (1), pp.1087-1096.

Yeoh, G.H.; Davis, V. and Leonardi, E., 1989. "Heat Transfer Across a Double-Glazed Window With Convective Boundary Conditions", Numerical Methods In Thermal Problems, Vol. VI (1), pp. 355-365.

Yin, S.H.; Wung, T.Y. and Chen, K., 1978. "Natural Convection in an Air Layer Enclosed Within Rectangular Cavities", I. J. Heat and Mass Transfer, Vol. 21, pp. 307-315.

APPENDIX A. THE PENALTY FUNCTION METHOD

A common technique, used to reduce the number of unknowns and also the number of governing equations from the original problem, consists of weakening the incompressibility constraint and is called the Penalty Function Method (PFM). In the PFM, the continuity equation (2.14a) is modified to:

$$\frac{\partial U}{\partial X}+\frac{\partial V}{\partial Y} = -\varepsilon P \tag{A.1}$$

where ε is called the penalty parameter.

This statement is equivalent to replacing the original incompressible fluid with a slightly compressible one. If the value of the penalty parameter, ε, is small enough, the loss of overall accuracy compared to the solution of the full system of governing equations will be insignificant, while the overall numerical solution complexity is reduced.

Applying the Galerkin's Method to the modified continuity equation (A.1), we obtain:

$$\left(\int_{A_e} \psi \frac{\partial \varphi^T}{\partial X} dA_e\right) U + \left(\int_{A_e} \psi \frac{\partial \varphi^T}{\partial Y} dA_e\right) V + \left(\varepsilon \int_{A_e} \psi \psi^T dA_e\right) P = 0 \tag{A.2}$$

Hence

$$P = -\left(\varepsilon \int_{A_e} \psi \psi^T dA_e\right)^{-1} \left(\left(\int_{A_e} \psi \frac{\partial \varphi^T}{\partial X} dA_e\right) U + \left(\int_{A_e} \psi \frac{\partial \varphi^T}{\partial Y} dA_e\right) V\right) \tag{A.3}$$

Upon evaluation of equations (3.17b) and (3.17c), the pressure term is replaced by

the expression from equation (A.3) and the matrix equation (3.18) becomes:

$$\begin{bmatrix} 2\boldsymbol{K}_{11}+\boldsymbol{K}_{22}+(1/\varepsilon)\,\boldsymbol{C}_1\boldsymbol{M}_P^{-1}\boldsymbol{C}_1^T & \boldsymbol{K}_{12}+(1/\varepsilon)\,\boldsymbol{C}_1\boldsymbol{M}_P^{-1}\boldsymbol{C}_2^T & \mathbf{0} \\ \boldsymbol{K}_{21}+(1/\varepsilon)\,\boldsymbol{C}_2\boldsymbol{M}_P^{-1}\boldsymbol{C}_1^T & \boldsymbol{K}_{11}+2\boldsymbol{K}_{22}+(1/\varepsilon)\,\boldsymbol{C}_2\boldsymbol{M}_P^{-1}\boldsymbol{C}_2^T & \boldsymbol{B} \\ \mathbf{0} & \mathbf{0} & \boldsymbol{L}_{11}+\boldsymbol{L}_{22} \end{bmatrix} \begin{bmatrix} \boldsymbol{U} \\ \boldsymbol{V} \\ \Theta \end{bmatrix}$$

$$\begin{bmatrix} \boldsymbol{A}_1(\boldsymbol{U})+\boldsymbol{A}_2(\boldsymbol{V}) & \mathbf{0} & \mathbf{0} \\ \mathbf{0} & \boldsymbol{A}_1(\boldsymbol{U})+\boldsymbol{A}_2(\boldsymbol{V}) & \mathbf{0} \\ \mathbf{0} & \mathbf{0} & \boldsymbol{D}_1(\boldsymbol{U})+\boldsymbol{D}_2(\boldsymbol{V}) \end{bmatrix} \begin{bmatrix} \boldsymbol{U} \\ \boldsymbol{V} \\ \Theta \end{bmatrix} = \begin{bmatrix} \boldsymbol{F}_1 \\ \boldsymbol{F}_2 \\ \boldsymbol{G} \end{bmatrix} \qquad \text{(A.4)}$$

where the coefficient matrices are the same as those in equation (3.19) and $\boldsymbol{M}_P$ is defined as

$$\boldsymbol{M}_P = \int_{A_e} \psi\psi^T dA_e \qquad \text{(A.5)}$$

APPENDIX B. INPUT AND OUTPUT FILES FOR THE FLOW OVER AN ISOTHERMAL VERTICAL FLAT PLATE AJACENT TO A VENETIAN BLIND (θ=45° and *d*=2.5cm)

1 INPUT FILE

```
*TITLE
NATURAL CONVECTION WITH BLINDS (θ=45°, d=2.5cm)
*FIMESH(IMAX=5,JMAX=19)
EXPI
1 15 0 19 33
EXPJ
1 9 13 17 21 25 29 33 37 41 45 49 53 57 61 65 69 73 81
POINT
1 1 1 1 0. 0.
2 1 2 1 0. 0.254
3 1 3 1 0. 0.3033
4 1 4 1 0. 0.6363
5 1 5 1 0. 0.9693
6 1 6 1 0. 1.3023
7 1 7 1 0. 1.6353
8 1 8 1 0. 1.9683
9 1 9 1 0. 2.3013
10 1 10 1 0. 2.6343
11 1 11 1 0. 2.9673
12 1 12 1 0. 3.3003
13 1 13 1 0. 3.6333
14 1 14 1 0. 3.9663
15 1 15 1 0. 4.2993
16 1 16 1 0. 4.6323
17 1 17 1 0. 4.9653
18 1 18 1 0. 5.25
19 1 19 1 0. 5.504
20 2 1 1 0.2104 0.
21 2 2 1 0.2104 0.254
22 2 3 1 0.2104 0.3033
23 2 4 1 0.2104 0.6363
24 2 5 1 0.2104 0.9693
25 2 6 1 0.2104 1.3023
26 2 7 1 0.2104 1.6353
```

27 2 8 1 0.2104 1.9683
28 2 9 1 0.2104 2.3013
29 2 10 1 0.2104 2.6343
30 2 11 1 0.2104 2.9673
31 2 12 1 0.2104 3.3003
32 2 13 1 0.2104 3.6333
33 2 14 1 0.2104 3.9663
34 2 15 1 0.2104 4.2993
35 2 16 1 0.2104 4.6323
36 2 17 1 0.2104 4.9653
37 2 18 1 0.2104 5.25
38 2 19 1 0.2104 5.504
39 4 1 1 0.4458 0.
40 4 2 1 0.4458 0.254
41 4 3 1 0.4458 0.5387
42 4 4 1 0.4458 0.8717
43 4 5 1 0.4458 1.2047
44 4 6 1 0.4458 1.5377
45 4 7 1 0.4458 1.8707
46 4 8 1 0.4458 2.2037
47 4 9 1 0.4458 2.5367
48 4 10 1 0.4458 2.8697
49 4 11 1 0.4458 3.2027
50 4 12 1 0.4458 3.5357
51 4 13 1 0.4458 3.8687
52 4 14 1 0.4458 4.2017
53 4 15 1 0.4458 4.5347
54 4 16 1 0.4458 4.8677
55 4 17 1 0.4458 5.2007
56 4 18 1 0.4458 5.25
57 4 19 1 0.4458 5.504
58 5 1 1 1. 0.
59 5 2 1 1. 0.254
60 5 3 1 1. 0.5387
61 5 4 1 1. 0.8717
62 5 5 1 1. 1.2047
63 5 6 1 1. 1.5377
64 5 7 1 1. 1.8707
65 5 8 1 1. 2.2037
66 5 9 1 1. 2.5367
67 5 10 1 1. 2.8697
68 5 11 1 1. 3.2027
69 5 12 1 1. 3.5357
70 5 13 1 1. 3.8687
71 5 14 1 1. 4.2017
72 5 15 1 1. 4.5347

73 5 16 1 1. 4.8677
74 5 17 1 1. 5.2007
75 5 18 1 1. 5.25
76 5 19 1 1. 5.504
LINE
/vertical line
1 20 3. 3
2 21 3. 3
10 29 3. 3
18 37 3. 3
19 38 3. 3
20 39
21 40
29 48
37 56
38 57
39 58
40 59
48 67
56 75
57 76
/horizontal line
1 2
2 3
3 4
4 5
5 6
6 7
7 8
8 9
9 10
10 11
11 12
12 13
13 14
14 15
15 16
16 17
17 18
18 19
21 22
22 23
23 24
24 25
25 26
26 27

27 28
28 29
29 30
30 31
31 32
32 33
33 34
34 35
35 36
36 37
40 41
41 42
42 43
43 44
44 45
45 46
46 47
47 48
48 49
49 50
50 51
51 52
52 53
53 54
54 55
55 56
58 59
59 60
60 61
61 62
62 63
63 64
64 65
65 66
66 67
67 68
68 69
69 70
70 71
71 72
72 73
73 74
74 75
75 76
SURFACE
1 76

```
BCNODE(UX)
1 19 0.
22 41 0.
23 42 0.
24 43 0.
25 44 0.
26 45 0.
27 46 0.
28 47 0.
29 48 0.
30 49 0.
31 50 0.
32 51 0.
33 52 0.
34 53 0.
35 54 0.
36 55 0.
BCNODE(UY)
2 18 0.
58 76 0.
22 41 0.
23 42 0.
24 43 0.
25 44 0.
26 45 0.
27 46 0.
28 47 0.
29 48 0.
30 49 0.
31 50 0.
32 51 0.
33 52 0.
34 53 0.
35 54 0.
36 55 0.
BCNODE(TEMPERATURE)
2 18 1.
58 76 0.
1 58 0.
ELEMENTS(QUADRILATERAL,NODES=9,ALL)
ELEMENTS(BOUNDARY,NODES=3)
2 18
19 76
58 76
1 58
1 2
```

```
18 19
END
*PROBLEM(NONLINEAR,TSTRONGLY)
*EXECUTION(restart)
*SOLUTION(s.s.=10,accf=0.5)
/STRATEGY(S.S.=2)
*POSTPROCESS
*NODES(FIMESH)
*ELEMENTS(QUADRILATERAL,NODES=9,FIMESH)
*ELEMENTS(PLOT,NODES=3,FIMESH)
*ELEMENTS(PLOT,NODES=3,FIMESH)
*ELEMENTS(PLOT,NODES=3,FIMESH)
*ELEMENTS(PLOT,NODES=3,FIMESH)
*ELEMENTS(PLOT,NODES=3,FIMESH)
*ELEMENTS(PLOT,NODES=3,FIMESH)
*DENSITY(CONSTANT=1098.1803)
*PRESSURE(PENALTY=1.E-8,DISCONTINUOUS)
*SPECIFICHEAT(CONSTANT=0.7110)
/BODYFORCE(CONSTANT)
/. -1. 0.
*printout(none)
*RENUMBER(PROFILE)
*END
```

2 OUTPUT FILE

```
FFFFFFFFFF    IIIIII    PPPPPPPPP      OOOOOOOOO      SSSSSSSS     TTTTTTTTTT
FFFFFFFFFF    IIIIII    PPPPPPPPPP    OOOOOOOOOOO    SSSSSSSSSS    TTTTTTTTTT
FF              II      PP      PPP   OO       OO   SSS              TT
FF              II      PP       PP   OO       OO   SS               TT
FF              II      PP      PPP   OO       OO   SSS              TT
FFFFFF          II      PPPPPPPPPP    OO       OO    SSSSSSS         TT
FFFFFF          II      PPPPPPPPP     OO       OO     SSSSSSS        TT
FF              II      PP            OO       OO          SSS        TT
FF              II      PP            OO       OO           SS        TT
FF              II      PP            OO       OO          SSS        TT
FF            IIIIII    PP            OOOOOOOOOOO    SSSSSSSSSS      TT
FF            IIIIII    PP             OOOOOOOOO     SSSSSSSS        TT

                        FIDAP  POST - PROCESSOR  PROGRAM

                              RELEASE  (  5.02 )
```

1

NUMBER OF NODAL POINTS	=	2673
NUMBER OF ELEMENTS	=	752
NUMBER OF ELEMENT GROUPS	=	7
NUMBER OF FACES	=	640
NUMBER OF EXTERNAL FACES	=	640
NUMBER OF EXTERNAL EDGES	=	2672
MEMORY FOR EXECUTION	=	1288435
DATABASE FILE (I3D)	=	INCORE
ELEMENT FILE (IELM)	=	INCORE

*** SOLUTION CONVERGED IN 6 ITERATIONS

*** 0.930 DATA STRUCTURE INITIALISATION TIME

F L U X C A L C U L A T I O N S

FLUX TYPE . . . . . (LFLUX) = 0
= 0 , TEMPERATURE (HEAT FLUX)
= 1 , SPECIES 1
= 2 , SPECIES 2

FLUX PLOT OPTION . . . . . (IFTYP) = 100
= 0 , NO PLOT; PRINT ONLY
= LMN, N=0 NO PLOT OF DIFFUSIVE FLUX
N=1 PLOT DIFFUSIVE FLUX
M=0 NO PLOT OF CONVECTIVE FLUX
M=1 PLOT CONVECTIVE FLUX
L=0 NO PLOT OF TOTAL FLUX
L=1 PLOT TOTAL FLUX

NUMBER OF ELEMENT SIDES(FACES) . . . . . (NSIDES) = 0
=-1 , PICK UP PREVIOUS SIDE DEFINITION
= 0 , INPUT BY ELEMENT GROUP LIST
= N , INPUT BY ELEMENT NUMBER AND SIDE

PRINT FLAG . . . . . (IPRF) = 0
= 0 , PRINT CALCULATED VALUES ON FPOUT
= 1 , NO PRINTOUT

DIRECTION FLAG . . . . . (LDIR) = 0
= 0 , LINE DIRECTION OK
= 1 , REVERSE LINE DIRECTION

SYMBOL FLAG . . . . . (LSYMB) = 0
=-1 , PLOT SYMBOL AT FIRST STEP ONLY
= 0 , PLOT SYMBOLS AT EACH TIME STEP
= 1 , PLOT SYMBOL AT LAST TIME STEP ONLY
= 2 , NO SYMBOLS PLOTTED AT EACH TIME STEP

GRID LINE FLAG . . . . . (ILINF) = 0
= 0 , NO GRID LINES
= 1 , HORIZONTAL AND VERTICAL GRID LINES
= 2 , VERTICAL GRID LINES
= 3 , HORIZONTAL GRID LINES

GROUP 1	GROUP 2	NGEN
2	0	0

LIST OF DEFINING GROUPS:
2

MAXIMUM STORAGE (INTEGER WORDS) REQUIRED FOR EXECUTION = 3505

ELEMENT	SIDE			INTEGRATION POINT FLUXES/QUANTITIES		INTEGRATED HEAT FLOW
65	4	DIFFUSIVE	NORMAL	-0.3656628E+02	-0.5911660E+02	-0.1179291E+01
			X	0.3656628E+02	0.5911660E+02	0.1179291E+01
			Y	0.1421085E-13	0.0000000E+00	0.1751488E-15
		CONVECTIVE	NORMAL	0.0000000E+00	0.0000000E+00	0.0000000E+00
			X	0.0000000E+00	0.0000000E+00	0.0000000E+00
			Y	0.0000000E+00	0.0000000E+00	0.0000000E+00
		TOTAL	NORMAL	-0.3656628E+02	-0.5911660E+02	-0.1179291E+01
			X	0.3656628E+02	0.5911660E+02	0.1179291E+01
			Y	0.1421085E-13	0.0000000E+00	0.1751488E-15
		COORDINATE	ARC LN	0.0000000E+00	0.1423168E-01	0.2465000E-01
			X	0.0000000E+00	0.0000000E+00	
			Y	0.2734408E+00	0.2592092E+00	
		NORMAL VEC	X	-0.1000000E+01	-0.1000000E+01	
			Y	0.0000000E+00	0.0000000E+00	
81	4	DIFFUSIVE	NORMAL	-0.2770070E+02	-0.3279319E+02	-0.7455871E+00
			X	0.2770070E+02	0.3279319E+02	0.7455871E+00
			Y	0.1421085E-13	0.0000000E+00	0.1751488E-15
		CONVECTIVE	NORMAL	0.0000000E+00	0.0000000E+00	0.0000000E+00
			X	0.0000000E+00	0.0000000E+00	0.0000000E+00
			Y	0.0000000E+00	0.0000000E+00	0.0000000E+00
		TOTAL	NORMAL	-0.2770070E+02	-0.3279319E+02	-0.7455871E+00
			X	0.2770070E+02	0.3279319E+02	0.7455871E+00
			Y	0.1421085E-13	0.0000000E+00	0.1751488E-15
		COORDINATE	ARC LN	0.2465000E-01	0.3888168E-01	0.2465000E-01
			X	0.0000000E+00	0.0000000E+00	
			Y	0.2980908E+00	0.2838592E+00	
		NORMAL VEC	X	-0.1000000E+01	-0.1000000E+01	
			Y	0.0000000E+00	0.0000000E+00	
97	4	DIFFUSIVE	NORMAL	-0.1849859E+02	-0.2344705E+02	-0.3491975E+01
			X	0.1849859E+02	0.2344705E+02	0.3491975E+01
			Y	0.0000000E+00	-0.1776357E-14	-0.1478817E-15
		CONVECTIVE	NORMAL	0.0000000E+00	0.0000000E+00	0.0000000E+00
			X	0.0000000E+00	0.0000000E+00	0.0000000E+00
			Y	0.0000000E+00	0.0000000E+00	0.0000000E+00
		TOTAL	NORMAL	-0.1849859E+02	-0.2344705E+02	-0.3491975E+01
			X	0.1849859E+02	0.2344705E+02	0.3491975E+01
			Y	0.0000000E+00	-0.1776357E-14	-0.1478817E-15
		COORDINATE	ARC LN	0.7927643E-01	0.1754053E+00	0.1665000E+00
			X	0.0000000E+00	0.0000000E+00	
			Y	0.4346144E+00	0.3384856E+00	
		NORMAL VEC	X	-0.1000000E+01	-0.1000000E+01	
			Y	0.0000000E+00	0.0000000E+00	
113	4	DIFFUSIVE	NORMAL	-0.1568084E+02	-0.1718204E+02	-0.2735835E+01
			X	0.1568084E+02	0.1718204E+02	0.2735835E+01
			Y	0.0000000E+00	-0.1776357E-14	-0.1478817E-15
		CONVECTIVE	NORMAL	0.0000000E+00	0.0000000E+00	0.0000000E+00
			X	0.0000000E+00	0.0000000E+00	0.0000000E+00
			Y	0.0000000E+00	0.0000000E+00	0.0000000E+00
		TOTAL	NORMAL	-0.1568084E+02	-0.1718204E+02	-0.2735835E+01
			X	0.1568084E+02	0.1718204E+02	0.2735835E+01
			Y	0.0000000E+00	-0.1776357E-14	-0.1478817E-15
		COORDINATE	ARC LN	0.2457764E+00	0.3419053E+00	0.1665000E+00
			X	0.0000000E+00	0.0000000E+00	
			Y	0.6011144E+00	0.5049856E+00	
		NORMAL VEC	X	-0.1000000E+01	-0.1000000E+01	
			Y	0.0000000E+00	0.0000000E+00	
129	4	DIFFUSIVE	NORMAL	-0.1399841E+02	-0.1487845E+02	-0.2403999E+01
			X	0.1399841E+02	0.1487845E+02	0.2403999E+01
			Y	-0.1776357E-14	0.0000000E+00	-0.1478817E-15
		CONVECTIVE	NORMAL	0.0000000E+00	0.0000000E+00	0.0000000E+00
			X	0.0000000E+00	0.0000000E+00	0.0000000E+00
			Y	0.0000000E+00	0.0000000E+00	0.0000000E+00
		TOTAL	NORMAL	-0.1399841E+02	-0.1487845E+02	-0.2403999E+01
			X	0.1399841E+02	0.1487845E+02	0.2403999E+01
			Y	-0.1776357E-14	0.0000000E+00	-0.1478817E-15
		COORDINATE	ARC LN	0.4122764E+00	0.5084053E+00	0.1665000E+00
			X	0.0000000E+00	0.0000000E+00	
			Y	0.7676144E+00	0.6714856E+00	
		NORMAL VEC	X	-0.1000000E+01	-0.1000000E+01	
			Y	0.0000000E+00	0.0000000E+00	

145	4	DIFFUSIVE	NORMAL	-0.1298547E+02	-0.1351997E+02	-0.2206578E+01
			X	0.1298547E+02	0.1351997E+02	0.2206578E+01
			Y	0.1776357E-14	0.0000000E+00	0.1478817E-15
		CONVECTIVE	NORMAL	0.0000000E+00	0.0000000E+00	0.0000000E+00
			X	0.0000000E+00	0.0000000E+00	0.0000000E+00
			Y	0.0000000E+00	0.0000000E+00	0.0000000E+00
		TOTAL	NORMAL	-0.1298547E+02	-0.1351997E+02	-0.2206578E+01
			X	0.1298547E+02	0.1351997E+02	0.2206578E+01
			Y	0.1776357E-14	0.0000000E+00	0.1478817E-15
		COORDINATE	ARC LN	0.5787764E+00	0.6749053E+00	0.1665000E+00
			X	0.0000000E+00	0.0000000E+00	
			Y	0.9341144E+00	0.8379856E+00	
		NORMAL VEC	X	-0.1000000E+01	-0.1000000E+01	
			Y	0.0000000E+00	0.0000000E+00	
161	4	DIFFUSIVE	NORMAL	-0.1219225E+02	-0.1262507E+02	-0.2066042E+01
			X	0.1219225E+02	0.1262507E+02	0.2066042E+01
			Y	-0.1776357E-14	0.1776357E-14	0.0000000E+00
		CONVECTIVE	NORMAL	0.0000000E+00	0.0000000E+00	0.0000000E+00
			X	0.0000000E+00	0.0000000E+00	0.0000000E+00
			Y	0.0000000E+00	0.0000000E+00	0.0000000E+00
		TOTAL	NORMAL	-0.1219225E+02	-0.1262507E+02	-0.2066042E+01
			X	0.1219225E+02	0.1262507E+02	0.2066042E+01
			Y	-0.1776357E-14	0.1776357E-14	0.0000000E+00
		COORDINATE	ARC LN	0.7452764E+00	0.8414053E+00	0.1665000E+00
			X	0.0000000E+00	0.0000000E+00	
			Y	0.1100614E+01	0.1004486E+01	
		NORMAL VEC	X	-0.1000000E+01	-0.1000000E+01	
			Y	0.0000000E+00	0.0000000E+00	
177	4	DIFFUSIVE	NORMAL	-0.1164849E+02	-0.1194254E+02	-0.1963954E+01
			X	0.1164849E+02	0.1194254E+02	0.1963954E+01
			Y	0.0000000E+00	0.0000000E+00	0.0000000E+00
		CONVECTIVE	NORMAL	0.0000000E+00	0.0000000E+00	0.0000000E+00
			X	0.0000000E+00	0.0000000E+00	0.0000000E+00
			Y	0.0000000E+00	0.0000000E+00	0.0000000E+00
		TOTAL	NORMAL	-0.1164849E+02	-0.1194254E+02	-0.1963954E+01
			X	0.1164849E+02	0.1194254E+02	0.1963954E+01
			Y	0.0000000E+00	0.0000000E+00	0.0000000E+00
		COORDINATE	ARC LN	0.9117764E+00	0.1007905E+01	0.1665000E+00
			X	0.0000000E+00	0.0000000E+00	
			Y	0.1267114E+01	0.1170986E+01	
		NORMAL VEC	X	-0.1000000E+01	-0.1000000E+01	
			Y	0.0000000E+00	0.0000000E+00	
193	4	DIFFUSIVE	NORMAL	-0.1116643E+02	-0.1143500E+02	-0.1881569E+01
			X	0.1116643E+02	0.1143500E+02	0.1881569E+01
			Y	0.0000000E+00	0.1776357E-14	0.1478817E-15
		CONVECTIVE	NORMAL	0.0000000E+00	0.0000000E+00	0.0000000E+00
			X	0.0000000E+00	0.0000000E+00	0.0000000E+00
			Y	0.0000000E+00	0.0000000E+00	0.0000000E+00
		TOTAL	NORMAL	-0.1116643E+02	-0.1143500E+02	-0.1881569E+01
			X	0.1116643E+02	0.1143500E+02	0.1881569E+01
			Y	0.0000000E+00	0.1776357E-14	0.1478817E-15
		COORDINATE	ARC LN	0.1078276E+01	0.1174405E+01	0.1665000E+00
			X	0.0000000E+00	0.0000000E+00	
			Y	0.1433614E+01	0.1337486E+01	
		NORMAL VEC	X	-0.1000000E+01	-0.1000000E+01	
			Y	0.0000000E+00	0.0000000E+00	
209	4	DIFFUSIVE	NORMAL	-0.1081404E+02	-0.1100622E+02	-0.1816537E+01
			X	0.1081404E+02	0.1100622E+02	0.1816537E+01
			Y	0.1776357E-14	0.0000000E+00	0.1478817E-15
		CONVECTIVE	NORMAL	0.0000000E+00	0.0000000E+00	0.0000000E+00
			X	0.0000000E+00	0.0000000E+00	0.0000000E+00
			Y	0.0000000E+00	0.0000000E+00	0.0000000E+00
		TOTAL	NORMAL	-0.1081404E+02	-0.1100622E+02	-0.1816537E+01
			X	0.1081404E+02	0.1100622E+02	0.1816537E+01
			Y	0.1776357E-14	0.0000000E+00	0.1478817E-15
		COORDINATE	ARC LN	0.1244776E+01	0.1340905E+01	0.1665000E+00
			X	0.0000000E+00	0.0000000E+00	
			Y	0.1600114E+01	0.1503986E+01	
		NORMAL VEC	X	-0.1000000E+01	-0.1000000E+01	
			Y	0.0000000E+00	0.0000000E+00	
225	4	DIFFUSIVE	NORMAL	-0.1048290E+02	-0.1067093E+02	-0.1761057E+01
			X	0.1048290E+02	0.1067093E+02	0.1761057E+01
			Y	0.0000000E+00	0.0000000E+00	0.0000000E+00
		CONVECTIVE	NORMAL	0.0000000E+00	0.0000000E+00	0.0000000E+00
			X	0.0000000E+00	0.0000000E+00	0.0000000E+00

			Y	0.0000000E+00	0.0000000E+00	0.0000000E+00
		TOTAL	NORMAL	-0.1048290E+02	-0.1067093E+02	-0.1761057E+01
			X	0.1048290E+02	0.1067093E+02	0.1761057E+01
			Y	0.0000000E+00	0.0000000E+00	0.0000000E+00
		COORDINATE	ARC LN	0.1411276E+01	0.1507405E+01	0.1665000E+00
			X	0.0000000E+00	0.0000000E+00	
			Y	0.1766614E+01	0.1670486E+01	
		NORMAL VEC	X	-0.1000000E+01	-0.1000000E+01	
			Y	0.0000000E+00	0.0000000E+00	
241	4	DIFFUSIVE	NORMAL	-0.1022227E+02	-0.1036563E+02	-0.1713942E+01
			X	0.1022227E+02	0.1036563E+02	0.1713942E+01
			Y	-0.1776357E-14	0.0000000E+00	-0.1478817E-15
		CONVECTIVE	NORMAL	0.0000000E+00	0.0000000E+00	0.0000000E+00
			X	0.0000000E+00	0.0000000E+00	0.0000000E+00
			Y	0.0000000E+00	0.0000000E+00	0.0000000E+00
		TOTAL	NORMAL	-0.1022227E+02	-0.1036563E+02	-0.1713942E+01
			X	0.1022227E+02	0.1036563E+02	0.1713942E+01
			Y	-0.1776357E-14	0.0000000E+00	-0.1478817E-15
		COORDINATE	ARC LN	0.1577776E+01	0.1673905E+01	0.1665000E+00
			X	0.0000000E+00	0.0000000E+00	
			Y	0.1933114E+01	0.1836986E+01	
		NORMAL VEC	X	-0.1000000E+01	-0.1000000E+01	
			Y	0.0000000E+00	0.0000000E+00	
257	4	DIFFUSIVE	NORMAL	-0.9973800E+01	-0.1011573E+02	-0.1672453E+01
			X	0.9973800E+01	0.1011573E+02	0.1672453E+01
			Y	0.1776357E-14	-0.1776357E-14	0.4437343E-30
		CONVECTIVE	NORMAL	0.0000000E+00	0.0000000E+00	0.0000000E+00
			X	0.0000000E+00	0.0000000E+00	0.0000000E+00
			Y	0.0000000E+00	0.0000000E+00	0.0000000E+00
		TOTAL	NORMAL	-0.9973800E+01	-0.1011573E+02	-0.1672453E+01
			X	0.9973800E+01	0.1011573E+02	0.1672453E+01
			Y	0.1776357E-14	-0.1776357E-14	0.4437343E-30
		COORDINATE	ARC LN	0.1744276E+01	0.1840405E+01	0.1665000E+00
			X	0.0000000E+00	0.0000000E+00	
			Y	0.2099614E+01	0.2003486E+01	
		NORMAL VEC	X	-0.1000000E+01	-0.1000000E+01	
			Y	0.0000000E+00	0.0000000E+00	
273	4	DIFFUSIVE	NORMAL	-0.9768061E+01	-0.9882414E+01	-0.1635902E+01
			X	0.9768061E+01	0.9882414E+01	0.1635902E+01
			Y	0.0000000E+00	0.0000000E+00	0.0000000E+00
		CONVECTIVE	NORMAL	0.0000000E+00	0.0000000E+00	0.0000000E+00
			X	0.0000000E+00	0.0000000E+00	0.0000000E+00
			Y	0.0000000E+00	0.0000000E+00	0.0000000E+00
		TOTAL	NORMAL	-0.9768061E+01	-0.9882414E+01	-0.1635902E+01
			X	0.9768061E+01	0.9882414E+01	0.1635902E+01
			Y	0.0000000E+00	0.0000000E+00	0.0000000E+00
		COORDINATE	ARC LN	0.1910776E+01	0.2006905E+01	0.1665000E+00
			X	0.0000000E+00	0.0000000E+00	
			Y	0.2266114E+01	0.2169986E+01	
		NORMAL VEC	X	-0.1000000E+01	-0.1000000E+01	
			Y	0.0000000E+00	0.0000000E+00	
289	4	DIFFUSIVE	NORMAL	-0.9570175E+01	-0.9683237E+01	-0.1602847E+01
			X	0.9570175E+01	0.9683237E+01	0.1602847E+01
			Y	0.0000000E+00	0.0000000E+00	0.0000000E+00
		CONVECTIVE	NORMAL	0.0000000E+00	0.0000000E+00	0.0000000E+00
			X	0.0000000E+00	0.0000000E+00	0.0000000E+00
			Y	0.0000000E+00	0.0000000E+00	0.0000000E+00
		TOTAL	NORMAL	-0.9570175E+01	-0.9683237E+01	-0.1602847E+01
			X	0.9570175E+01	0.9683237E+01	0.1602847E+01
			Y	0.0000000E+00	0.0000000E+00	0.0000000E+00
		COORDINATE	ARC LN	0.2077276E+01	0.2173405E+01	0.1665000E+00
			X	0.0000000E+00	0.0000000E+00	
			Y	0.2432614E+01	0.2336486E+01	
		NORMAL VEC	X	-0.1000000E+01	-0.1000000E+01	
			Y	0.0000000E+00	0.0000000E+00	
305	4	DIFFUSIVE	NORMAL	-0.9401387E+01	-0.9495802E+01	-0.1573191E+01
			X	0.9401387E+01	0.9495802E+01	0.1573191E+01
			Y	0.0000000E+00	0.1776357E-14	0.1478817E-15
		CONVECTIVE	NORMAL	0.0000000E+00	0.0000000E+00	0.0000000E+00
			X	0.0000000E+00	0.0000000E+00	0.0000000E+00
			Y	0.0000000E+00	0.0000000E+00	0.0000000E+00
		TOTAL	NORMAL	-0.9401387E+01	-0.9495802E+01	-0.1573191E+01
			X	0.9401387E+01	0.9495802E+01	0.1573191E+01
			Y	0.0000000E+00	0.1776357E-14	0.1478817E-15
		COORDINATE	ARC LN	0.2243776E+01	0.2339905E+01	0.1665000E+00
			X	0.0000000E+00	0.0000000E+00	

			Y	0.2599114E+01	0.2502986E+01	
		NORMAL VEC	X	-0.1000000E+01	-0.1000000E+01	
			Y	0.0000000E+00	0.0000000E+00	
321	4	DIFFUSIVE	NORMAL	-0.9237741E+01	-0.9331139E+01	-0.1565859E+01
			X	0.9237741E+01	0.9331139E+01	0.1565859E+01
			Y	-0.1776357E-14	-0.1776357E-14	-0.2957634E-15
		CONVECTIVE	NORMAL	0.0000000E+00	0.0000000E+00	0.0000000E+00
			X	0.0000000E+00	0.0000000E+00	0.0000000E+00
			Y	0.0000000E+00	0.0000000E+00	0.0000000E+00
		TOTAL	NORMAL	-0.9237741E+01	-0.9331139E+01	-0.1565859E+01
			X	0.9237741E+01	0.9331139E+01	0.1565859E+01
			Y	-0.1776357E-14	-0.1776357E-14	-0.2957634E-15
		COORDINATE	ARC LN	0.2410276E+01	0.2506405E+01	0.1665000E+00
			X	0.0000000E+00	0.0000000E+00	
			Y	0.2765614E+01	0.2669486E+01	
		NORMAL VEC	X	-0.1000000E+01	-0.1000000E+01	
			Y	0.0000000E+00	0.0000000E+00	
337	4	DIFFUSIVE	NORMAL	-0.9095121E+01	-0.9174839E+01	-0.1520974E+01
			X	0.9095121E+01	0.9174839E+01	0.1520974E+01
			Y	0.0000000E+00	-0.1776357E-14	-0.1478817E-15
		CONVECTIVE	NORMAL	0.0000000E+00	0.0000000E+00	0.0000000E+00
			X	0.0000000E+00	0.0000000E+00	0.0000000E+00
			Y	0.0000000E+00	0.0000000E+00	0.0000000E+00
		TOTAL	NORMAL	-0.9095121E+01	-0.9174839E+01	-0.1520974E+01
			X	0.9095121E+01	0.9174839E+01	0.1520974E+01
			Y	0.0000000E+00	-0.1776357E-14	-0.1478817E-15
		COORDINATE	ARC LN	0.2576776E+01	0.2672905E+01	0.1665000E+00
			X	0.0000000E+00	0.0000000E+00	
			Y	0.2932114E+01	0.2835986E+01	
		NORMAL VEC	X	-0.1000000E+01	-0.1000000E+01	
			Y	0.0000000E+00	0.0000000E+00	
353	4	DIFFUSIVE	NORMAL	-0.8956193E+01	-0.9035037E+01	-0.1497770E+01
			X	0.8956193E+01	0.9035037E+01	0.1497770E+01
			Y	0.0000000E+00	0.0000000E+00	0.0000000E+00
		CONVECTIVE	NORMAL	0.0000000E+00	0.0000000E+00	0.0000000E+00
			X	0.0000000E+00	0.0000000E+00	0.0000000E+00
			Y	0.0000000E+00	0.0000000E+00	0.0000000E+00
		TOTAL	NORMAL	-0.8956193E+01	-0.9035037E+01	-0.1497770E+01
			X	0.8956193E+01	0.9035037E+01	0.1497770E+01
			Y	0.0000000E+00	0.0000000E+00	0.0000000E+00
		COORDINATE	ARC LN	0.2743276E+01	0.2839405E+01	0.1665000E+00
			X	0.0000000E+00	0.0000000E+00	
			Y	0.3098614E+01	0.3002486E+01	
		NORMAL VEC	X	-0.1000000E+01	-0.1000000E+01	
			Y	0.0000000E+00	0.0000000E+00	
369	4	DIFFUSIVE	NORMAL	-0.8833072E+01	-0.8901020E+01	-0.1476363E+01
			X	0.8833072E+01	0.8901020E+01	0.1476363E+01
			Y	0.0000000E+00	0.1776357E-14	0.1478817E-15
		CONVECTIVE	NORMAL	0.0000000E+00	0.0000000E+00	0.0000000E+00
			X	0.0000000E+00	0.0000000E+00	0.0000000E+00
			Y	0.0000000E+00	0.0000000E+00	0.0000000E+00
		TOTAL	NORMAL	-0.8833072E+01	-0.8901020E+01	-0.1476363E+01
			X	0.8833072E+01	0.8901020E+01	0.1476363E+01
			Y	0.0000000E+00	0.1776357E-14	0.1478817E-15
		COORDINATE	ARC LN	0.2909776E+01	0.3005905E+01	0.1665000E+00
			X	0.0000000E+00	0.0000000E+00	
			Y	0.3265114E+01	0.3168986E+01	
		NORMAL VEC	X	-0.1000000E+01	-0.1000000E+01	
			Y	0.0000000E+00	0.0000000E+00	
385	4	DIFFUSIVE	NORMAL	-0.8712907E+01	-0.8779866E+01	-0.1456273E+01
			X	0.8712907E+01	0.8779866E+01	0.1456273E+01
			Y	-0.1776357E-14	0.1776357E-14	-0.8874685E-30
		CONVECTIVE	NORMAL	0.0000000E+00	0.0000000E+00	0.0000000E+00
			X	0.0000000E+00	0.0000000E+00	0.0000000E+00
			Y	0.0000000E+00	0.0000000E+00	0.0000000E+00
		TOTAL	NORMAL	-0.8712907E+01	-0.8779866E+01	-0.1456273E+01
			X	0.8712907E+01	0.8779866E+01	0.1456273E+01
			Y	-0.1776357E-14	0.1776357E-14	-0.8874685E-30
		COORDINATE	ARC LN	0.3076276E+01	0.3172405E+01	0.1665000E+00
			X	0.0000000E+00	0.0000000E+00	
			Y	0.3431614E+01	0.3335486E+01	
		NORMAL VEC	X	-0.1000000E+01	-0.1000000E+01	
			Y	0.0000000E+00	0.0000000E+00	
401	4	DIFFUSIVE	NORMAL	-0.8604989E+01	-0.8662453E+01	-0.1437515E+01
			X	0.8604989E+01	0.8662453E+01	0.1437515E+01

			Y	0.1776357E-14	0.0000000E+00	0.1478817E-15
		CONVECTIVE	NORMAL	0.0000000E+00	0.0000000E+00	0.0000000E+00
			X	0.0000000E+00	0.0000000E+00	0.0000000E+00
			Y	0.0000000E+00	0.0000000E+00	0.0000000E+00
		TOTAL	NORMAL	-0.8604989E+01	-0.8662453E+01	-0.1437515E+01
			X	0.8604989E+01	0.8662453E+01	0.1437515E+01
			Y	0.1776357E-14	0.0000000E+00	0.1478817E-15
		COORDINATE	ARC LN	0.3242776E+01	0.3338905E+01	0.1665000E+00
			X	0.0000000E+00	0.0000000E+00	
			Y	0.3598114E+01	0.3501986E+01	
		NORMAL VEC	X	-0.1000000E+01	-0.1000000E+01	
			Y	0.0000000E+00	0.0000000E+00	
417	4	DIFFUSIVE	NORMAL	-0.8499643E+01	-0.8555692E+01	-0.1419857E+01
			X	0.8499643E+01	0.8555692E+01	0.1419857E+01
			Y	0.1776357E-14	0.0000000E+00	0.1478817E-15
		CONVECTIVE	NORMAL	0.0000000E+00	0.0000000E+00	0.0000000E+00
			X	0.0000000E+00	0.0000000E+00	0.0000000E+00
			Y	0.0000000E+00	0.0000000E+00	0.0000000E+00
		TOTAL	NORMAL	-0.8499643E+01	-0.8555692E+01	-0.1419857E+01
			X	0.8499643E+01	0.8555692E+01	0.1419857E+01
			Y	0.1776357E-14	0.0000000E+00	0.1478817E-15
		COORDINATE	ARC LN	0.3409276E+01	0.3505405E+01	0.1665000E+00
			X	0.0000000E+00	0.0000000E+00	
			Y	0.3764614E+01	0.3668486E+01	
		NORMAL VEC	X	-0.1000000E+01	-0.1000000E+01	
			Y	0.0000000E+00	0.0000000E+00	
433	4	DIFFUSIVE	NORMAL	-0.8403987E+01	-0.8450971E+01	-0.1403175E+01
			X	0.8403987E+01	0.8450971E+01	0.1403175E+01
			Y	-0.1776357E-14	-0.1776357E-14	-0.2957634E-15
		CONVECTIVE	NORMAL	0.0000000E+00	0.0000000E+00	0.0000000E+00
			X	0.0000000E+00	0.0000000E+00	0.0000000E+00
			Y	0.0000000E+00	0.0000000E+00	0.0000000E+00
		TOTAL	NORMAL	-0.8403987E+01	-0.8450971E+01	-0.1403175E+01
			X	0.8403987E+01	0.8450971E+01	0.1403175E+01
			Y	-0.1776357E-14	-0.1776357E-14	-0.2957634E-15
		COORDINATE	ARC LN	0.3575776E+01	0.3671905E+01	0.1665000E+00
			X	0.0000000E+00	0.0000000E+00	
			Y	0.3931114E+01	0.3834986E+01	
		NORMAL VEC	X	-0.1000000E+01	-0.1000000E+01	
			Y	0.0000000E+00	0.0000000E+00	
449	4	DIFFUSIVE	NORMAL	-0.8310668E+01	-0.8355617E+01	-0.1387468E+01
			X	0.8310668E+01	0.8355617E+01	0.1387468E+01
			Y	-0.1776357E-14	-0.1776357E-14	-0.2957634E-15
		CONVECTIVE	NORMAL	0.0000000E+00	0.0000000E+00	0.0000000E+00
			X	0.0000000E+00	0.0000000E+00	0.0000000E+00
			Y	0.0000000E+00	0.0000000E+00	0.0000000E+00
		TOTAL	NORMAL	-0.8310668E+01	-0.8355617E+01	-0.1387468E+01
			X	0.8310668E+01	0.8355617E+01	0.1387468E+01
			Y	-0.1776357E-14	-0.1776357E-14	-0.2957634E-15
		COORDINATE	ARC LN	0.3742276E+01	0.3838405E+01	0.1665000E+00
			X	0.0000000E+00	0.0000000E+00	
			Y	0.4097614E+01	0.4001486E+01	
		NORMAL VEC	X	-0.1000000E+01	-0.1000000E+01	
			Y	0.0000000E+00	0.0000000E+00	
465	4	DIFFUSIVE	NORMAL	-0.8224606E+01	-0.8261193E+01	-0.1372443E+01
			X	0.8224606E+01	0.8261193E+01	0.1372443E+01
			Y	0.0000000E+00	0.0000000E+00	0.0000000E+00
		CONVECTIVE	NORMAL	0.0000000E+00	0.0000000E+00	0.0000000E+00
			X	0.0000000E+00	0.0000000E+00	0.0000000E+00
			Y	0.0000000E+00	0.0000000E+00	0.0000000E+00
		TOTAL	NORMAL	-0.8224606E+01	-0.8261193E+01	-0.1372443E+01
			X	0.8224606E+01	0.8261193E+01	0.1372443E+01
			Y	0.0000000E+00	0.0000000E+00	0.0000000E+00
		COORDINATE	ARC LN	0.3908776E+01	0.4004905E+01	0.1665000E+00
			X	0.0000000E+00	0.0000000E+00	
			Y	0.4264114E+01	0.4167986E+01	
		NORMAL VEC	X	-0.1000000E+01	-0.1000000E+01	
			Y	0.0000000E+00	0.0000000E+00	
481	4	DIFFUSIVE	NORMAL	-0.8139584E+01	-0.8175079E+01	-0.1358196E+01
			X	0.8139584E+01	0.8175079E+01	0.1358196E+01
			Y	-0.1776357E-14	0.1776357E-14	-0.1824241E-29
		CONVECTIVE	NORMAL	0.0000000E+00	0.0000000E+00	0.0000000E+00
			X	0.0000000E+00	0.0000000E+00	0.0000000E+00
			Y	0.0000000E+00	0.0000000E+00	0.0000000E+00
		TOTAL	NORMAL	-0.8139584E+01	-0.8175079E+01	-0.1358196E+01
			X	0.8139584E+01	0.8175079E+01	0.1358196E+01

			Y	-0.1776357E-14	0.1776357E-14	-0.1824241E-29
		COORDINATE	ARC LN	0.4075276E+01	0.4171405E+01	0.1665000E+00
			X	0.0000000E+00	0.0000000E+00	
			Y	0.4430614E+01	0.4334486E+01	
		NORMAL VEC	X	-0.1000000E+01	-0.1000000E+01	
			Y	0.0000000E+00	0.0000000E+00	
497	4	DIFFUSIVE	NORMAL	-0.8058717E+01	-0.8088951E+01	-0.1344293E+01
			X	0.8058717E+01	0.8088951E+01	0.1344293E+01
			Y	-0.1776357E-14	0.0000000E+00	-0.1478817E-15
		CONVECTIVE	NORMAL	0.0000000E+00	0.0000000E+00	0.0000000E+00
			X	0.0000000E+00	0.0000000E+00	0.0000000E+00
			Y	0.0000000E+00	0.0000000E+00	0.0000000E+00
		TOTAL	NORMAL	-0.8058717E+01	-0.8088951E+01	-0.1344293E+01
			X	0.8058717E+01	0.8088951E+01	0.1344293E+01
			Y	-0.1776357E-14	0.0000000E+00	-0.1478817E-15
		COORDINATE	ARC LN	0.4241776E+01	0.4337905E+01	0.1665000E+00
			X	0.0000000E+00	0.0000000E+00	
			Y	0.4597114E+01	0.4500986E+01	
		NORMAL VEC	X	-0.1000000E+01	-0.1000000E+01	
			Y	0.0000000E+00	0.0000000E+00	
513	4	DIFFUSIVE	NORMAL	-0.7980460E+01	-0.8011879E+01	-0.1331362E+01
			X	0.7980460E+01	0.8011879E+01	0.1331362E+01
			Y	-0.1776357E-14	0.0000000E+00	-0.1478817E-15
		CONVECTIVE	NORMAL	0.0000000E+00	0.0000000E+00	0.0000000E+00
			X	0.0000000E+00	0.0000000E+00	0.0000000E+00
			Y	0.0000000E+00	0.0000000E+00	0.0000000E+00
		TOTAL	NORMAL	-0.7980460E+01	-0.8011879E+01	-0.1331362E+01
			X	0.7980460E+01	0.8011879E+01	0.1331362E+01
			Y	-0.1776357E-14	0.0000000E+00	-0.1478817E-15
		COORDINATE	ARC LN	0.4408276E+01	0.4504405E+01	0.1665000E+00
			X	0.0000000E+00	0.0000000E+00	
			Y	0.4763614E+01	0.4667486E+01	
		NORMAL VEC	X	-0.1000000E+01	-0.1000000E+01	
			Y	0.0000000E+00	0.0000000E+00	
529	4	DIFFUSIVE	NORMAL	-0.7920628E+01	-0.7940761E+01	-0.1320461E+01
			X	0.7920628E+01	0.7940761E+01	0.1320461E+01
			Y	0.0000000E+00	0.1776357E-14	0.1478817E-15
		CONVECTIVE	NORMAL	0.0000000E+00	0.0000000E+00	0.0000000E+00
			X	0.0000000E+00	0.0000000E+00	0.0000000E+00
			Y	0.0000000E+00	0.0000000E+00	0.0000000E+00
		TOTAL	NORMAL	-0.7920628E+01	-0.7940761E+01	-0.1320461E+01
			X	0.7920628E+01	0.7940761E+01	0.1320461E+01
			Y	0.0000000E+00	0.1776357E-14	0.1478817E-15
		COORDINATE	ARC LN	0.4574776E+01	0.4670905E+01	0.1665000E+00
			X	0.0000000E+00	0.0000000E+00	
			Y	0.4930114E+01	0.4833986E+01	
		NORMAL VEC	X	-0.1000000E+01	-0.1000000E+01	
			Y	0.0000000E+00	0.0000000E+00	
545	4	DIFFUSIVE	NORMAL	-0.7959458E+01	-0.7912975E+01	-0.1129720E+01
			X	0.7959458E+01	0.7912975E+01	0.1129720E+01
			Y	0.0000000E+00	0.0000000E+00	0.0000000E+00
		CONVECTIVE	NORMAL	0.0000000E+00	0.0000000E+00	0.0000000E+00
			X	0.0000000E+00	0.0000000E+00	0.0000000E+00
			Y	0.0000000E+00	0.0000000E+00	0.0000000E+00
		TOTAL	NORMAL	-0.7959458E+01	-0.7912975E+01	-0.1129720E+01
			X	0.7959458E+01	0.7912975E+01	0.1129720E+01
			Y	0.0000000E+00	0.0000000E+00	0.0000000E+00
		COORDINATE	ARC LN	0.4736173E+01	0.4818359E+01	0.1423500E+00
			X	0.0000000E+00	0.0000000E+00	
			Y	0.5077568E+01	0.4995382E+01	
		NORMAL VEC	X	-0.1000000E+01	-0.1000000E+01	
			Y	0.0000000E+00	0.0000000E+00	
561	4	DIFFUSIVE	NORMAL	-0.8296006E+01	-0.8104746E+01	-0.1167323E+01
			X	0.8296006E+01	0.8104746E+01	0.1167323E+01
			Y	0.0000000E+00	0.0000000E+00	0.0000000E+00
		CONVECTIVE	NORMAL	0.0000000E+00	0.0000000E+00	0.0000000E+00
			X	0.0000000E+00	0.0000000E+00	0.0000000E+00
			Y	0.0000000E+00	0.0000000E+00	0.0000000E+00
		TOTAL	NORMAL	-0.8296006E+01	-0.8104746E+01	-0.1167323E+01
			X	0.8296006E+01	0.8104746E+01	0.1167323E+01
			Y	0.0000000E+00	0.0000000E+00	0.0000000E+00
		COORDINATE	ARC LN	0.4878523E+01	0.4960709E+01	0.1423500E+00
			X	0.0000000E+00	0.0000000E+00	
			Y	0.5219918E+01	0.5137732E+01	
		NORMAL VEC	X	-0.1000000E+01	-0.1000000E+01	
			Y	0.0000000E+00	0.0000000E+00	

```
T O T A L   H E A T   F L O W:     DIFFUSIVE =  -0.5261981E+02
                                  CONVECTIVE =   0.0000000E+00
                                  TOTAL     =  -0.5261981E+02

T O T A L   S I D E   L E N G T H:                0.4996000E+01

A V E R A G E   H E A T   F L U X:  DIFFUSIVE =  -0.1053239E+02
                                  CONVECTIVE =   0.0000000E+00
                                  TOTAL     =  -0.1053239E+02

***    6.760 COMMAND EXECUTION TIME
```

N O D A L - C O O R D I N A T E   P L O T

```
        NODAL DEGREE OF FREEDOM  . . . . . . . . . . . . . . . . . . . (NDEG)   =        6
            = 1 , X COMPONENT OF VELOCITY , U
            = 2 , Y COMPONENT OF VELOCITY , V
            = 3 , Z COMPONENT OF VELOCITY , W
            = 4 , SPEED ( SQRT(U*U+V*V+W*W) )
            = 5 , PRESSURE
            = 6 , TEMPERATURE
            = 7 , TURBULENT KINETIC ENERGY
            = 8 , TURBULENT DISSIPATION
            = 9 , STREAMLINE
            =10 , VORTICITY
            =11 , USER DEFINED VARIABLE
            =12 , X COORDINATE
            =13 , Y COORDINATE
            =14 , Z COORDINATE
            =15 , TURBULENT VISCOSITY
            =16 , NON-NEWTONIAN VISCOSITY
            =17 , SPECIES 1
            =18 , SPECIES 2
            =19 , DENSITY
            =20 , CELL REYNOLDS NO.
            =21 , USER VECTOR FUNCTION MAGNITUDE
            =22 , SHEAR RATE
            =23 , FLUX (3-D ONLY)
            =24 , FLOWRATE (3-D ONLY)
            =25 , COEFFICIENT (3-D ONLY)
            =26 , STRESS MAGNITUDE (3-D ONLY)
            =27 , CELL PECLET NO. (TEMPERATURE)
            =28 , CELL PECLET NO. (SPECIES1)
            =29 , CELL PECLET NO. (SPECIES2)

        LINE DEFINITION OPTION FLAG  . . . . . . . . . . . . . . . (LTYPE)   =        2
            < 0 , PREVIOUS LINE, OPPOSITE DIRECTION
            = 1 , NODAL POINT AND A VECTOR
            = 2 , POINT AND A VECTOR
            = 3 , TWO NODAL POINTS
            = 4 , TWO POINTS
            = 5 , THREE NODAL POINTS
            = 6 , THREE POINTS
            = 7 , LINE COEFFICIENTS
            = 8 , PARALLEL TO EXISTING LINE THROUGH NODE
            = 9 , PARALLEL TO EXISTING LINE THROUGH POINT
            =10 , PERPENDICULAR TO EXISTING PLANE THROUGH NODE
            =11 , PERPENDICULAR TO EXISTING PLANE THROUGH POINT
            =12 , LIST OF NODES
            =13 , BOUNDARY ELEMENT GROUP

        SYMBOL FLAG  . . . . . . . . . . . . . . . . . . . . . . . (LSYMB)   =        0
            =-1 , PLOT SYMBOL AT FIRST STEP ONLY
            = 0 , PLOT SYMBOLS AT EACH TIME STEP
            = 1 , PLOT SYMBOL AT LAST TIME STEP ONLY
            = 2 , NO SYMBOLS PLOTTED AT EACH TIME STEP

        GRID LINE FLAG . . . . . . . . . . . . . . . . . . . . . . (ILINE)   =        0
            = 0 , NO GRID LINES
            = 1 , HORIZONTAL AND VERTICAL GRID LINES
            = 2 , VERTICAL GRID LINES
            = 3 , HORIZONTAL GRID LINES
```

LINE DEFINITION

POINT (X COORDINATE) . . . . . (POINT(1))=0.0000E+00

POINT (Y COORDINATE) . . . . . (POINT(2))=0.2752E+01

POINT (Z COORDINATE) . . . . . (POINT(3))=0.0000E+00

VECTOR (X COMPONENT) . . . . . (VECTOR(1)=0.1000E+01

VECTOR (Y COMPONENT) . . . . . (VECTOR(2)=0.0000E+00

VECTOR (Z COMPONENT) . . . . . (VECTOR(3)=0.0000E+00

RESULTING LINE : POINT : 0.0000E+00 0.2752E+01 0.0000E+00
DIRECTION : 1.0000 0.0000 0.0000

MAXIMUM STORAGE (INTEGER WORDS) REQUIRED FOR EXECUTION = 1288425

POINT	COORDINATE	VALUE
1	0.00000E+00	0.10000E+01
2	0.50144E-02	0.95352E+00
3	0.85543E-02	0.92099E+00
4	0.12094E-01	0.88856E+00
5	0.17109E-01	0.84223E+00
6	0.23046E-01	0.78799E+00
7	0.27238E-01	0.75003E+00
8	0.31430E-01	0.71305E+00
9	0.37368E-01	0.66026E+00
10	0.44399E-01	0.60084E+00
11	0.49362E-01	0.55921E+00
12	0.54326E-01	0.52078E+00
13	0.61357E-01	0.46605E+00
14	0.69683E-01	0.40875E+00
15	0.75560E-01	0.36853E+00
16	0.81438E-01	0.33445E+00
17	0.89764E-01	0.28605E+00
18	0.99623E-01	0.24002E+00
19	0.10658E+00	0.20791E+00
20	0.11354E+00	0.18384E+00
21	0.12340E+00	0.14890E+00
22	0.13508E+00	0.11957E+00
23	0.14332E+00	0.99940E-01
24	0.15156E+00	0.86807E-01
25	0.16323E+00	0.67914E-01
26	0.17706E+00	0.54298E-01
27	0.18682E+00	0.43663E-01
28	0.19658E+00	0.35710E-01
29	0.21040E+00	0.27694E-01
30	0.21477E+00	0.15812E-01
31	0.25909E+00	0.10978E-01
32	0.26923E+00	0.88553E-02
33	0.32810E+00	0.36991E-02
34	0.38697E+00	0.10780E-02
35	0.39711E+00	0.10051E-02
36	0.41143E+00	0.84245E-03
37	0.44580E+00	0.40069E-03
38	0.46900E+00	0.26379E-03
39	0.48539E+00	0.19019E-03
40	0.50177E+00	0.16053E-03
41	0.52497E+00	0.86553E-04
42	0.54818E+00	0.52283E-04
43	0.56456E+00	0.36990E-04
44	0.58094E+00	0.30503E-04
45	0.60414E+00	0.16474E-04
46	0.62735E+00	0.10161E-04
47	0.64373E+00	0.69916E-05
48	0.66011E+00	0.56488E-05
49	0.68331E+00	0.31422E-05
50	0.70652E+00	0.19857E-05
51	0.72290E+00	0.13451E-05
52	0.73928E+00	0.10758E-05
53	0.76249E+00	0.60722E-06
54	0.78569E+00	0.38770E-06
55	0.80207E+00	0.26014E-06

```
      56      0.81845E+00     0.20672E-06
      57      0.84166E+00     0.11600E-06
      58      0.86486E+00     0.73110E-07
      59      0.88124E+00     0.47835E-07
      60      0.89762E+00     0.37247E-07
      61      0.92083E+00     0.19281E-07
      62      0.94403E+00     0.10739E-07
      63      0.96041E+00     0.57206E-08
      64      0.97680E+00     0.36123E-08
      65      0.10000E+01     0.00000E+00

***   10.440 COMMAND EXECUTION TIME
```

N O D A L - C O O R D I N A T E P L O T

```
         NODAL DEGREE OF FREEDOM . . . . . . . . . . . . . . . . . . (NDEG)   =        2
            = 1 , X COMPONENT OF VELOCITY , U
            = 2 , Y COMPONENT OF VELOCITY , V
            = 3 , Z COMPONENT OF VELOCITY , W
            = 4 , SPEED ( SQRT(U*U+V*V+W*W) )
            = 5 , PRESSURE
            = 6 , TEMPERATURE
            = 7 , TURBULENT KINETIC ENERGY
            = 8 , TURBULENT DISSIPATION
            = 9 , STREAMLINE
            =10 , VORTICITY
            =11 , USER DEFINED VARIABLE
            =12 , X COORDINATE
            =13 , Y COORDINATE
            =14 , Z COORDINATE
            =15 , TURBULENT VISCOSITY
            =16 , NON-NEWTONIAN VISCOSITY
            =17 , SPECIES 1
            =18 , SPECIES 2
            =19 , DENSITY
            =20 , CELL REYNOLDS NO.
            =21 , USER VECTOR FUNCTION MAGNITUDE
            =22 , SHEAR RATE
            =23 , FLUX (3-D ONLY)
            =24 , FLOWRATE (3-D ONLY)
            =25 , COEFFICIENT (3-D ONLY)
            =26 , STRESS MAGNITUDE (3-D ONLY)
            =27 , CELL PECLET NO. (TEMPERATURE)
            =28 , CELL PECLET NO. (SPECIES1)
            =29 , CELL PECLET NO. (SPECIES2)

         LINE DEFINITION OPTION FLAG . . . . . . . . . . . . . . . . (LTYPE)   =        2
            < 0 , PREVIOUS LINE, OPPOSITE DIRECTION
            = 1 , NODAL POINT AND A VECTOR
            = 2 , POINT AND A VECTOR
            = 3 , TWO NODAL POINTS
            = 4 , TWO POINTS
            = 5 , THREE NODAL POINTS
            = 6 , THREE POINTS
            = 7 , LINE COEFFICIENTS
            = 8 , PARALLEL TO EXISTING LINE THROUGH NODE
            = 9 , PARALLEL TO EXISTING LINE THROUGH POINT
            =10 , PERPENDICULAR TO EXISTING PLANE THROUGH NODE
            =11 , PERPENDICULAR TO EXISTING PLANE THROUGH POINT
            =12 , LIST OF NODES
            =13 , BOUNDARY ELEMENT GROUP

         SYMBOL FLAG . . . . . . . . . . . . . . . . . . . . . . . . (LSYMB)   =        0
            =-1 , PLOT SYMBOL AT FIRST STEP ONLY
            = 0 , PLOT SYMBOLS AT EACH TIME STEP
            = 1 , PLOT SYMBOL AT LAST TIME STEP ONLY
            = 2 , NO SYMBOLS PLOTTED AT EACH TIME STEP

         GRID LINE FLAG . . . . . . . . . . . . . . . . . . . . . . . (ILINE)   =        0
            = 0 , NO GRID LINES
            = 1 , HORIZONTAL AND VERTICAL GRID LINES
            = 2 , VERTICAL GRID LINES
            = 3 , HORIZONTAL GRID LINES
```

LINE DEFINITION

```
          POINT (X COORDINATE) . . . . . (POINT(1))=0.0000E+00

          POINT (Y COORDINATE) . . . . . (POINT(2))=0.2752E+01

          POINT (Z COORDINATE) . . . . . (POINT(3))=0.0000E+00

          VECTOR (X COMPONENT) . . . . . (VECTOR(1)=0.1000E+01

          VECTOR (Y COMPONENT) . . . . . (VECTOR(2)=0.0000E+00

          VECTOR (Z COMPONENT) . . . . . (VECTOR(3)=0.0000E+00

RESULTING LINE  :  POINT     :   0.0000E+00  0.2752E+01  0.0000E+00
                   DIRECTION :       1.0000      0.0000      0.0000

   MAXIMUM STORAGE (INTEGER WORDS) REQUIRED FOR EXECUTION =  1288425
```

POINT	COORDINATE	VALUE
1	0.00000E+00	0.00000E+00
2	0.50144E-02	0.17783E+00
3	0.85543E-02	0.30448E+00
4	0.12094E-01	0.40076E+00
5	0.17109E-01	0.53576E+00
6	0.23046E-01	0.64628E+00
7	0.27238E-01	0.72541E+00
8	0.31430E-01	0.77215E+00
9	0.37368E-01	0.83678E+00
10	0.44399E-01	0.86570E+00
11	0.49362E-01	0.88717E+00
12	0.54326E-01	0.88109E+00
13	0.61357E-01	0.87141E+00
14	0.69683E-01	0.82761E+00
15	0.75560E-01	0.79718E+00
16	0.81438E-01	0.75279E+00
17	0.89764E-01	0.68980E+00
18	0.99623E-01	0.60841E+00
19	0.10658E+00	0.55025E+00
20	0.11354E+00	0.49321E+00
21	0.12340E+00	0.41618E+00
22	0.13508E+00	0.33769E+00
23	0.14332E+00	0.28072E+00
24	0.15156E+00	0.23586E+00
25	0.16323E+00	0.17276E+00
26	0.17706E+00	0.11854E+00
27	0.18682E+00	0.79775E-01
28	0.19658E+00	0.51946E-01
29	0.21040E+00	0.20825E-01
30	0.24477E+00	-.12612E-01
31	0.25909E+00	-.33013E-01
32	0.26923E+00	-.28159E-01
33	0.32810E+00	0.00000E+00
34	0.38697E+00	-.12088E-01
35	0.39711E+00	-.14172E-01
36	0.41143E+00	-.14106E-01
37	0.44580E+00	-.12336E-01
38	0.46900E+00	-.10588E-01
39	0.48539E+00	-.90646E-02
40	0.50177E+00	-.60789E-02
41	0.52497E+00	-.42307E-02
42	0.54818E+00	-.30460E-02
43	0.56456E+00	-.20882E-02
44	0.58094E+00	-.14442E-02
45	0.60414E+00	-.98718E-03
46	0.62735E+00	-.69288E-03
47	0.64373E+00	-.43290E-03
48	0.66011E+00	-.31997E-03
49	0.68331E+00	-.20209E-03
50	0.70652E+00	-.12637E-03
51	0.72290E+00	-.79588E-04
52	0.73928E+00	-.61442E-04
53	0.76249E+00	-.33210E-04
54	0.78569E+00	-.15244E-04
55	0.80207E+00	-.89345E-05
56	0.81845E+00	-.76969E-05
57	0.84166E+00	-.18255E-05
58	0.86486E+00	0.17303E-05

```
      59      0.88124E+00      0.12803E-05
      60      0.89762E+00      0.30508E-06
      61      0.92083E+00      0.10524E-05
      62      0.94403E+00      0.14734E-05
      63      0.96041E+00      0.62944E-06
      64      0.97680E+00      0.66152E-07
      65      0.10000E+01      0.00000E+00

***   16.250 COMMAND EXECUTION TIME
```

N O D A L - C O O R D I N A T E P L O T

```
NODAL DEGREE OF FREEDOM . . . . . (NDEG)  =  2
    = 1 , X COMPONENT OF VELOCITY , U
    = 2 , Y COMPONENT OF VELOCITY , V
    = 3 , Z COMPONENT OF VELOCITY , W
    = 4 , SPEED ( SQRT(U*U+V*V+W*W) )
    = 5 , PRESSURE
    = 6 , TEMPERATURE
    = 7 , TURBULENT KINETIC ENERGY
    = 8 , TURBULENT DISSIPATION
    = 9 , STREAMLINE
    =10 , VORTICITY
    =11 , USER DEFINED VARIABLE
    =12 , X COORDINATE
    =13 , Y COORDINATE
    =14 , Z COORDINATE
    =15 , TURBULENT VISCOSITY
    =16 , NON-NEWTONIAN VISCOSITY
    =17 , SPECIES 1
    =18 , SPECIES 2
    =19 , DENSITY
    =20 , CELL REYNOLDS NO.
    =21 , USER VECTOR FUNCTION MAGNITUDE
    =22 , SHEAR RATE
    =23 , FLUX (3-D ONLY)
    =24 , FLOWRATE (3-D ONLY)
    =25 , COEFFICIENT (3-D ONLY)
    =26 , STRESS MAGNITUDE (3-D ONLY)
    =27 , CELL PECLET NO. (TEMPERATURE)
    =28 , CELL PECLET NO. (SPECIES1)
    =29 , CELL PECLET NO. (SPECIES2)

LINE DEFINITION OPTION FLAG . . . . . (LTYPE)  =  2
    < 0 , PREVIOUS LINE, OPPOSITE DIRECTION
    = 1 , NODAL POINT AND A VECTOR
    = 2 , POINT AND A VECTOR
    = 3 , TWO NODAL POINTS
    = 4 , TWO POINTS
    = 5 , THREE NODAL POINTS
    = 6 , THREE POINTS
    = 7 , LINE COEFFICIENTS
    = 8 , PARALLEL TO EXISTING LINE THROUGH NODE
    = 9 , PARALLEL TO EXISTING LINE THROUGH POINT
    =10 , PERPENDICULAR TO EXISTING PLANE THROUGH NODE
    =11 , PERPENDICULAR TO EXISTING PLANE THROUGH POINT
    =12 , LIST OF NODES
    =13 , BOUNDARY ELEMENT GROUP

SYMBOL FLAG . . . . . (LSYMB)  =  0
    =-1 , PLOT SYMBOL AT FIRST STEP ONLY
    = 0 , PLOT SYMBOLS AT EACH TIME STEP
    = 1 , PLOT SYMBOL AT LAST TIME STEP ONLY
    = 2 , NO SYMBOLS PLOTTED AT EACH TIME STEP

GRID LINE FLAG . . . . . (ILINE)  =  0
    = 0 , NO GRID LINES
    = 1 , HORIZONTAL AND VERTICAL GRID LINES
    = 2 , VERTICAL GRID LINES
    = 3 , HORIZONTAL GRID LINES
```

LINE DEFINITION

```
          POINT (X COORDINATE) . . . . . (POINT(1))=0.0000E+00

          POINT (Y COORDINATE) . . . . . (POINT(2))=0.1250E+01

          POINT (Z COORDINATE) . . . . . (POINT(3))=0.0000E+00

          VECTOR (X COMPONENT) . . . . . (VECTOR(1)=0.1000E+01

          VECTOR (Y COMPONENT) . . . . . (VECTOR(2)=0.0000E+00

          VECTOR (Z COMPONENT) . . . . . (VECTOR(3)=0.0000E+00

RESULTING LINE  :  POINT     :   0.0000E+00  0.1250E+01  0.0000E+00
                   DIRECTION :       1.0000      0.0000      0.0000

   MAXIMUM STORAGE (INTEGER WORDS) REQUIRED FOR EXECUTION =  1288425
```

POINT	COORDINATE	VALUE
1	0.00000E+00	0.00000E+00
2	0.53740E-02	0.14861E+00
3	0.85543E-02	0.23856E+00
4	0.11735E-01	0.30190E+00
5	0.17109E-01	0.40544E+00
6	0.23472E-01	0.47854E+00
7	0.27238E-01	0.52401E+00
8	0.31004E-01	0.54361E+00
9	0.37368E-01	0.57393E+00
10	0.44903E-01	0.57009E+00
11	0.49362E-01	0.56905E+00
12	0.53822E-01	0.55110E+00
13	0.61357E-01	0.51993E+00
14	0.70280E-01	0.46639E+00
15	0.75560E-01	0.43453E+00
16	0.80841E-01	0.39980E+00
17	0.89764E-01	0.34207E+00
18	0.10033E+00	0.28054E+00
19	0.10658E+00	0.24304E+00
20	0.11284E+00	0.21291E+00
21	0.12340E+00	0.16338E+00
22	0.13591E+00	0.12104E+00
23	0.14332E+00	0.94055E-01
24	0.15072E+00	0.74522E-01
25	0.16323E+00	0.46219E-01
26	0.17805E+00	0.20950E-01
27	0.18682E+00	0.67501E-02
28	0.19558E+00	0.23217E-02
29	0.21040E+00	-.19406E-01
30	0.24264E+00	-.37895E-01
31	0.25868E+00	-.38499E-01
32	0.26965E+00	-.45695E-01
33	0.32793E+00	-.45004E-01
34	0.32803E+00	-.44970E-01
35	0.32810E+00	-.44988E-01
36	0.32852E+00	-.44863E-01
37	0.38738E+00	-.25529E-01
38	0.39674E+00	-.26146E-01
39	0.40948E+00	-.14874E-01
40	0.44580E+00	0.29081E-02
41	0.46734E+00	0.64840E-02
42	0.48539E+00	0.18708E-01
43	0.50343E+00	0.15540E-01
44	0.52497E+00	0.15299E-01
45	0.54651E+00	0.14743E-01
46	0.56456E+00	0.13209E-01
47	0.58260E+00	0.12003E-01
48	0.60414E+00	0.11184E-01
49	0.62568E+00	0.10470E-01
50	0.64373E+00	0.96368E-02
51	0.66177E+00	0.88541E-02
52	0.68331E+00	0.82272E-02
53	0.70485E+00	0.76362E-02
54	0.72290E+00	0.69035E-02
55	0.74095E+00	0.62021E-02
56	0.76249E+00	0.56396E-02
57	0.78403E+00	0.51137E-02
58	0.80207E+00	0.44200E-02
59	0.82012E+00	0.37787E-02
60	0.84166E+00	0.32829E-02
61	0.86320E+00	0.28427E-02

```
      62       0.88124E+00      0.22368E-02
      63       0.89929E+00      0.17132E-02
      64       0.92083E+00      0.13252E-02
      65       0.94237E+00      0.10202E-02
      66       0.96041E+00      0.56594E-03
      67       0.97846E+00      0.21851E-03
      68       0.10000E+01      0.00000E+00

***   20.320 COMMAND EXECUTION TIME

 ********** END OF RUN --     4  PLOTS COMPLETED
```